MUSCULOSKELETAL DYNAMICS ANALYSIS OF LOWER LIMB AND ITS APPLICATION USINF A WEARABLE SENSOR SYSTEM

Rencheng Zheng

A dissertation submitted to
Kochi University of Technology
in partial fulfillment of the requirements
for the degree of

Doctor of Philosophy

Special Course for International Students
Graduate School of Engineering
Kochi University of Technology
Kochi, Japan

March 2009

Abstract

Human motion analysis is fundamental for rehabilitating and clinical applications but data are commonly obtained by means of the traditional laboratory-restricted equipment such as a force plate and optical camera system. A wearable sensor system was developed for an ambulatory and unobtrusive motion measurement of lower limb in everyday activities instead of the traditional one. Moreover, musculoskeletal dynamics analysis of lower limb can provide a deeply and quantitatively understanding of motion mechanism and assessment of motion abilities. In this dissertation, musculoskeletal dynamics analysis of lower limb and its application using the wearable sensor system were presented for developing a new biomechanical analysis technique.

Firstly, the wearable sensor system integrating force sensor and motion sensor was introduced. Then, a new method based on the sensing signals and gait cycle was demonstrated for kinematics analysis of ankle, knee and hip joints. And an inverse method suitable to the wearable sensor signals was developed for joint dynamics analysis. In experimental study, a force plate & optical camera system as a reference, the sensing signals and the results of joints kinematics and dynamics analysis using the wearable sensor system were validated through statistical analysis.

For musculoskeletal kinematics analysis, a reliable processing was designed to estimate individual dynamic musculotendon lengths and moment arms of lower limb in vivo. Regression equations inputting skeletal morphological parameters for calculating musculotendon origin-insertion coordinates and anthropometric method measuring skeletal morphological parameters ensure that the method can be conveniently operated. In virtue of muscle mechanical properties, static optimization method to calculate muscle forces was presented, and surface electromyography signals as a reference to evaluate the predicted results of muscle force.

In this study, the whole analytical processes of musculoskeletal dynamics of lower limb were built, meanwhile, feasibility and effectiveness of the musculoskeletal dynamics analysis and its application was testified using the wearable sensor system.

Keywords: Wearable Sensor System, Musculoskeletal Model, Joint Dynamics, Musculotendon Parameters, Muscle Force

Acknowledgements

I am deeply thankful to have had the opportunity to work with Professor Yoshio Inoue. As my principal advisor, Professor Inoue has been a constant source of insight and encouragement. His enthusiasm, attension to detail, and frindship will continue to influence my study in the year to come.

I greatly thank Associate Professor Kyoko Shibata. As my vice advisor, Associate Professor Shibata gave me a lot of helps in my study activities. Her valuable suggestions in the regular meeting have been especially constructive.

I gratefully acknowledge the contributions of my senior, Dr. Tao Liu, his excellent researches laid a foundation on the study about wearable sensor system. He also gave me a lot of valuable suggestion on my studying activities.

Thanks to Mr. Matsazuku Kurihara, as my tutor, he helped me so much when I just went to Japan. I will never forget his warm heart and kindness.

I have benefitted for daily interactions with friends at Robotics and Dynamic Lab in Kochi University of Technology. Mr. Masafumi Nakahama, Mr. Takashi Mori, Mr. Hiroki Yamaoka, Mr. Shingo Fukii, Mr. Nozomu Imanishi, Mr. Hajime Utsunomiya, Mr. Shinji Ymamoto, and Mr. Takuto Shirakawa have been especially helpful.

At last, thanks to scholarship of Speacial Schorlar Program by Kochi University of Technology supporting my living for three years in Japan.

Contents

1 Introduction

1.1 Background

The body motion analysis is fundamental for rehabilitation and clinical diagnosis but data are commonly obtained by means of the laboratory-restricted equipment such as a force plate and optical camera system. The force plate and optical camera analysis system, as a traditional motion analysis system, are expensive, space-consuming and need professional calibration knowledge, so they are limited to laboratory studies. A wearable sensor system is needed for an ambulatory and unobtrusive motion measuring instead of the traditional ones. The wearable sensor system can be conveniently used in daily environments, such as in living room, upstairs and downstairs, up-slope and down-slope, and in doctor’s office. Moreover, musculoskeletal dynamics analysis can provide a deeply and quantitatively understanding about motion mechanism, motion abilities and healthy condition of lower limb. Especially, joint moments and muscle forces of lower limb are important data for medical assessment and diagnosis. It is emergent to developing an inverse method for the musculoskeletal dynamics analysis of lower limb using a wearable sensor system, and eventually developing a new biomechanical assessment technique.

1.2 Historical Method

In general, a measurement system of human motion consisting of force plate and optical camera system has several disadvantages to everyday application. Firstly, the measurement system is mainly restricted to the gait laboratory. The force plate and optical camera system are fixed on the ground, and cannot be moved after the system calibration process. Secondly, the system is inconvenient for everyday human activities, since the reflective marker of an optical camera system has to be attached to the subject's body, and the subject should commonly placed their feet completed on the force plate for a correct measurement. Moreover, in the case of successive gait trials, an instrumented treadmill device[(1)] or multiple force plates have to be prepared, and for staircases, a complex system by multiple force plate are usually constructed[(2)]. Furthermore, in both of the above cases, the synchronous measurement of body movement is difficult due to the limited measurement dimensions of optical camera system. Especially, when a stand-up training

machine[3] or a walking aid[4] are used to enhance subjects' motion abilities in a daily healthcare course, since force plate and optical camera system cannot be employed in this condition due to their limitations, a sensor system is necessary to implement the real-time feedback of subject movement information for monitoring subject behavior. For measurement of body movement, an alternative for overcoming the drawbacks of the optical camera system is to use inertial sensors, which commonly consist of accelerometers and gyroscopes[5]. However, integrating accelerometers and gyroscopes consistently involved some drift error of the position and orientation. Up to the present time, few studies have mentioned a wearable sensor system, which can simultaneously get sufficient information including GRF, CoP and body movement data for ankle, knee and hip joints kinetics analysis, which can make a significant contribution to the understanding of human movement in everyday activities. The first goal of this study is to improve a wearable sensor system to measure GRF, CoP and segments movement of lower limb. In addition, considering the sensor system features, a new method was applied to estimate the joint position and orientation, and an inverse kinetic method to calculate the joint kinetics.

Dynamic musculotendon parameters are vital to understand muscle functions and estimate muscle force in vivo, and the parameters are eventually applied on the clinical diagnosis for patients. Generally, non-invasive estimation of dynamic musculotendon length and moment arm during gait is dependent on the use of musculoskeletal model of lower limb. Through determination of the muscle force action line and coordinates of origin-insertion and via point, and rescaling the coordinates to measurable external landmarks, musculotendon parameters can be estimated based on anatomical musculoskeletal models[6]. Length and moment arm of human leg muscles as a function of knee and hip-joint angles[7] were studied respectively. A prior computer program[8] calculate musculotendons kinematics and moment arm of six muscles of lower extremity for subject performing movements in the sagittal plane. Following this step, musculoskeletal modeling software of AnyBody[9], SIMM[10] and OpenSim[11] are successively developed for musculoskeletal motion simulation, even for dynamics simulation based on musculoskeletal anatomical models. But up to now, the most of existing musculoskeletal data were measured by European and American. However, studies[14, 15] demonstrated the musculoskeletal structure of different human race existed remarkable discrepancies that means the most of the data are not suitable to analyze Asian musculoskeletal structure.

Recently, researchers begin to use magnetic resonance image (MRI) or ultrasound scanning (US) techniques to restructure the subject-specific musculoskeletal model of lower limb for estimating the moment arm length. Moreover, the personalized MRI-based musculoskeletal models were compared to rescaled generic models in the presence of increased femoral

anteversion effects on hip moment arm lengths[12]. The further researching results suggested that the calculated musculotendon length and moment arm during gait differ substantially using MRI-based versus rescaled generic lower-limb musculoskeletal models[13]. However, study[14] concluded that the combination of MRI and graphics-based musculoskeletal modeling provides a more accurate means of estimating musculotendon and moment arms in vivo. Anyway, MRI and US yield time and cost consideration, and suffer a lot of the limitations by MRI or ultrasound scanning equipments. A newly attempt is to use a novel non-invasive protocol[15] to determine the personalized moment arms of knee and ankle muscles. This method is designed for superficial muscles only, and the validity of the results depends on the accuracy of the data recorded during motion analysis. The error is obvious, and difficult to be taken into account.

Many researchers commonly use the musculoskeletal modeling method to analyze the muscle cooperation problem during human motion, since we can not destroy muscle organization and simultaneously maintain muscle lively. Correspondingly, estimation of muscle force is an important way to understand muscle activities, and can provide diagnosis information for relevant patient. In our study, linear-weight-sum method as a new method is proposed to estimate optical muscle force based on multiple musculoskeletal model. Recently, human motion modeling and simulation becomes a very active research field. There is an increasing need of tools that permit to know or evaluate in vivo muscle force with noninvasive techniques. The most of studies is in virtue of the comprehensive achievements by Zajac[16], and he[17,18] suggested that dynamic optimization is a powerful method to estimate muscle force but static optimization has several disadvantages, even though static optimization has been used extensively to estimate in vivo muscle forces during gait.

Unfortunately, dynamic optimization incurs so much computational expense that relatively few dynamic solutions for gait have been found. Further, for gait, this approach has required that the dynamic models be simplified to such an extent that it has been difficult to ascertain whether its computational expense is justified. Thus, for normal gait, if one can accurately solve the inverse dynamics problem and if one seeks only to estimate muscle forces, the use of dynamic optimization rather than static optimization is currently not justified[19]. Since static optimization method may provide reasonably accurate estimation of muscle force during gait, objective function as an important impact factor to the estimation results had be paid a lot of attentions. Minimum energy expenditure, minimum muscle fatigue, and minimum sense of effort seem to be the most promising function to solve the optimization problem[20]. EMG-to-force processing approach[21] had became a reliable technique to estimate muscle force, however, Sofia[22] proposed static optimization method can get more accurate muscle force results than EMG-to-force

processing approach.

1.3 **Thesis Overview**

In this chapter, background, historical methods and researching goals of this study was introduced.

In chapter 2, the structures of a wearable sensor systems are presented, and the measuring signals was validated by a standard reference of a force plate & optical camera system in our experimental system.

In chapter 3, the kinematics analysis of ankle, knee and hip joints in the sagittal plane by using the sensor system on human normal level walking during whole gait phases are introduced integrating the sensing signals and walking cycle principle.

In chapter 4, kinetics analysis method of ankle, knee and hip joints using a wearable sensor system are demonstrated, and the validating experiments are also presented in turn.

In chapter 5, we concentrates on the estimation processes of the individual dynamic musculotendon lengths and moment arms of lower limb in vivo to extend our research.

In chapter 6, muscular forces are estimated using static optimization from joint moments, meanwhile, the whole processes was presented in detail.

In chapter 7, the contributions, practical applications and future work of this study are concluded.

References

(1) Frédéric Dierick, Massimo Penta, David Renaut and Christine Detrembleur, A force measuring treadmill in clinical gait analysis, Gait & Posture, Vol. 20, No. 3, (2004), pp. 299-303.

(2) Alex Stacoff, Christian Diezi, Gerhard Luder, Edgar Stüssi and Inès A. Kramers-de Quervain, Ground reaction forces on stairs: effects of stair inclination and age, Gait & Posture, Vol. 21, No. 1, (2005), pp. 24-38.

(3) Kyoko Shibata, Yoshio Inoue, Study on standing-up training machine with posture sensor system, Proceeding of the Welfare Engineering Symposium, (2007), Japan, pp. 41-43.

(4) Yusuke, Ouchi, Osamu Matsumoto, Seong-SiK Yoon, Yoji Yamada, Study on prediction of falling when using a walking aid, Proceeding of the Welfare Engineering Symposium, (2007), Japan, pp. 70-71.

(5) Ruth E. Mayagoitia, Anand V. Nene and Peter H. Veltink, Accelerometer and rate gyroscope measurement of kinematics: an inexpensive alternative to optical motion analysis systems,

Journal of Biomechanics, Vol. 35, No. 4, (2002), pp. 537-542.

(6) R. A. Brand, R. D. Crowninshield, C. E. Wittstock, D. R. Pederson, C. R. Clark, A model of lower extremity muscular anatomy, Journal of Biomechanical Engineering, Vol. 104, No. 4 (1984), pp. 304-10.

(7) J.J. Visser, J.E. Hoogkamer, M.F. Bobbert, P.A. Huijing, Length and moment arm of human leg muscles as a function of knee and hip-joint angles, European Journal of Applied Physiology, (1990), pp. 453-460.

(8) David Hawkins, Software for determining lower extremity muscle-tendon kinematics and moment arm lengths during flexion/extension, Computers in Biology and Medicine, Vol. 22, No. 1/2 (1992), pp. 59-71.

(9) Delp, S.L., Loan, J.P., A graphics-based software system to develop and analyze models of musculoskeletal structures, Computers in Biology and Medicine, Vol. 25, No. 1 (1995), pp. 21-34.

(10) Michael Damsgaard, John Rasmussen, Soren Torholm Christensen, Egidijus Surma, Mark de Zee, Analysis of musculoskeletal systems in the AnyBody Modeling System, Simulation Modelling Practice and Theory, Vol. 14, No. 8 (2006), pp. 1100-1111.

(11) Delp, S.L., Frank C. Andersen, Allison S. Arnold, Peter Loan, Ayman Habib, Chand T. John, Eran Guendelman, Darryl G. Thelen, OpenSim: open-source of software to create and analyze dynamic simulations of movement, IEEE Transactions on Biomechanical Engineering, Vol. 54, No. 11 (2007), pp. 1940-1947.

(12) Constantinos N. Maganaris, Vasilios Baltzopoulos, Dimitrios Tsaopoulos, Muscle fiber length-moment arm ratios in the human lower limb determined in vivo, Journal of Biomechanics, Vol. 39, No. 9 (2006), pp. 1663-1668.

(13) Lennart Scheys, Arhur Spaepen, Paul Suetens, Ilse Jonkers, Calculated moment-arm and muscle-tendon lengths during gait differ substantially using MR based versus rescaled generic lower-limb musculoskeletal models, Gait & Posture, Vol. 28, No. 3 (2008), pp. 358-365.

(14) Lennart Scheys, Anja Van Campenhout, Arhur Spaepen, Paul Suetens, Ilse Jonkers, Personalized MR-based musculoskeletal models compared to rescaled generic models in the presence of increased femoral anteversion: Effect on hip moment arm lengths, Gait & Posture, Vol. 28, No. 4 (2008), pp. 640-648.

(15) A. Bonnefoy, N. Doriot, M. Senk, B. Dohin, D. Pradon, L. Cheze, A non-invasive protocol to determine the personalized moment arms of knee and ankle muscle, Journal of Biomechanics, Vol. 40, No. 8 (2007), pp. 1776-1785.

(16) Zajac Felix E., Muscle and tendon: properties, models, scaling, and application to biomechanics and motor control, Critical Reviews in Biomedical Engineering, Vol. 17, No. 4, pp.359-411, 1989.

(17) Zajac Felix E., Richard R. Neptune, Steven A. Kautz, Biomechanics and muscle coordination of human walking Part I: introduction of concepts, power transfer, dynamics and simulations, Gait & Posture, Vol. 16, No. 3, pp.215-232, 2002.

(18) Zajac Felix E., Richard R. Neptune, Steven A. Kautz, Biomechanics and muscle coordination of human walking Part II: Lessons from dynamical simulations and clinical implications, Gait & Posture , Vol. 17, No. 1, pp.1-17, 2003.

(19) Anderson Frank C., Marcus G. Pandy, Static and dynamic optimization solutions for gait are practically equivalent, Journal of Biomechanics, Vol. 34, No. 2, pp.153-161, 2001.

(20) Prilutsky, Boris I., Zatsiorsky, Vladimir M., Optimization-based models of muscles coordination, Exercise & Sports Sciences Reviews, Vol. 30, No. 1, 2002.

(21) Louis N., A. Bonnefoy, D. Pradon, P. Gorce, A preliminary report. Muscle forces during reaching: EMG-to-force processing, Computer Methods in Biomechanics and Biomedical Engineering, Vol. 10, S. 1, pp.57-58, 2007.

(22) Sofia Heintz, Elena M Gutierrez-Farewik, Static optimization of muscle forces during gait in comparison to EMG-to-force processing approach, Gait & Posture, Vol. 26, No. 2, 2007.

2 Wearable Sensor Systems

Human motion analysis is fundamental for rehabilitation and clinical diagnosis but data are commonly obtained by means of the laboratory-restricted equipment such as a force plate and optical camera system, which usually require complicated computing programs and professional operation. In our study, a wearable sensor system was developed to measure body movement in daily activities. The wearable sensor system is composed of a shoe-based force sensor which measures ground reaction force (GRF) and center of pressure (CoP), and a leg-attached motion sensor consisting of three uniaxial gyroscopes units which detect lower limbs movement. In this chapter, firstly structure of the wearable sensor system is introduced. Then, in the experimental study, a force & optical camera system as a reference, the measuring accuracy of the wearable sensor system was validated.

2.1 Introduction

Segmental motion, GRF and CoP are usually measured by a combination of force plate and optical camera system in a gait laboratory. However, with increasing applications of human motion analysis in the medical-related fields, the lab-restricted measurement system is not suitable for applications in everyday environments, especially for healthcare evaluation to the elder in homes and medical diagnosis for patients in rehabilitation sites. There is a need for a measurement system which can measure GRF, CoP and body movement conveniently in daily activities, such as a miniature sensor system which can be worn on the human body and does not restrict human movement, namely a wearable sensor system.

In general, a measurement system consisting of force plate and optical camera system has several disadvantages to everyday application. Firstly, the measurement system is mainly restricted to the gait laboratory. The force plate and optical camera system are fixed on the ground, and cannot be moved after the system calibration process. Secondly, the system is inconvenient for everyday human activities, since the reflective marker of an optical camera system has to be attached to the subject's body, and the subject should commonly placed their feet completed on the force plate for a correct measurement. Moreover, in the case of successive gait trials, an

instrumented treadmill device[1] or multiple force plates have to be prepared, and for staircases, a complex system by multiple force plate are usually constructed [2]. Furthermore, in both of the above cases, the synchronous measurement of body movement is difficult due to the limited measurement dimensions of optical camera system. Especially, when a stand-up training machine[3] or a walking aid[4] are used to enhance subjects' motion abilities in a daily healthcare course, since force plate and optical camera system cannot be employed in this condition due to their limitations, a sensor system is necessary to implement the real-time feedback of subject movement information for monitoring subject behavior. In fact, in pioneering research by Kljajic and Krajnik[5], pressure sensors were widely used to make instrumented insoles for measurement of the vertical component of GRF and CoP[6-8]. In the research[9, 10], the novel shoes were developed by placing two six-axial force sensors in the front part and rear part of the structure to measure complete GRF and CoP in ambulatory walking. In further research, by arrangement of the inertial sensor and six-axial force sensors together, the orientation of the force sensor could be measured for an accurate estimation of GRF. For measurement of body movement, an alternative for overcoming the drawbacks of the optical camera system is to use inertial sensors, which commonly consist of accelerometers and gyroscopes[11-13]. For our developed wearable sensor system, GRF, CoP and segmental movement of lower limb can be measured by the integrating sensor system.

2.2 Wearable Sensor Systems

A wearable sensor system was developed by integration of an instrumented shoe, a motion sensor systems and a logger. Two force sensors were mounted into a common shoe as a prototype of the instrumented shoe in this research. A 6-axial force sensor[14] was fixed on the heel part of the shoe, and a smart 3-axial force sensor (Tec Gihan, Japan) on the forefoot part of the shoe to measure GRF and CoP. Three motion sensor units were worn on the foot, calf and thigh respectively. A segmental model of lower limb wore the wearable sensor system is shown in Fig. 1.1(a).

Each of the motion units consisting of an electrical baseboard was specially designed for integrating uniaxial gyroscope chip (Murata ENC-03J). Gyroscopes are used to measure angular velocities of the foot, shank and thigh. The sensitive axis is vertical to the medial-lateral plane so that the angular velocity in the sagittal plane can be detected. The gyroscope measures the Coriolis acceleration, which is generated when a rotational angular velocity is applied to the oscillating piezoelectric bimorph. The gyroscope can work under low energy consumption (4.6 mA at 5V). The signals from the gyroscopes are amplified and low-pass filtered (cutoff frequency: 25Hz) to remove electronic noise.

A micro-computer PIC (16F877A) was used to design a pocketed multi-channel logger, and sampling data from the sensors can be saved in a SRAM, which can keep recording for five minutes. An off-line motion analysis can be performed by means of the sampled data saved in the SRAM to a personal computer through a RS232 communication module. The wearable sensor system was powered by a battery of 300mAh (NiMH 30R7H). The logger is strapped around the waist part as shown in the Fig. 1.1(a). In here, Each of ankle, knee and hip joints is assumed as an ideal joint model[(1)].

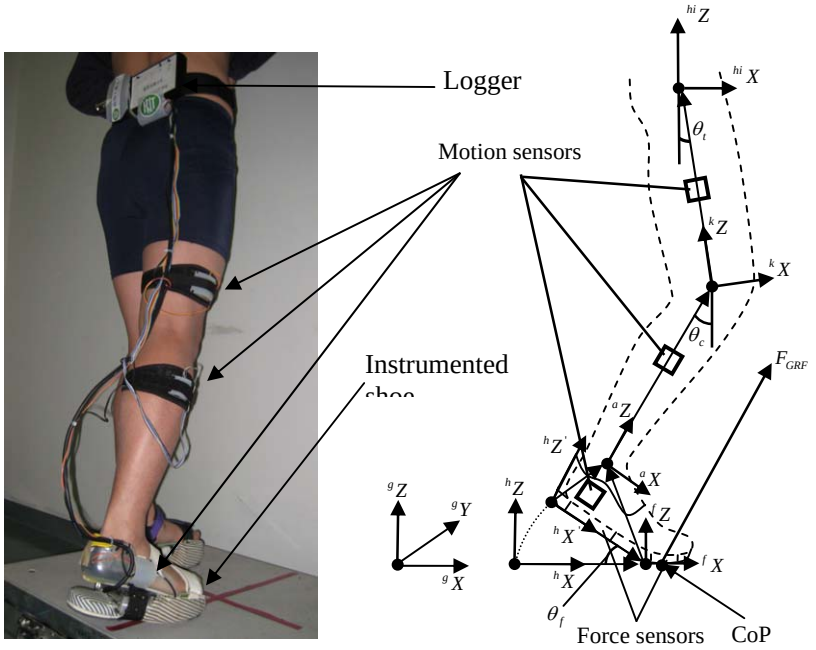

Fig.1.1. Diagram of lower extremity wearing the wearable sensor system. (a) Wearable sensor system. (b) Segmental model and coordinates systems of a lower extremity.

For calculation purposes, all the vectors should be expressed in global coordinates system. As shown in Fig. 1.1(b), an orthogonal right-handed coordinate system (${}^{g}X-{}^{g}Y-{}^{g}Z$) was defined as the global coordinates system, in which positive X is along the forward direction of gait, positive Z is directed upward and positive Y is perpendicular to the X and Z direction. The origin and orientation of this global coordinates system are renewed for each stride to coincide with the segment and sensor coordinates systems. The coordinates systems of heel (${}^{h}X-{}^{h}Z$), foot joint (${}^{f}X-{}^{f}Z$), ankle (${}^{a}X-{}^{a}Z$), knee (${}^{k}X-{}^{k}Z$) and hip joint (${}^{hi}X-{}^{hi}Z$) were also established, and their Y directions were decided by X and Z direction of themselves. The displaced heel coordinates systems (${}^{h}X'-{}^{h}Z'$) were also constructed in Fig. 1.1(b). The ankle, knee and hip joint orientations

were decided by the angular velocities of foot $\dot{\theta}_f$, calf $\dot{\theta}_c$ and thigh $\dot{\theta}_t$ from the three gyroscopes signals respectively. In the integration of the angular velocities, we can get the angular displacements of foot θ_f, calf θ_c and thigh θ_t.

Joint moment and power are useful to obtain a full biomechanical analysis of body movement in daily activities. Before calculation of joint moment and power, we have to combine the GRFs, ${}^{s1}F_{GRF}$ and ${}^{s2}F_{GRF}$, and the moments, ${}^{s1}M_{GRF}$ and ${}^{s2}M_{GRF}$, from the two sensors, and transfer all of the measurement results to the global coordinates by

$$ {}^{g}F_{GRF} = {}^{g}_{s1}[T]\,{}^{s1}F_{GRF} + {}^{g}_{s2}[T]\,{}^{s2}F_{GRF} \tag{1.1} $$

$$ {}^{g}M_{GRF} = {}^{g}_{s1}[T]\,{}^{s1}M_{GRF} + {}^{g}_{s2}[T]\,{}^{s2}M_{GRF} \tag{1.2} $$

where the GRF and the moment in the global frame are presented by ${}^{g}F_{GRF}$ and ${}^{g}M_{GRF}$. ${}^{g}_{s1}[T]$ and ${}^{g}_{s2}[T]^{s2}$ are the transformation matrix to represent conversion of coordinates systems from the two sensors' frames to the global frames respectively. The GRF and the moment are expressed by the vectors in equation (1.3), and the coordinates of CoP ${}^{g}x_{CoP}$ in the global frame is calculated by

$$ {}^{g}F_{GRF} = \begin{pmatrix} {}^{g}F_x \\ {}^{g}F_y \\ {}^{g}F_z \end{pmatrix} \qquad {}^{g}M_{GRF} = \begin{pmatrix} {}^{g}M_x \\ {}^{g}M_y \\ {}^{g}M_z \end{pmatrix} \qquad {}^{g}x_{CoP} = \begin{pmatrix} \dfrac{{}^{g}M_y}{{}^{g}F_z} \\ \dfrac{{}^{g}M_y}{{}^{g}F_z} \\ 0 \end{pmatrix} \tag{1.3} $$

2.3 Validation Experiments

In this study, a series of experiments were accomplished for validation of the wearable sensor system. During the experiments, each of subjects wearing the sensor system was asked to normally walk over a force plate (EFP-S-2KNSA12, KYOWA, Japan); meanwhile, the movement information of the reflective markers on the lower extremity was captured by optical camera system (Hi-DCam, NAC Image Tech., Japan).

The sampling data from the gyroscope sensors, the force sensors in the instrumented shoe, and the force plate was acquired at same sample rate of 100 Hz. The force sensors in the instrumented shoe and the force plate were calibrated before each trial. Frame rate of Hi-DCam 4-camera systems was 100 Hz, and shutter speed was 1000 Hz. Calibration value of 3-D residuals before measurement by the camera systems was (0.5485 ± 0.2316) (mean $\pm$ standard deviation) mm, and ward length was (500.01 ± 0.86) mm. The possible gaps of the Hi-DCam data were dealt with by Join Cubic. The synchronization of the motion sensor system and Hi-DCam was done by maximizing the correlation of the angular velocities of the lower limb between the two systems.

10 healthy subjects (8 males and 2 females) as volunteers cooperated with us in the experiments. Ages of the subjects are (28.1 ± 1.99) (mean $\pm$ standard deviation), heights (1.692 ± 0.0424) m, and weights (66.26 ± 9.179) kg. The definition of thigh is from greater trochanteric head to center of the knee joint, calf from center of the knee joint to center of the ankle joint, foot from acropodion to heel. The length of thigh about the subjects is (0.4165 ± 0.0224) m (mean $\pm$ standard deviation), shank (0.3715 ± 0.03) m, and foot (0.2453 ± 0.008) m.

2.4 Results and Discussions

The force plate and optical camera system was used as a reference to validate the measurement results by the wearable sensor system, including GRF and CoP, segmental angular displacement, and the calculation results of the joint moment and power. The root mean square (RMS) difference as a statistic indexes was used to compare the closeness in amplitude of the results between the two systems.

As shown in Fig. 1.2(a), 1.2(b) and 1.2(c), the comparisons of the three components of GRF measured by wearable sensor systems and force plate systems were demonstrated in a representative trial. The results of GRF were normalized with respect to body weight. The results show good correspondence between two methods, which is confirmed by comparison analysis of the GRF (see Fig. 1.2(d)) and errors analysis of the GRF (see Fig. 1.2(e)), and RMS differences by 10 subjects' trials of (0.045 ± 0.003) N/N (mean $\pm$ standard deviation), which corresponds to (4.26 ± 0.34)% of the maximal GRF magnitude. A separate analysis of each component of the GRF results for the vertical component in an RMS difference of (0.046 ± 0.002) N/N, being (4.8 ± 0.2)% of the maximal GRF magnitude, or (4.2 ± 0.2)% of the maximal vertical components. For the X direction component of the horizontal GRF, RMS difference is (0.011 ± 0.008) N/N, being (1.07 ± 0.91)% to the maximal GRF magnitude, or (10.3 ± 2.2)% to the maximal X direction component. For the Y direction component of the horizontal GRF, RMS difference is

(0.014 ± 0.002) N/N, being (1.17 ± 0.12)% to the maximal GRF magnitude, or (10.1 ± 3.6)% to the maximal Y direction component.

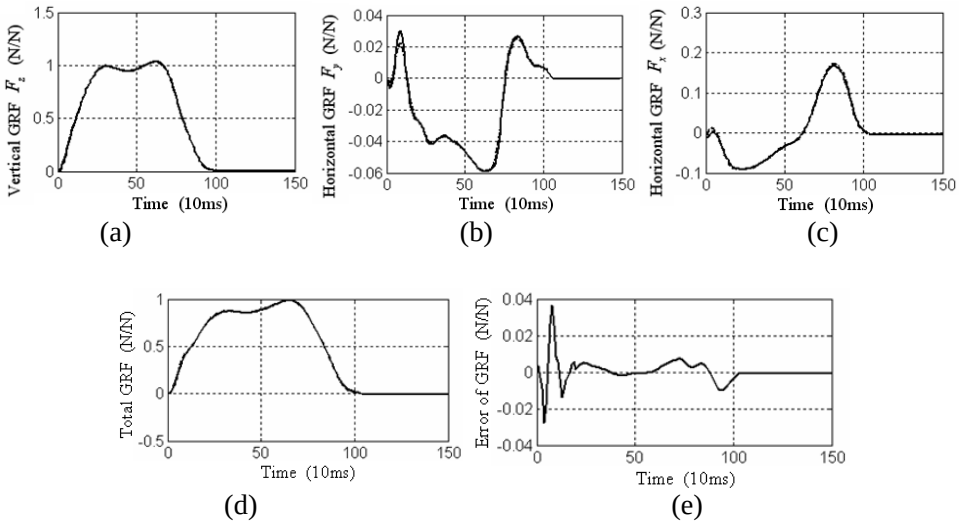

Fig. 1.2. GRF measured by wearable sensor systems (solid line) and force plate (dashed line). (a) Vertical components, F_z. (b) Horizontal components, F_y. (c) Horizontal components, F_x. (d) Total GRF. (e) Error of GRF between two systems.

The estimation of the position of the CoP is shown in Fig. 1.3. The trajectories agree well, resulting in an RMS difference between both methods of (10.4 ± 1.2) mm, corresponding to (3.7 ± 0.5)% of the length of the instrumented shoe.

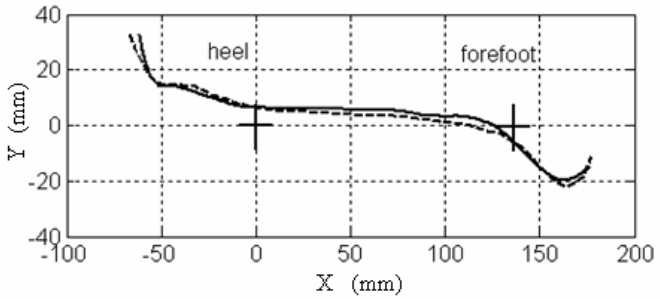

Fig. 1.3. Center of pressure (CoP) measured by wearable sensor systems (solid line) and force plate (dashed line) expressed in global coordinates system. The center of each force sensor is indicated by the black cross.

As shown in Fig. 1.4, the segmental angular displacements estimated using the wearable

sensor system and Hi-DCam camera systems was also compared. For the foot angular displacement, the RMS difference between the results estimated using the two systems was calculated as (2.91 ± 0.12) degree, being (5.6 ± 0.35) % of the maximal magnitude of the foot angular displacement. For the calf angular displacement, the RMS difference between the two methods is (2.61 ± 0.93) degree, being (4.71 ± 1.4) % of the maximal magnitude of the calf angular displacement. For the thigh angular displacement, the RMS difference between the two methods is (1.3 ± 0.39) degree, being (4.71 ± 2.05)% of the maximal magnitude of the thigh angular displacement.

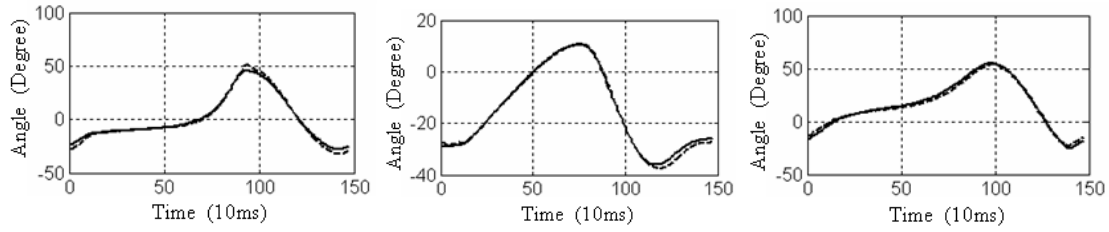

(a) (b) (c)

Fig. 1.4. Segmental angular displacements measured by wearable sensor systems (solid line) and Hi-DCam camera systems (dashed line). (a) Foot angular displacements. (b) Calf angular displacements. (c) Thigh angular displacements.

2.5 Conclusions

In this chapter, the improved wearable sensor system was validated for the application feasibilities by our experimental study. The GRF, CoP and segmental movement were measured by the wearable sensor system, and the data were used for joint kinematics and dynamics analysis in the next step study. In the validation experiments, the analysis of the RMS difference between the two systems was implemented, including the RMS differences of X, Y and Z components of GRF, segmental angular displacements. The results of the RMS differences demonstrated the measurement results have high consistence between the wearable sensor system and the force plate & optical camera system.

Two sensors were mounted on the heel and forefoot parts in a common shoe, and GRF can be accurately measured in the whole gait phase. One of the gyroscopes was fixed on the instrumented shoe during gait to measure the movement of sensor on the heel part. The independent movement of sensor in the forefoot part was omitted during pre swing period since the movement is negligible[16]. Considering the movement of the force sensor, the accurate results of the GRF were obtained by equation (1.1). The RMS difference analysis of the complete GRF and the GRF's errors indicated that the GRF's errors mainly occurred in loading response period,

since measurement accuracy of the sensors was influenced by the collision of the instrumented shoe initially contacting on the floor. This point suggested that a more flexible instrumented shoe should be designed for the further improvement of the wearable sensor. About the application of the instrumented shoe to measure GRF, an important problem should be made clear that is about the difference between using the barefoot method and the footwear method in gait analysis. Wolf et al.[17] manifested a flexible shoe have very few affects to motion analysis comparing to the barefoot method. Gait parameters by using an instrumented shoe was compared to the data by using normal, light and heavy shoes, and only a significant difference was found in the maximal GRF[18]. The announced result[18] was also validated in our related experiments. For the viewpoint[17], the instrumented shoe should be improved to be more flexible for subject's walking, and the improvements can result in a more accurately measurement of GRF. Since the prototype of the instrumented shoe applied the 6-axial sensor, which was designed by us using the whole aluminum contractures. The 6-axial sensor is a little large and rather stiff, and the RMS differences of X and Y components of GRF are about 10% to their maximal magnitude as mentioned in the results. Based on above analyses, the instrumented shoe should be improved to resolve the above problems by means of the optimal design in our future work.

In the chapter, a wearable sensor system combining a force sensor and motion sensor was used to measure GRF, CoP and collect segmental movement of lower limb. In the experimental study, RMS differences with a force plate and optical camera system as a reference testified to the wearable sensor system's accuracy. In the next chapter, kinematics analysis of ankle, knee and hip joints will be presented using the measuring data by the wearable sensor system.

References

(1) Frédéric Dierick, Massimo Penta, David Renaut and Christine Detrembleur, A force measuring treadmill in clinical gait analysis, Gait & Posture, Vol. 20, No. 3, pp. 299-303, 2004.

(2) Alex Stacoff, Christian Diezi, Gerhard Luder, Edgar Stüssi and Inès A. Kramers-de Quervain, Ground reaction forces on stairs: effects of stair inclination and age, Gait & Posture, Vol. 21, No. 1, pp. 24-38, 2005.

(3) Kyoko Shibata, Yoshio Inoue, Study on standing-up training machine with posture sensor system, Proceeding of the Welfare Engineering Symposium, Japan, pp. 41-43, 2007.

(4) Yusuke, Ouchi, Osamu Matsumoto, Seong-SiK Yoon, Yoji Yamada, Study on prediction of falling when using a walking aid, Proceeding of the Welfare Engineering Symposium, Japan, pp. 70-71, 2007.

(5) M Kljajic and J Krajnik, The use of ground reaction measuring shoes in gait evaluation, Clin. Phys. Physiol. Meas., Vol. 8, pp. 133-142, 1987.

(6) Sue Barnett, James L. Cunningham and Steven West, A Comparison of vertical force and temporal parameters produced by an in-shoe pressure measuring system and a force platform, Clinical Biomechanics, Vol. 15, No. 10, pp. 781-785, 2000.

(7) Kenneth J. Chesnin, Lisa Selby-Silverstein and Marcus P. Besser, Comparison of an in-shoe pressure measurement device to a force plate: concurrent validity of center of pressure measurements, Gait & Posture**,** Vol. 12, No. 2, pp. 128-133, 2000.

(8) Arnaud Faivre, Marc Dahan, Bernard Parratte and Guy Monnier**,** Instrumented shoes for pathological gait assessment, Mechanics Research Communications, Vol. 31, No. 5, pp. 627-632, 2004.

(9) Chao L.-P., Yin C.-Y., The six-component force sensor for measuring the loading of the feet in locomotion, Materials and Design, Vol. 20, No. 5, pp. 237-244, 1999.

(10) Peter H. Veltink, Christian Liedtke, Herman van der Kooij, Ambulatory measurement of ground reaction forces, IEEE Transactions on Neural Systems and Rehabilitation Engineering, Vol. 13, No.3, pp. 423-427, 2005.

(11) Ruth E. Mayagoitia, Anand V. Nene and Peter H. Veltink, Accelerometer and rate gyroscope measurement of kinematics: an inexpensive alternative to optical motion analysis systems, Journal of Biomechanics, Vol. 35, No. 4, pp. 537-542, 2002.

(12) Karol J. O'Donovan, Roman Kamnik, Derek T. O'Keeffe, An inertial and magnetic sensor based technique for joint angle measurement, Journal of biomechanics, Vol. 40, No. 12, pp. 2604-2611, 2007.

(13) Roetenberg, D. Baten, C.T.M. Veltink, P.H. Xsens Technol., Enschede, Estimation body segment orientation by applying inertial and magnetic sensing near ferromagnetic materials, Neural Systems and Rehabilitation Engineering, Vol. 15, No. 3, pp. 469-471, 2007.

(14) Tao Liu, Yoshio Inoue, Kyoko Shibata, Wearable force sensor with parallel structure for measurement of ground-reaction force, Measurement, Vol. 40, pp. 644-653, 2007.

(15) Sylvia Ounpuu, Roy B. Davis, Peter A. Deluca, Joint kinetics: method, interpretation and treatment decision-making in children with cerebral palsy and myelomeningocele, Gait & Posture, Vol. 4, No. 1, pp. 62-78, 1996.

(16) Jessica Rose, James G. Gamble, Human Walking, Lippincott Williams & Wilkins, New York, 2006.

(17) Wolf S, Simon J, Patikas D, Schuster W, Armbrust P, Döderlein L, Foot motion in children shoes: a comparison of barefoot walking with shod walking in conventional and flexible shoes, Gait & Posture,Vol. 27, No. 1, pp. 51-59, 2008.

(18) H. Martin Schepers, H. F. J. M. Koopman, Peter H. Veltink, Ambulatory Assessment of ankle and foot dynamics, IEEE Transactions on Biomedical Engineering, Vol. 54, No. 5, pp. 895-902, 2007.

3 Joint Kinematics Analysis

The kinematical analysis of ankle, knee and hip joints is necessary to for joints dynamics analysis. In our study, the developed sensor system is composed of a shoe-based force sensor which measures ground reaction force (GRF) and center of pressure (CoP), and a leg-attached motion sensor consisting of three uniaxial gyroscopes units which detect lower limbs movement. Accordingly, the kinematics analysis techniques for fitting the wearable sensor system should be studied by means of the inverse method. In order to estimate the joint kinetics, an inverse kinematical analysis method based on the sensing signals and gait characteristics was developed. This chapter presents the kinematics analysis of ankle, knee and hip joints in the sagittal plane by using the sensor system on human normal level walking during whole gait phases.

3.1 Introduction

For measurement of body movement, an alternative for overcoming the drawbacks of the optical camera system is to use inertial sensors, which commonly consist of accelerometers and gyroscopes[1-3]. However, integrating accelerometers and gyroscopes consistently involved some drift error of the position and orientation. A complicated algorithm had to be used based on assumption of the zero velocity update and knowledge of position and orientation of body movement[4]. Obviously, the simpler method should be studied based on the sensor system and the kinematical knowledge of body movement. This paper concentrates on how to use measuring data by the wearable sensor system to do joints kinematics analysis.

3.2 Identification of Gait Periods

Identification of gait periods is the basis for gait analysis using a wearable sensor system. A cycle is a recurrent series of events. The gait cycle is the basis for understanding normal and pathological human walking. We speak of the gait cycle as applying separately to each lower extremity, and we define the gait cycle as the events that occur from one heel strike to the next.

Normal Gait. Initially, we can divide the gait cycle into phases, stance phase when the foot is in contact with the ground, and swing phase when the foot is in the air. Stance phase account for

60% of the cycle, and swing account for the remaining 40%. We can subdivide stance into five periods know as: 1) initial contact, 2) loading response, 3) midstance, 4) terminal stance, and 5) preswing. In addition, we can divide swing into three periods: 1) initial swing, 2) midswing, and 3) terminal swing. Gait phase (Fig. 3.1) are defined in detail as followings:

(1) Initial contact: This phase includes the moment when the foot just touches the floor. The joint postures presented at this time determine the limb's loading response pattern.

(2) Loading response: This is the initial double stance period. The phase begins with initial floor contact and continues until the other foot is lifted for swing. Using the heel as a rocker, the knee is flexed for shock absorption. Ankle plantar flexion limits the heel rocker by forefoot contact with floor.

(3) Mid stance: This is the first half of the single limb support interval. In this phase, the limb advances over the stationary foot by ankle dorsiflexion (ankle rocker) while the knee and hip extend. It begins as the other foot is lifted and continues until body weight is aligned over the forefoot.

(4) Terminal stance: This phase complete single limb support. It begins with heel rise and continues until the other foot strikes the ground, in which the heel rise and the limb advance over the forefoot rocker. Throughout his phase body weight moves ahead of the forefoot.

(5) Pre-swing: This final phase of stance is the second double stance interval in the gait cycle. It begins with initial contact of the opposite limb and end with ipsilateral toe-off. Objective of this phase is position the limb for swing.

(6) Initial swing: This phase is approximately one-third of the swing period. It begins with lift of the foot from the floor and ends when the swinging foot is opposite the stance foot. In this phase, the foot is lifted and limb advanced by hip flexion and increased knee flexion.

(7) Mid swing: This phase begins as the swinging limb is opposite the stance limb and ends when the swinging limb is forward and the tibia is vertical (i.e., hip and keen flexion postures are equal). The knee is allowed to extend in response to gravity while the ankle continues dorsiflexion to neural.

(8) Terminal swing: This final phase of swing begins with a vertical tibia and ends when the foot strikes the floor. Limb advancement is completed as the leg (shank) moves ahead of the thigh. In this phase the limb advancement is completed by knee extension, and the hip maintains its earlier flexion, and the ankle remains dorsiflexed to neural.

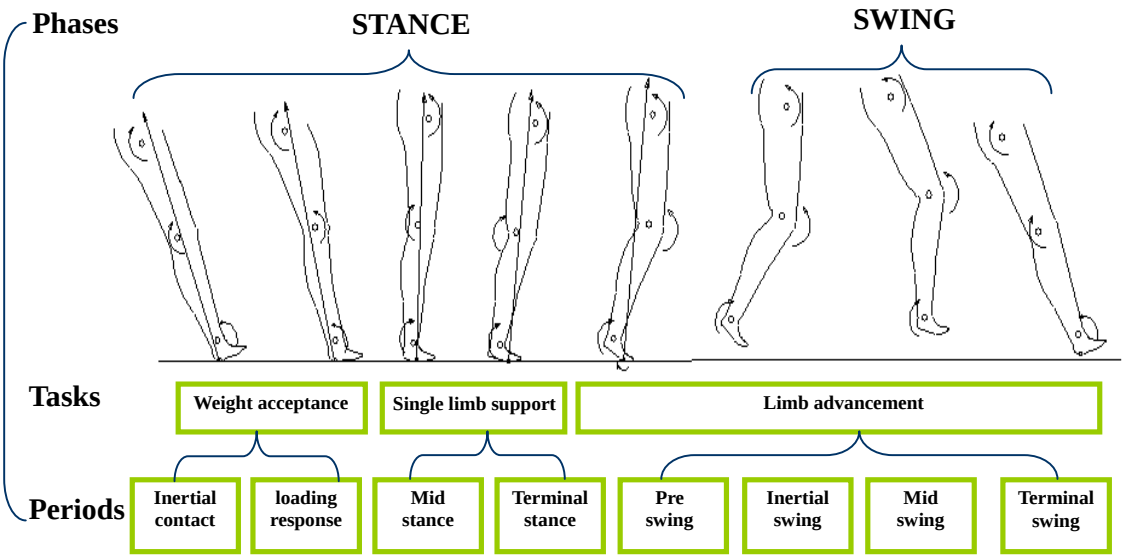

Fig. 3.1 The two phases of the gait cycle: stance phase when the foot is on the floor, and swing phase when the foot is in the air. The gait cycle is further subdivided into tasks as well as periods known as () initial contact, (2) loading response, (3) midstance, (4) terminal stance, and (5) preswing, (6) initial swing, (7) midswing, and (8) terminal swing.

Signal Analysis. The ankle, knee and hip joint orientations were decided by the angular velocities of foot $\dot{\theta}_f$, calf $\dot{\theta}_c$ and thigh $\dot{\theta}_t$ from the three gyroscopes signals respectively. In the integration of the angular velocities, we can get the angular displacements of foot θ_f, calf θ_c and thigh θ_t. It is difficult to know joint position only using the sensing signals. However, consider certain movement principles of lower extremity in normal gait cycle[(18)], a new method can be developed to obtain joint position. Based on the knowledge of normal gait cycle, we redefined the gait periods for estimation of joints positions. In our research, gait phase is subdivided into four periods (1) weight acceptance (WA), including inertial contact and loading response, (2) single limb support (SLS), including mid stance and terminal stance, (3) pre swing (PS), and (4) swing phase (SW), include inertial swing, mid swing, terminal swing. The former gait periods from WA to PS occur in stance phase (ST). The start and the end of a stride, and stance phase and swing phase are determined by the GRF's data from force sensors. When $F_{GRF} \neq 0$, gait phase is being in stance phase, and when $F_{GRF} = 0$, being in swing phase. The identification of different periods in stance phase is based on the signals of the foot angular displacement θ_f. When $\theta_f > 0$, gait phase is being in weight acceptance, when $\theta_f = 0$, being

in single limb support; and when $\theta_f < 0$, being in pre swing. The identification processes are as shown in Fig. 3.2.

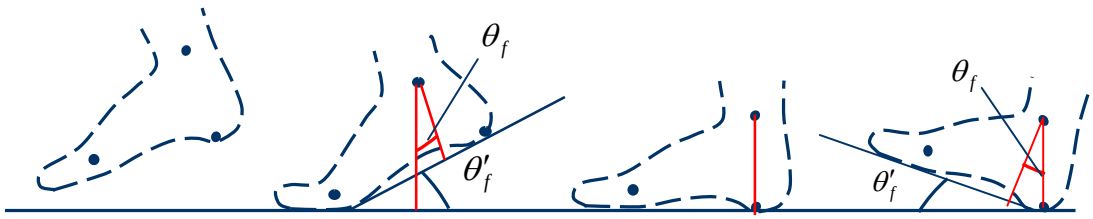

Fig. 3.2 Diagram of identification of gait period by signal analysis

3.3 Joint Position and Orientation

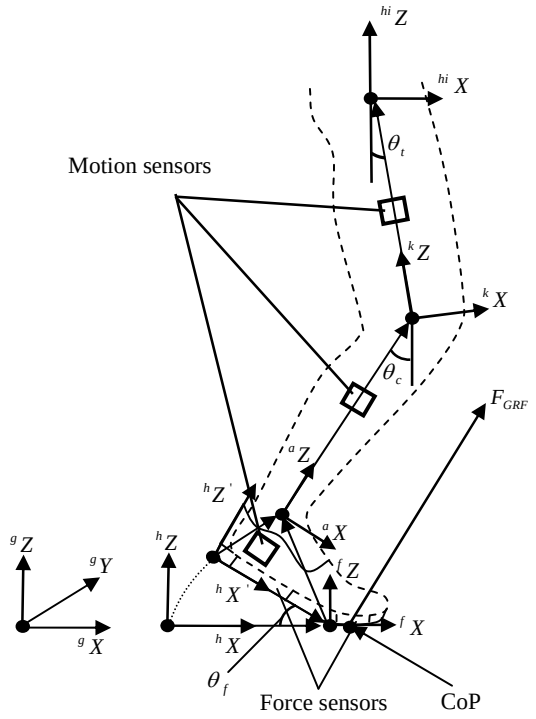

Fig. 3.3 Segmental model and coordinates systems of lower Limb

Estimation of joint position and orientation is a basement of joint kinetics analysis. For calculation purposes, all the vectors should be expressed in global coordinates system. As shown in Fig. 3.3, an orthogonal right-handed coordinate system ($^{g}X-^{g}Y-^{g}Z$) was defined as the global coordinates system, in which positive X is along the forward direction of gait, positive Z is directed upward and positive Y is perpendicular to the X and Z direction. The origin and orientation of this global coordinates system are renewed for each stride to coincide with the

segment and sensor coordinates systems. The coordinates systems of heel (${}^{h}X-{}^{h}Z$), foot joint (${}^{f}X-{}^{f}Z$), ankle (${}^{a}X-{}^{a}Z$), knee (${}^{k}X-{}^{k}Z$) and hip joint (${}^{hi}X-{}^{hi}Z$) were also established, and their Y directions were decided by X and Z direction of themselves. The displaced heel coordinates systems (${}^{h}X'-{}^{h}Z'$) were also constructed in Fig. 3.3.

In WA, heel strike to floor and foot begin to rotate around the heel stroked point forward to floor. The heel stroked point is used as supporting and rotation point. In SLS, whole foot sole touch the floor for supporting body, and in PS, foot joint as supporting and rotation point drive leg to leave the floor. In whole stance phases, segments of leg rotate around ankle, knee and hip joint successively. In SW, leg's segments swing forward around hip joint, knee and ankle successively. Based on the above knowledge, movement of lower extremity during gait can be described as a rotation and displace movement in their coordinates systems. In this way, joint position can be derived from the mutual movements in the joints and segments coordinates systems during gait. A homogeneous transformation matrix ${}^{j}_{i}[T]$ was used to denote the combination of rotation and displacement between two coordinates systems[19]

$$ {}^{i}_{j}[T] = \begin{bmatrix} {}^{i}_{j}[R] & {}^{i}_{j}\{Q\} \\ 0 & 1 \end{bmatrix} \tag{3.1} $$

where ${}^{i}_{j}[R]$ is a rotation matrix representing the transformation of coordinates between frame $\{j\}$ and frame $\{i\}$ rotated with respect to each other, superscript i represent reference frame $\{i\}$, and j represent frame $\{j\}$. ${}^{i}_{j}\{Q\}$ is a displacement vector representing the coordinates of the origin of frame $\{j\}$ expressed in frame $\{i\}$.

In stance phase, the ankle position in the global frame in the three successive gait periods are expressed by the position vectors ${}^{g}\{P\}_{ank-wa}$, ${}^{g}\{P\}_{ank-sls}$ and ${}^{g}\{P\}_{ank-pw}$, and can be estimated by

$$ {}^{g}\{P\}_{ank-wa} = \begin{bmatrix} {}^{g}_{h}[R] & {}^{g}_{h}\{Q\} \\ 0 & 1 \end{bmatrix} {}^{h}\{P\}_{ank-wa} \tag{3.2} $$

$$ {}^{g}\{P\}_{ank-sls} = \begin{bmatrix} I & {}^{g}_{h}\{Q\} \\ 0 & 1 \end{bmatrix} {}^{h}\{P\}_{ank-sls} \tag{3.3} $$

$$ {}^{g}\{P\}_{ank-pw} = \begin{bmatrix} {}^{g}_{f}[R] & {}^{g}_{f}\{Q\} \\ 0 & 1 \end{bmatrix} {}^{f}\{P\}_{ank-pw} \tag{3.4} $$

where ${}^{h}\{P\}_{ank-wa}$ and ${}^{h}\{P\}_{ank-sls}$ represent the initial ankle position vector in the heel frame in WA and in SLS respectively, and ${}^{f}\{P\}_{ank-pw}$ represent the initial position vector of ankle in the heel frame in PW. ${}^{g}_{h}[R]$ and ${}^{g}_{f}[R]$ represent the rotation matrices representing the rotation relation between the heel frame and the global frame and between the foot joint frame and the global frame. I is a unit matrix. ${}^{g}_{h}\{Q\}$ and ${}^{g}_{f}\{Q\}$ are the displacement vectors representing the heel frame and the foot joint frame respectively expressed in global frame.

In stance phase, since calf rotate around ankle and thigh rotate around knee, the knee position vector in the global frame ${}^{g}\{P\}_{kne-st}$ and the hip position vector in the global frame ${}^{g}\{P\}_{hip-st}$ can be estimated by

$$ {}^{g}\{P\}_{kne-st} = \begin{bmatrix} {}^{g}_{a}[R] & {}^{g}_{a}\{Q\} \\ 0 & 1 \end{bmatrix} {}^{a}\{P\}_{kne-st} \tag{3.5} $$

$$ {}^{g}\{P\}_{hip-st} = \begin{bmatrix} {}^{g}_{k}[R] & {}^{g}_{a}\{Q\}+{}^{a}_{k}\{Q\} \\ 0 & 1 \end{bmatrix} {}^{k}\{P\}_{hip-st} \tag{3.6} $$

where ${}^{a}\{P\}_{kne-st}$ and ${}^{k}\{P\}_{hip-st}$ represent the initial knee position vector in the ankle frame and the initial hip position vector in the knee frame in stance phase. ${}^{g}_{k}[R]$ and ${}^{g}_{a}[R]$ represent the rotation matrices representing the rotation relation between the heel frame and the global frame and between the foot joint frame and the global frame. ${}^{g}_{a}\{Q\}$ and ${}^{a}_{k}\{Q\}$ are the displacement vectors representing the ankle frame expressed in global frame, and the knee frame

expressed in global frame.

In swing phase, hip joint only has a displacement relative to the global frame. Thigh rotates around hip joint, calf around knee joint, and foot around ankle joint. So the position vectors of hip joint ${}^{g}\{P\}_{hip-sw}$, knee ${}^{g}\{P\}_{kne-sw}$ and ankle ${}^{g}\{P\}_{ank-sw}$ can be sequentially calculated by

$$ {}^{g}\{P\}_{hip-sw} = \begin{bmatrix} I & {}^{g}_{hi}\{Q\} \\ 0 & 1 \end{bmatrix} {}^{g}\{P\}_{hip'} \tag{3.7} $$

$$ {}^{g}\{P\}_{kne-sw} = \begin{bmatrix} {}^{g}_{hi}[R] & {}^{g}_{hi}\{Q\} \\ 0 & 1 \end{bmatrix} {}^{hi}\{P\}_{kne-sw} \tag{3.8} $$

$$ {}^{g}\{P\}_{ank-sw} = \begin{bmatrix} {}^{g}_{k}[R] & {}^{g}_{hi}\{Q\} + {}^{hi}_{k}\{Q\} \\ 0 & 1 \end{bmatrix} {}^{k}\{P\}_{ank-sw} \tag{3.9} $$

where ${}^{g}\{P\}_{hip'}$, ${}^{hi}\{P\}_{kne-sw}$ and ${}^{k}\{P\}_{ank-sw}$ represent the initial hip position vector in the global frame, the initial knee position vector in the hip joint frame, and the initial ankle position vector in the global frame in swing phase. ${}^{g}_{hi}[R]$ and ${}^{g}_{k}[R]$ represent the rotation matrices representing the rotation relation between the hip joint frame and the global frame, and between the knee frame and the global frame. ${}^{g}_{hi}\{Q\}$ and ${}^{hi}_{k}\{Q\}$ are the displacement vectors representing the hip joint frame expressed in global frame, and the knee frame expressed in the hip joint frame.

In whole gait cycle, ankle positions can be expressed in vector (3.10) from equations (3.2), (3.3), (3.4) and (3.7), knee positions in vector (3.11) from equations (3.5) and (3.8), and hip joint positions in vector (3.12) by equations (3.6) and (3.9).

$$ {}^{g}\{P\}_{ank} = \{ {}^{g}\{P\}_{ank-wa}, {}^{g}\{P\}_{ank-sls}, {}^{g}\{P\}_{ank-pw}, {}^{g}\{P\}_{ank-sw} \} \tag{3.10} $$

$$ {}^{g}\{P\}_{kne} = \{ {}^{g}\{P\}_{kne-st}, {}^{g}\{P\}_{kne-sw} \} \tag{3.11} $$

$$ {}^{g}\{P\}_{hip} = \{ {}^{g}\{P\}_{hip-st}, {}^{g}\{P\}_{hip-sw} \} \tag{3.12} $$

${}^{g}\{P\}_{ank}$, ${}^{g}\{P\}_{kne}$ and ${}^{g}\{P\}_{hip}$ are the position vectors of the ankle, knee and hip joints respectively in the global frame.

3.4 Conclusions

Usually, the motion sensor consisting gyroscope, accelerometer or magnetometer are applied to measure movement of lower limb. When the inertial sensors consisting of accelerometers and gyroscopes are used to estimate joint position, the complicated algorithm has to be applied to overcome the drift errors caused by integration of accelerometers and gyroscopes. In our study, a simpler motion system only consisting three gyroscopes was applied for estimation of the joint positions based on gait characteristics. The key of the method is how to confirm the heel point touching on the floor in every strike. Therefore, the identification of different periods in stance phase was developed to resolve the problem. Our experiments showed the errors about the touching point in every stride are negligible. The substantive experiments demonstrated the method to estimate joint position is reliable, and the yielded results have high consistent with the results obtained by using the optical camera system.

References

(1) Ruth E. Mayagoitia, Anand V. Nene and Peter H. Veltink, Accelerometer and rate gyroscope measurement of kinematics: an inexpensive alternative to optical motion analysis systems, Journal of Biomechanics, Vol. 35, No. 4, pp. 537-542, 2002.

(2) Karol J. O'Donovan, Roman Kamnik, Derek T. O'Keeffe, An inertial and magnetic sensor based technique for joint angle measurement, Journal of biomechanics, Vol. 40, No. 12, pp. 2604-2611, 2007.

(3) Roetenberg, D. Baten, C.T.M. Veltink, P.H. Xsens Technol., Enschede, Estimation body segment orientation by applying inertial and magnetic sensing near ferromagnetic materials, Neural Systems and Rehabilitation Engineering, Vol. 15, No. 3, pp. 469-471, 2007.

(4) H. Martin Schepers, H. F. J. M. Koopman, Peter H. Veltink, Ambulatory Assessment of ankle and foot dynamics, IEEE Transactions on Biomedical Engineering, Vol. 54, No. 5, pp. 895-902, 2007.

4 Joint Dynamics Analysis

The dynamics analysis of ankle, knee and hip joints is important for rehabilitation and clinical diagnosis. This chapter presents a kinetics analysis of ankle, knee and hip joints in the sagittal plane by using the sensor system on human normal level walking during whole gait phases. In order to estimate the joint kinetics, an inverse kinetics method based on the sensing signals and gait characteristics was developed. Meanwhile, in the validation experiments with 10 subjects, joint kinetics was calculated using data synchronously measured by the sensor system and a force plate & optical camera system. The root mean square (RMS) differences of the ankle, knee and hip joints moments between the two systems in a gait cycle were (2 ± 0.34) (mean $\pm$ standard deviation) Nm, (7.2 ± 1.34) Nm and (11.2 ± 1.3) Nm, being (5.4 ± 0.7)%, (6 ± 0.32)% and (6.1 ± 0.25)% of the maximal magnitude of ankle, knee and hip joints moments respectively. The RMS differences of the ankle, knee and hip joints powers between the two systems in a gait cycle were (4.2 ± 0.4) W, (5.7 ± 2.1) W and (5.7 ± 0.3) W, being (8.4 ± 0.4)%, (4.1 ± 0.5)% and (6.4 ± 0.4)% of the maximal magnitude of joint powers respectively. The experimental results demonstrate the feasibility and effectiveness of the joint kinetics analysis using the wearable sensor system for a daily application in gait analysis.

4.1 Introduction

Joint kinetics, specifically joint moment and power, had been as an important part of healthcare evaluation and clinical diagnosis of body movement abilities in daily activities[(1)]. Body movement, GRF and CoP are usually measured by a combination of force plate and optical camera system in a gait laboratory. However, with increasing applications of human motion analysis in the medical-related fields, the lab-restricted measurement system is not suitable for applications in everyday environments, especially for healthcare evaluation to the elder in homes and medical diagnosis for patients in rehabilitation sites. There is a need for a measurement system which can measure GRF, CoP and body movement conveniently in daily activities, such as a miniature sensor system which can be worn on the human body and does not restrict human movement, namely a wearable sensor system. Accordingly, the kinetics analysis techniques for fitting the wearable sensor system should be studied by means of the inverse method.

With regard to joint kinetics analysis, an ambulatory sensor system had been used to assess foot and ankle dynamics, but only the GRF factor was considered and body inertial parameters were neglected[(2)]. Up to the present time, few studies have mentioned a wearable sensor system, which can simultaneously get sufficient information including GRF, CoP and body movement data for ankle, knee and hip joints kinetics analysis, which can make a significant contribution to the understanding of human movement in everyday activities.

The first goal of this study is to develop an analysis method for ankle, knee and hip joints kinetics using an improved wearable sensor system. The GRF, CoP and body movement were measured by means of the wearable sensor system. Considering the sensor system features, a new method was applied to estimate the joint position and orientation, and an inverse kinetic method to calculate the joint kinetics. In our gait experiments, the wearable sensor system was validated by a standard reference of a force plate and optical camera system, and the calculated kinetics results based on the two systems were also compared for validation of the joint kinetics analysis using the wearable sensor system.

This chapter concentrates on kinetics analysis of ankle, knee and hip joints to extend the work by Tao Liu et al.[(3)]. The analysis method of joint kinetics and the validation experiments are presented in turn.

4.2 *Joint Moments*

Joint moment and power are useful to obtain a full biomechanical analysis of body movement in daily activities. For calculation purposes, all the vectors are expressed in global coordinates system. As shown in Fig. 4.1, an orthogonal right-handed coordinate system (${}^{g}X-{}^{g}Y-{}^{g}Z$) was defined as the global coordinates system, in which positive X is along the forward direction of gait, positive Z is directed upward and positive Y is perpendicular to the X and Z direction. The origin and orientation of this global coordinates system are renewed for each stride to coincide with the segment and sensor coordinates systems. The coordinates systems of heel (${}^{h}X-{}^{h}Z$), foot joint (${}^{f}X-{}^{f}Z$), ankle (${}^{a}X-{}^{a}Z$), knee (${}^{k}X-{}^{k}Z$) and hip joint (${}^{hi}X-{}^{hi}Z$) were also established, and their Y directions were decided by X and Z direction of themselves. The displaced heel coordinates systems (${}^{h}X'-{}^{h}Z'$) were also constructed in Fig. 1.

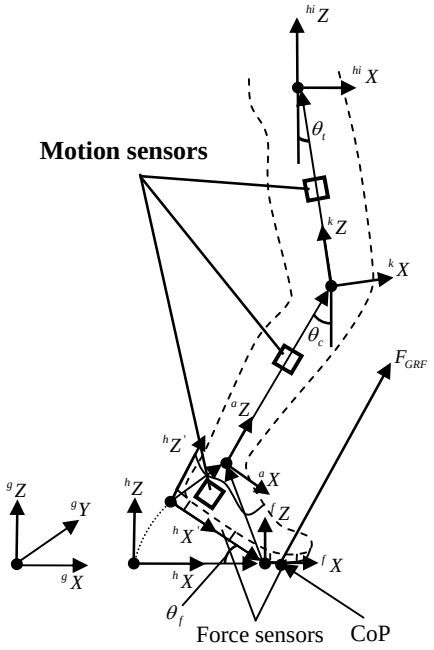

Fig. 4.1 Segmental model and coordinates systems of a lower extremity

Before calculation of joint moment and power, we have to combine the GRFs, ${}^{s1}F_{GRF}$ and ${}^{s2}F_{GRF}$, and the moments, ${}^{s1}M_{GRF}$ and ${}^{s2}M_{GRF}$, from the two sensors, and transfer all of the measurement results to the global coordinates by

$$ {}^{g}F_{GRF} = {}^{g}_{s1}[T]^{s1}F_{GRF} + {}^{g}_{s2}[T]^{s2}F_{GRF} \tag{4.1} $$

$$ {}^{g}M_{GRF} = {}^{g}_{s1}[T]^{s1}M_{GRF} + {}^{g}_{s2}[T]^{s2}M_{GRF} \tag{4.2} $$

where the GRF and the moment in the global frame are presented by ${}^{g}F_{GRF}$ and ${}^{g}M_{GRF}$. ${}^{g}_{s1}[T]$ and ${}^{g}_{s2}[T]^{s2}$ are the transformation matrix to represent conversion of coordinates systems from the two sensors' frames to the global frames respectively. The GRF and the moment are expressed by the vectors in (4.3), and the coordinates of CoP ${}^{g}x_{CoP}$ in the global frame is calculated by

$$ {}^{g}F_{GRF} = \begin{pmatrix} {}^{g}F_x \\ {}^{g}F_y \\ {}^{g}F_z \end{pmatrix} \qquad {}^{g}M_{GRF} = \begin{pmatrix} {}^{g}M_x \\ {}^{g}M_y \\ {}^{g}M_z \end{pmatrix} \qquad {}^{g}x_{CoP} = \begin{pmatrix} \dfrac{{}^{g}M_y}{{}^{g}F_z} \\ \dfrac{{}^{g}M_y}{{}^{g}F_z} \\ 0 \end{pmatrix} \tag{4.3} $$

By using the GRF as an input variable, equation is developed for computing the joint forces and moments by A.L. Hof[4]. This approach has certain advantages when the goal is to compute the joint forces and moments of the supporting leg. Consider the case of a moving subject who has one foot on a force plate in Fig. 4.2. The ground action is measured, and positions and accelerations of segments are determined. It is assumed that the foot does not exert a free moment on the force plate. The biomechanical model is a linked of n rigid bodies.

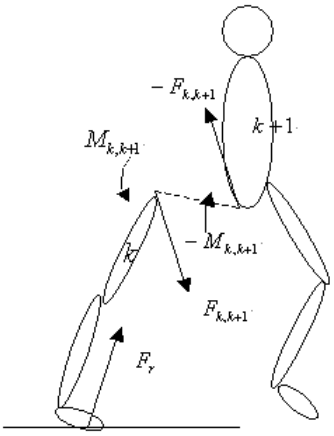

Fig. 4.2 Model of a subject walking over a force plate. The n-link chain is divided into two subsets, one containing the links from 1 to k and the other from k+1 to n.

In our case, the ankle, knee and hip joint moments in the global coordinates systems are calculated using the inverse dynamic method by

$$ {}^{g}M_{k,k+1} = -({}^{g}r_{CoP} - {}^{g}r_{k,k+1}) \times F_{GRF} - \sum_{i=1}^{k}\left[\left({}^{g}r_i - {}^{g}r_{k,k+1}\right) \times m_i \cdot g\right] $$
$$ + \sum_{i=1}^{k}\left[\left({}^{g}r_i - {}^{g}r_{k,k+1}\right) \times m_i \cdot a_i\right] + \sum_{i=1}^{k}\frac{d}{dt}\left(I_i \cdot \dot{\theta}_i\right) \qquad \text{, k=1, 2, 3,} \tag{4.4} $$

Where ${}^{g}M_{k,k+1}$ is the general term of the joint moment, and ${}^{g}M_{1,2}$, ${}^{g}M_{2,3}$ and ${}^{g}M_{3,4}$ from ${}^{g}M_{k,k+1}$ represent the ankle, knee and hip joint moments respectively. ${}^{g}r_{CoP}$ is the position vector from the origin of the global coordinates systems to the point of the CoP. ${}^{g}r_1$, ${}^{g}r_2$ and ${}^{g}r_3$ are the position vectors from the origin of the global coordinates systems to the center of mass (CoM) of ankle, knee and hip joint. ${}^{g}r_{1,2}$, ${}^{g}r_{2,3}$ and ${}^{g}r_{3,4}$ are the position vectors from the origin of the global coordinates systems to the center of ankle, knee and hip joint respectively. The mass of foot, calf and thigh are given by m_1, m_2 and m_3, the acceleration of foot, calf and thigh by a_1, a_2 and a_3, the moment of inertia of foot, calf and thigh by I_1, I_2 and I_3, and the angular velocity of foot, calf and thigh by $\dot{\theta}_1$, $\dot{\theta}_2$ and $\dot{\theta}_3$ respectively.

4.3 Joint Powers

The joint powers of ankle ${}^{g}P_{ank}$, knee ${}^{g}P_{kne}$ and hip joint ${}^{g}P_{hip}$ were calculated by the products of the ankle moment ${}^{g}M_{ank}$ and the ankle angular velocity ${}^{g}\dot{\theta}_{ank}$, the knee moment ${}^{g}M_{kne}$ and the knee angular velocity ${}^{g}\dot{\theta}_{kne}$, and the hip moment ${}^{g}M_{hip}$ and the hip angular velocity ${}^{g}\dot{\theta}_{hip}$. The ankle angular velocity is the differential value between the calf angular velocity ${}^{g}\dot{\theta}_c$ and the foot angular velocity ${}^{g}\dot{\theta}_f$. The knee angular velocity is the differential value between the thigh angular velocity ${}^{g}\dot{\theta}_t$ and the calf angular velocity ${}^{g}\dot{\theta}_c$. The hip joint angular velocity ${}^{g}\dot{\theta}_{hip}$ is equal to the thigh angular velocity ${}^{g}\dot{\theta}_t$, since the trunk angular velocity to hip joint is negligible for keeping body stability during level walking. The calculation equations are expressed by

$$ {}^{g}P_{ank} = {}^{g}M_{ank} \cdot {}^{g}\dot{\theta}_{ank} = {}^{g}M_{ank} \cdot ({}^{g}\dot{\theta}_c - {}^{g}\dot{\theta}_f) \tag{4.5} $$

$$ {}^{g}P_{kne} = {}^{g}M_{kne} \cdot {}^{g}\dot{\theta}_{kne} = {}^{g}M_{kne} \cdot ({}^{g}\dot{\theta}_t - {}^{g}\dot{\theta}_c) \tag{4.6} $$

$$ {}^{g}P_{hip} = {}^{g}M_{hip} \cdot {}^{g}\dot{\theta}_{hip} = {}^{g}M_{hip} \cdot {}^{g}\dot{\theta}_t \tag{4.7} $$

4.4 Validation Experiments

In this study, a series of experiments were accomplished for validation of the wearable sensor system. During the experiments, each of subjects wearing the sensor system was asked to normally walk over a force plate (EFP-S-2KNSA12, KYOWA, Japan); meanwhile, the movement information of the reflective markers on the lower extremity was captured by optical camera system (Hi-DCam, NAC Image Tech., Japan).

The sampling data from the gyroscope sensors, the force sensors in the instrumented shoe, and the force plate was acquired at same sample rate of 100 Hz. The force sensors in the instrumented shoe and the force plate were calibrated before each trial. Frame rate of Hi-DCam 4-camera systems was 100 Hz, and shutter speed was 1000 Hz. Calibration value of 3-D residuals before measurement by the camera systems was (0.5485 ± 0.2316) (mean $\pm$ standard deviation) mm, and ward length was (500.01 ± 0.86) mm. The possible gaps of the Hi-DCam data were dealt with by Join Cubic. The synchronization of the motion sensor system and Hi-DCam was done by maximizing the correlation of the angular velocities of the lower limb between the two systems.

10 healthy subjects (8 males and 2 females) as volunteers cooperated with us in the experiments. Ages of the subjects are (28.1 ± 1.99) (mean $\pm$ standard deviation), heights (1.692 ± 0.0424) m, and weights (66.26 ± 9.179) kg. Segmental inertial parameters of the lower extremities about the subjects were estimated by the empirical regression method[(5)]. The definition of thigh is from greater trochanteric head to center of the knee joint, calf from center of the knee joint to center of the ankle joint, foot from acropodion to heel. The length of thigh about the subjects is (0.4165 ± 0.0224) m (mean $\pm$ standard deviation), shank (0.3715 ± 0.03) m, and foot (0.2453 ± 0.008) m.

The masses of foot, calf and thigh about the subjects are (0.7355 ± 0.0635) kg, (3.1043 ± 0.3902) kg and 7.6924 ± 0.8436 (Error: male $2.1 \pm 1.3\%$, female $1.9 \pm 1.4\%$). The ratio of the center of gravity was calculated as the mean value of the percentage of the segment length measured from the proximal end. The ratios of the center of gravity of foot, calf and thigh are 59.5%, 40.6% and 0.475% for male, 59.4%, 41% and 45.8% for female. The moments of inertia of foot, calf and thigh are ($0.00037732 \pm 0.00000365$) kgm^2, (0.0302 ± 0.0101) kgm^2 and (0.0973 ± 0.0139) kgm^2.

4.5 Results and Discussions

The force plate and optical camera system was used as a reference to validate the results by the wearable sensor system, including GRF and CoP, segmental angular displacement, and the calculation results of the joint moment and power. The root mean square (RMS) difference as a

statistic indexes was used to compare the closeness in amplitude of the results between the two systems.

The comparing results of the joint moments of the ankle, knee and hip in the sagittal plane between the two systems are shown in Fig. 4.3(a), (b) and (c) respectively. The RMS difference of the ankle moments calculated by using the two systems is (2 ± 0.34) Nm, being (5.4 ± 0.7) % of the maximal magnitude of the ankle moments during a whole gait cycle. The RMS difference of the knee moments calculated by using the two systems is (7.2 ± 1.34) Nm, being (6 ± 0.32) % of the maximal magnitude of the knee moments. The RMS difference of the hip moments calculated by using the two systems is (11.2 ± 1.3) Nm, being (6.1 ± 0.25) % of the maximal magnitude of the hip joint moments.

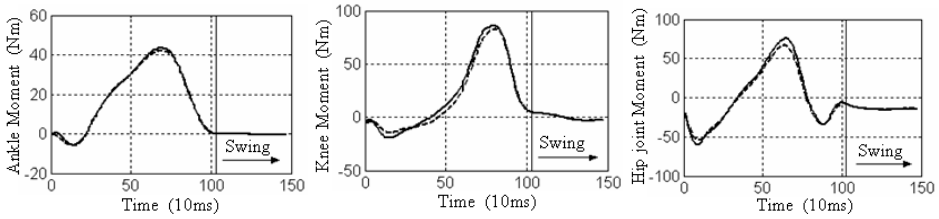

(a) (b) (c)

Fig. 4.3. Joint moments estimated by wearable sensor systems (solid line), and force plate & Hi-DCam camera systems (dashed line). Ankle plantarflexor, knee extensor, and hip flexor are positive, and ankle dorsiflexion, knee flexor, and hip extensor are negative. (a) Ankle moments. (b) Knee moments. (c) Hip joint moments.

The estimation of the joint powers of the ankle, knee and hip using wearable sensor systems and force plate & Hi-DCam camera systems were also implemented for a full understanding human waling kinetics. The comparison of the ankle, knee and hip joint power between the results using the two methods is shown in Fig. 4.4(a), (b) and (c) respectively. The RMS difference of the ankle power calculated by using the two systems is (4.2 ± 0.4) W, being (8.4 ± 0.4)% of the maximal magnitude of the ankle powers during a whole gait cycle. The RMS difference of the knee powers calculated by using the two systems is (5.7 ± 2.1) W, being (4.1 ± 0.5)% of the maximal magnitude of the knee powers. The RMS difference of the hip joint powers calculated by using the two systems is (5.7 ± 0.3) W, being (6.4 ± 0.4)% of the maximal magnitude of the hip joint powers.

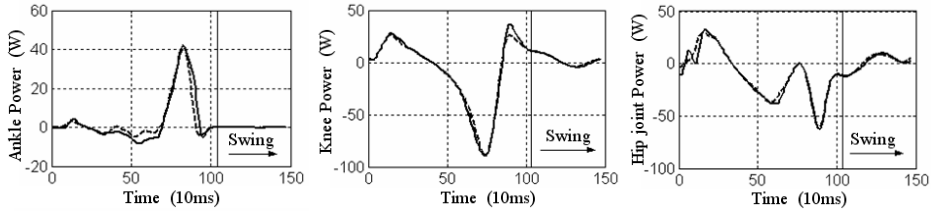

Fig. 6. Joint powers estimated by wearable sensor systems (solid line), and force plate & Hi-DCam camera systems (dashed line). (a) Ankle powers. (b) Knee powers. (c) Hip joint powers.

4.6 Conclusions

The kinetics analysis of ankle, knee and hip joints using a wearable sensor system is an important tendency. Firstly, relatively to a force plate and optical camera system, the wearable characteristics show the wearable sensor system has good prospects for applications on the human motion analysis in everyday activities. On the other hand, joint kinetics data have more contributions to the understanding of the cause of certain gait abnormalities and the motion mechanism of human walking, which are not provided by the other measurements, such as joint kinematics, temporal and stride parameters and electromyography. Therefore, the improved wearable sensor system was validated for the application feasibilities by our research. The GRF, CoP and body movement were measured by the wearable sensor system, and the data were used to estimate joint kinetics results by means of an inverse method for fitting the wearable sensor system. In the validation experiments, the analysis of the RMS difference between the two systems was implemented, including the RMS differences of X, Y and Z components of GRF, segmental angular displacements, and joint moments and joint powers. The results of the RMS differences demonstrated the measurement results and the kinetics results have high consistence between the wearable sensor system and the force plate & optical camera system.

In the calculation of joint moment and power, an inverse dynamics method was applied based on the use of GRF as a main input factor; meanwhile, other factors affected on joint kinetics result were also taken into account. The calculated joint moments consisted of four parts, moments of the GRF, moments of the weights of the segments, moments of the effective forces acting at the center of moment (CoM) of the segments, and moments due to segments' moment of inertia. However, when the empirical regression equations and the direct measurement method are used to estimate the weights of the segments, the position of CoM of the segments, and the moment of inertia of the segments, the errors indispensably occured[5]. Our preliminary study[6] about the wearable sensor system demonstrated that the joint moments are mainly caused by the

GRF, and the contributions to joint moments by other factors are negligible. The above conclusion is also supported by the research in the barefoot condition[7]. The conclusion suggest that the joint moments are caused by the inertial parameters of body segments can be neglected for convenient application of kinetics analysis in daily activities. On the other hand, the conclusion indicates the RMS differences about the joint moments and the joint powers in our results are mainly caused by the GRF. If we eliminate of the measurement errors of the GRF measured by the force plate, obviously, the measurement errors of the GRF from the wearable sensor are the main influencing factors on the RMS differences of the joint moments and the joint powers.

In the study, a wearable sensor system combining a force sensor and motion sensor was used to measure GRF, CoP and collect body movement information. A new kinematics analysis method for fitting the wearable sensor system was developed based on normal gait cycle principles. The complete data of kinematics and kinetics of ankle, knee and hip joint in the sagittal plane were obtained using the inverse kinetics method. In the experimental study, RMS differences with a force plate and optical camera system as a reference testified to the wearable sensor system's accuracy. The experimental study suggested that the wearable sensor system is feasible for joint kinetics analysis during normal gait, even though the system is a footwear and leg-attached equipment. Joint kinetics analysis for a normal walking by the healthy subject was fulfilled by the wearable sensor system. In the next step, we will use the system to estimate muscle force from joint moment dependent on a static optimization method and a musculoskeletal model of lower limb, since muscle force provide further details about human physiological data during gait.

References

(1) Sylvia Ounpuu, Roy B. Davis, Peter A. Deluca, Joint kinetics: method, interpretation and treatment decision-making in children with cerebral palsy and myelomeningocele, Gait & Posture, Vol. 4, No. 1, pp. 62-78, 1996.

(2) H. Martin Schepers, H. F. J. M. Koopman, Peter H. Veltink, Ambulatory Assessment of ankle and foot dynamics, IEEE Transactions on Biomedical Engineering, Vol. 54, No. 5, pp. 895-902, 2007.

(3) Tao Liu, Yoshio Inoue, Kyoko Shibata, Measurement of human lower limb orientations and reaction forces using wearable sensor systems, IEEE/ASME International Conference on Advanced Intelligent Mechotronics, Zurich, Switzerland, pp. 1-6, 2007.

(4) At L. Hof, An explicit expression for the moment in multibody systems, Journal of

Biomechanics, Vol. 25, No. 10, pp: 1209-1211, 1992

(5) M. Ae, H. Tang, T. Yokoi, Body segment parameters of Japanese adults, Journal of the Society of Biomechanisms, Vol. 11, pp. 23-33, 1992.

(6) Rencheng Zheng, Tao Liu, Yoshio Inoue, Kyoko Shibata, Calculation of joint moment using wearable sensor systems, 3rd Asian Pacific Conference on Biomechanics, Tokyo, Japan, pp.192, 2007.

(7) Roy B. Davis, Sylvia, Peter A. DeLuca, Joint moments: evaluation of ground reaction, inertial and segmental weight effects, Gait & Posture, Vol. 2, No. 1, pp. 58, 1994.

5 *Musculotendon Kinematics Analysis*

The main problem of musculotendon kinematics analysis is how to calculate dynamic musculotendon parameters. Musculotendon length and moment arm as dynamic musculotendon parameters during gait are the foundation of biomechanical analysis of human musculoskeletal system. The purpose of this study was to estimate individual dynamic musculotendon length and moment arm of lower limb in the sagittal plane during gait by means of a wearable sensor system. The wearable sensor system for body motion analysis was used to measure kinematical data for lower limbs during gait instead of an optical camera system.

Moreover, a series of regression equations obtained by inputting skeletal morphological parameters of lower limb was structured to calculate musculotendon origin-insertion coordinates in musculoskeletal coordinates system. The anthropometric method of measuring skeletal morphological parameters of lower limb was designed to represent individual bony features, which method can be conveniently operated on subject's body in vivo. By integrating the kinematical data and the origin-insertion coordinates, an algorithm was developed to calculate dynamic musculotendon parameters. This algorithm is applied to calculate the dynamic parameters of simple articular musculotendons and biarticular musculotendons. Moreover, the effects of the moving patella on the dynamic musculotendon parameters are also discussed in detail.

In an experimental and computational study of 10 subjects, data of the dynamic musculotendon parameters were collected in the sagittal plane during normal walking. Data collected were typical dynamic musculotendon parameters of lower limb, including musculotendons of Soleus (SO), Tibilis Anterior (TA), Biceps Femoris Caput Breve (BS), Glusteus (GU), Vastus (VS), Iliopsoas (IL), Gastrocnemius (GA), Rectus Femoris (RF) and Hamstring (HA). The results suggest that the method used in our study is feasible for estimating personalized dynamic musculotendon parameters in human daily activities.

5.1 Introduction

Dynamic musculotendon parameters, specifically dynamic musculotendon length and moment arm, reflect physiological condition of body movement. The musculotendon length is

physiological variable when musculotendon fibers lengthening and contracting during body movements. The musculotendon moment arm length, defined as the perpendicular distance from the rotation center of joint to the muscle force action line, transforms the linear movement of musculotendon into joint angular displacement. Both of the dynamic musculotendon parameters are vital to understand muscle functions and estimate muscle force in vivo[1, 2], and the parameters are eventually applied on the clinical diagnosis for patients [3].

Generally, non-invasive estimation of dynamic musculotendon length and moment arm during gait is dependent on the use of musculoskeletal model of lower limb. Through determination of the muscle force action line and coordinates of origin-insertion and via point, and rescaling the coordinates to measurable external landmarks, musculotendon parameters can be estimated based on anatomical musculoskeletal models[4, 5]. Length and moment arm of human leg muscles as a function of knee and hip-joint angles[6] and in vivo moment arm lengths for hip extensor muscle at different angles of hip flexion[7] were studied respectively. But in above early studies, the calculation accuracy of the musculotendon parameters was mainly limited by the lack of the intact musculoskeletal anatomical data. A prior computer program[8] calculate musculotendons kinematics and moment arm of six muscles of lower extremity for subject performing movements in the sagittal plane. Since the data was normalized by only three cadaver specimens and inputted the program few subject's anthropometric values, it is possible that a given individual have values markedly different than the results by the computer program. Following this step, musculoskeletal modeling software of AnyBody[9], SIMM[10] and OpenSim[11] are successively developed for musculoskeletal motion simulation, even for dynamics simulation based on musculoskeletal anatomical models. But we should discuss two important issues again. One issue addressed is how to find an appropriate anthropometric scaling factor for the musculoskeletal parameters normalization. It is often assumed that the musculotendon parameters could be normalized to body segment lengths or limb circumferences, but actual experimental data contract this notion. Few researches use skeletal morphological parameters to estimate origin-insertion coordinate to manifest individual musculoskeletal features. Another is that intact musculoskeletal anatomical data should be used to appropriate human group. Whole body muscles origin-insertion coordinates[12] and intact morphological musculoskeletal parameters of lower limb[13] have be provided based on the cadavers studies. Up to now, the most of existing musculoskeletal data were measured by European and American. However, studies[14, 15] demonstrated the musculoskeletal structure of different human race existed remarkable discrepancies that means the most of the data are not suitable to analyze Asian musculoskeletal structure.

Recently, researchers begin to use magnetic resonance image (MRI) or ultrasound scanning (US) techniques to restructure the subject-specific musculoskeletal model of lower limb for estimating the moment arm length[16] and length-to-moment ratios[17]. Moreover, the personalized MRI-based musculoskeletal models were compared to rescaled generic models in the presence of increased femoral anteversion effects on hip moment arm lengths[18]. The further researching results suggested that the calculated musculotendon length and moment arm during gait differ substantially using MRI-based versus rescaled generic lower-limb musculoskeletal models[19]. However, study[20] concluded that the combination of MRI and graphics-based musculoskeletal modeling provides a more accurate means of estimating musculotendon and moment arms in vivo. Anyway, MRI and US yield time and cost consideration, and suffer a lot of the limitations by MRI or ultrasound scanning equipments. A newly attempt is to use a novel non-invasive protocol[21] to determine the personalized moment arms of knee and ankle muscles. This method is designed for superficial muscles only, and the validity of the results depends on the accuracy of the data recorded during motion analysis. The error is obvious, and difficult to be taken into account. Meanwhile, an optical camera system for motion analysis is expensive, space-consuming and need professional calibration knowledge, which is limited in gait laboratory and not suitable for efficient measurement of human motion in daily activities [22]. In our former research, a wearable sensor system[23] was successful used to assess joints kinematics and kinetics as an ambulatory motion analysis system, and was validated by an optical camera system. In this way, how to assess individual dynamic musculotendon parameters using the sensor system becomes to be an interesting topic.

This chapter concentrates on the estimation processes of the individual dynamic musculotendon parameters of lower limb during gait to extend our research projects. In the study, kinematics analysis of lower-limb joints by a wearable sensor system was simply introduced. Then, musculoskeletal model, regression equations of musculotendon origin-insertion coordinates, and anthropometric methods of measuring morphological parameters were demonstrated on sequence. Moreover, a calculation algorithm for the dynamic parameters is described on the examples of simple articular and biarticular musculotendons. At last, results of the joint angular displacements, the dynamic musculotendon lengths and the moment arms during gait were presented and discussed.

5.2 Collection of Joint Kinematical Data

For body motion analysis, a wearable sensor system[0] was developed by integrating of a motion sensor system, an instrumented shoe and a data logger. Three motion sensor units are worn on the

part of the foot, calf and thigh respectively. Each of the units consists of a biaxial gyroscope. Two force sensors are inserted into a modified common shoe as a prototype of the instrumented shoe. A 6-axial force sensor is under the heel part of the shoe, and a smart triaxial force sensor under the forefoot part of the shoe. The data logger was strapped around the waist part. A segmental model of human lower limb wore the sensor system during gait is shown in Fig.5.1. θ_f , θ_c and θ_t are the segmental angular displacements of foot, calf and thigh respectively. Joint angles of ankle, knee angle and hip were defined in the figure, and joint angular displacements of ankle (θ_a), knee (θ_k) and hip (θ_h) can be calculated by

$$\theta_a = 90 + \theta_f - \theta_c \tag{5.1}$$

$$\theta_k = 180 + \theta_t - \theta_c \tag{5.2}$$

$$\theta_h = 180 + \theta_t \tag{5.3}$$

In equation (5.3), the assumption is that the contribution of the trunk angular displacements to the angle of hip joint is negligible, because the trunk part, especially pelvic part, is relative stable for keeping body balance during normal walking.

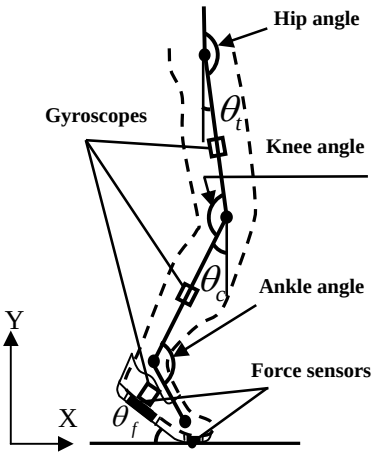

Fig.5.1 Model of lower

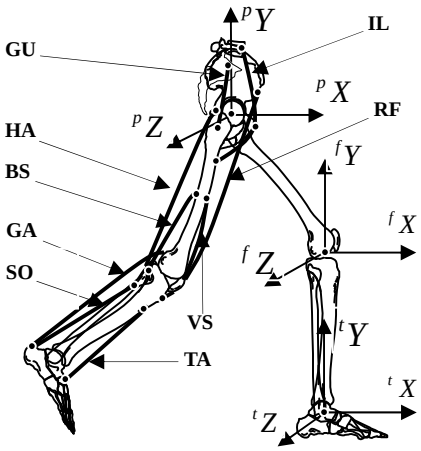

Fig.5.2 Musculoskeletal model

5.3 Musculoskeletal model Study

Musculoskelel Model. The musculoskeletal model of lower limb is built as four rigid-body segments: pelvis, femur, tibia and foot. We assumed that the segments are articulated by frictionless and single degree-of-freedom joints at the hip, knee and ankle. An orthogonal

coordinates system of the musculoskeletal model is constructed by pelvic, femoral and tibial coordinates. The coordinates' origins are assumed at the ideal rotation joint centres of hip, knee and ankle respectively. The origins and directions of the coordinates are shown in the left limb of Fig. 5.2. Nine musculotendons, including Soleus (SO), Tibilis Anterior (TA), Biceps Femoris Caput Breve (BS), Glusteus Maximus (GU), Vastus (VS), Iliopsoas (IL), Gastrocnemius (GA) of Medial head, Rectus Femoris (RF) and Hamstring (HA), are approximately assumed as a straight force action line from origins to insertions. The musculotendons are around the joints in the sagittal plane during normal walking as is shown in the right limb of Fig. 5.2.

Origin-insertion regression equations of musculotendon. In our research, data of 3-dimentional coordinates of musculotendon origin-insertion and skeletal morphological parameters come from the anatomical study of eight fresh cadavers of Asian, namely 16 specimens of lower limbs [24]. Height of cadavers is 1.7525 ± 0.0836 m (Mean $\pm$ S. D.), and age is 38.75 ± 10.61 year-old. Data include 38 musculotendons of lower limb. In order to apply data of the cadavers' studies on living subjects, we have to build regression equations to in vivo estimate musculotendon origin-insertion coordinates of lower limb. Firstly, skeletal morphological parameters are chosen as independent variables, and musculotendon origin-insertion coordinates were chosen as dependent variables respectively. Then, the regression equations were built between the skeletal morphological parameters and the musculotendon origin-insertion coordinates through progressive statistic analysis. At last, for validation of application reliability and effectivity of regression equations on living body, statistic error analysis of the regression equations were completed.

TA, SO, BS, GU, IL and VS are simple articular musculotendon. Regression equations of origin-insertion coordinates of TA are presented by skeletal morphological parameters in Eqs.(5.4)and(5.5) as a representative of simple articular musculotendons. $O(x, y, z)$ and $I(x, y, z)$ are origin and insertion coordinates in the reference frame. TA origin coordinates is described in tibial reference frame by

$$\begin{aligned} O_x &= -3.63 + 0.17 \times C4, && (r = 0.693) \\ O_y &= 23.49 - 2.02 \times C8 + 2.66 \times C3, && (r = 0.978) \\ O_z &= 6.37 - 0.14 \times C5, && (r = 0.695) \end{aligned} \tag{5.4}$$

TA insertion coordinates is described in tibial reference frame by

$$
\begin{aligned}
I_x &= 9.04 - 1.05 \times D2 + 0.78 \times D4, \qquad (r = 0.98) \\
I_y &= -14.34 + 0.54 \times D4 + 1.07 \times D5, \qquad (r = 0.738) \\
I_z &= -2.47 + 1.13 \times D2 - 0.9 \times D4, \qquad (r = 0.928)
\end{aligned} \tag{5.5}
$$

where, C3 is the width of malleolus (intervals between lateral malleolus to medial malleolus), C4 is the intervals from the head of fibula to medial malleolus, C5 is the intervals between medial condyle and medial malleolus, D2 is the intervals between tuber calcaneus and inner surface of lateral malleolus, D4 is the foot width (intervals between the middle point of first phalanx distal and the middle point of fifth phalanx distal), D5 is the malleolus width (intervals between lateral malleolus and medial malleolus). 'r' is correlation coefficient to present the closeness between the results of origin-insertion coordinates of musculotendons, which calculated by the regression equations, and the results, which measured by the specimens in the cadaver study.

GA, RF and HA are biarticular musculotendon, which morphologies and functions are different with the simple articular ones. GA includes lateral head and medial head, and we chose origin coordinate of medial head of GA as computational coordinates. The insertion coordinates of lateral head and medial head of GA are same with TA ones. Origin coordinate of medial head of GA is described in femoral reference frame by

$$
\begin{aligned}
O_x &= 4.51 - 1.05 \times C2 + 0.55 \times C8, \qquad (r = 0.913) \\
O_y &= -12.23 - 3.97 \times C1 + 0.55 \times C2, \qquad (r = 0.988) \\
O_z &= -1.67 - 0.68 \times C2 + 1.24 \times C3, \qquad (r = 0.809)
\end{aligned} \tag{5.6}
$$

where, C1 is the condyle intervals (transverse breadth of lateral condyle), C2 is the vertical breadth of lateral condyle and medial condyle, C8 is the tibial tuberosity intervals of medical condyle. The above skeletal morphological parameters are measured using anthropometric method through confirming body surficial bony landmarks.

Skeletal Morphological Parameters. Musculotendon is located on skeletal surfaces and its functions are substantially dependent on specific skeletal morphological features. Skeletal morphological parameters selected to estimate musculotendon origin-insertion coordinate should adequately represent morphological features of the skeleton, and anthropometric operations for the parameters should be simple and easy. In each skeletal coordinates, eight skeletal morphological parameters are chosen to estimate musculotendon origin-insertion coordinates. The regression analysis was computed between the morphological parameters as independent variable and musculotendon origin-insertion coordinate as dependent variable. Each dependent

variable is expressed by the most correlative independent variables of 1, 2 or 3 numbers. Morphological parameters of pelvic skeleton, femoral skeleton, tibial skeleton and foot skeleton are presented in Tables 5.1-4, respectively. The original value of skeletal morphological parameters is also given as a referential value, which data come from same data sample with the musculotendon origin-insertion coordinates.

Table 5.1 Pelvic morphological parameters (cm)

Item	A1	A2	A3	A4	A5	A6	A7	A8
Mean value	23.74	8.76	27.72	15.84	20.36	21.22	14.84	17.08
S.D.	± 0.82	± 0.49	± 0.49	± 0.49	± 0.53	± 0.52	± 0.46	± 0.96

In table 5.1, A1 is the intervals between the left anterior superior iliac spine and the right one, A2 is the intervals between the left posterior superior iliac spine and the right one, A3 is the intervals between the two iliac crest tuberosities, A4 is the intervals between anterior superior iliac spine and posterior superior iliac spine, A5 is the intervals between iliac crest tuberosity and coccyx apex, A6 is the height of pelvic pedestal (intervals between ischium tuberosity and the upper limb of iliac crest), A7 is the perpendicular distance from anterior superior iliac spine to ischium tuberosity (seating posture), A8 is the perpendicular distance from posterior superior iliac spine to ischium tuberosity (seating postrure).

Table 5.2 Femoral morphological parameters (cm)

Item	B1	B2	B3	B4	B5	B6	B7	B8
Mean value	4.93	7.54	7.50	41.47	41.13	42.09	8.93	8.93
S.D.	± 0.16	± 0.18	± 0.27	± 0.97	± 1.55	± 1.50	± 0.18	± 0.17

In table 5.2, B1 is the patella width, B2 is the intervals between the middle point of patella and lateral epicondyle, B3 is the intervals between the middle point of patella and medial epicondyle, B4 is the intervals between greater trochanter and the middle point of patella, B5 is the intervals of greater trochanter apex and lateral epicondyle, B6 is the intervals of greater trochanter apex and medial epicondyle, B7 is the intervals between medial epicondyle and lateral epicondyle, B8 is the vertical breadth of medial epicondyle and lateral epicondyle (Perpendicular distance from the frontal mid-point of patella to the link between the posterior border of medial epicondyle and the posterior border of lateral epicondyle).

Table 5.3 Tibial morphological parameters (cm)

Item	C1	C2	C3	C4	C5	C6	C7	C8
Mean value	8.23	8.79	6.84	34.56	38.47	32.75	6.85	9.37
S.D.	± 0.23	± 0.27	± 0.09	± 1.38	± 1.39	± 1.68	± 0.38	± 0.40

In table 5.3, C6 is the intervals between tibial tuberosity and malleolus (between the middle point of tibial tuberosity and the middle point of the link of lateral malleolus and medial malleolus), C7 is the tuberosity intervals of the head of fibula.

Table 5.4 Foot morphological parameters (cm)

Item	D1	D2	D3	D4	D5	D6	D7	D8
Mean value	7.81	7.63	17.99	8.53	6.84	14.11	14.54	2.11
S.D.	± 0.34	± 0.32	± 0.54	± 0.20	± 0.09	± 0.51	± 1.05	± 0.05

In table 5.4, D1 is the foot height (perpendicular distance from the inner surface of lateral malleolus to the sole plane), D3 is the foot length from the tuber calcaneus to middle point of first phalanx distal, D6 is the intervals between fifth metatarsals and lateral malleolus, D7 is the intervals between first metatarsals and medial malleolus, D8 is the ratio between foot length and foot width.

The above skeletal morphological parameters are measured by tactual bony landmarks. Even though the accuracy of the origin-insertion coordinates are affected by anthropometric operation errors, however, it is necessary to use anthropometric method to confirm inner physical structures and bony landmarks in medical engineering. For improvement of anthropometric accuracy, specific operations to comprehend bony landmarks have been normalized. The contents including body physical structures, surficial bony landmarks, and anthropometric postures are demonstrated by Figs.5.3-6.

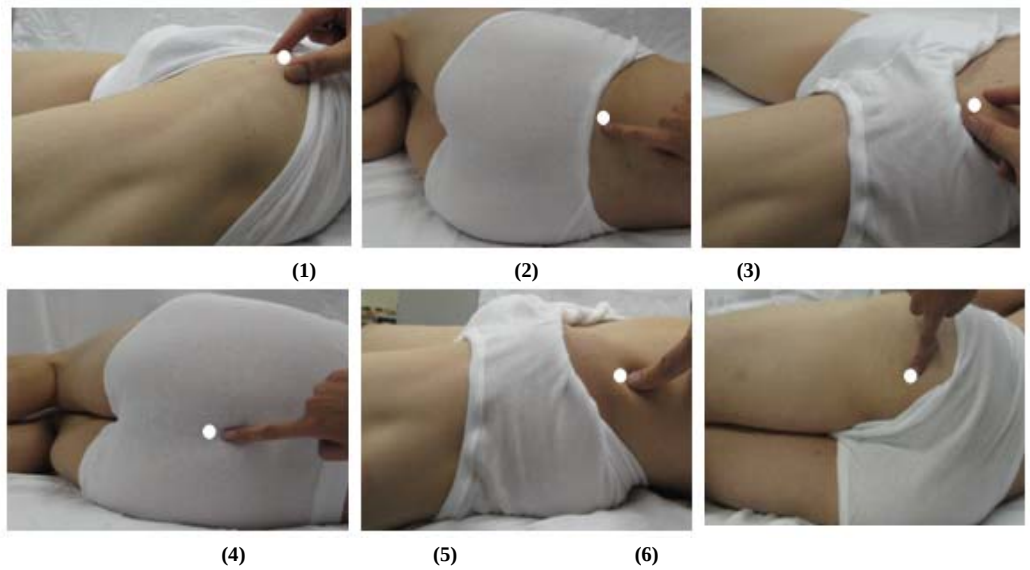

Fig.5.3 Bony landmarks of pelvic skeleton. (1) Anterior superior iliac spine. (2) Posterior superior iliac spine. (3) Iliac crest tuberosities. (4) Coccyx apex, (5) Upper limb of iliac crest. (6) Ischium tuberosity.

(1) (2) (3)

(4) (5) (6)

Fig.5.4 Bony landmarks of femoral skeleton. (1) Upper point of patella. (2) Lower point of patella. (3) Middle point of patella. (4) Lateral epicondyle. (5) Medial epicondyle. (6) Greater trochanter apex.

(1) (2) (3)

Fig.5.5 Bony landmarks of tibial skeleton. (1) Tibial tuberosity. (2) Fibula capitulun. (3) Tibial capitulum.

(1) (2)

Fig.5.6 Bony landmarks of foot skeleton. (1) First and fifth metatarsals capitulum (2) Tuber calcaneus, lateral and medial malleolus.

5.4 Musculotendon lengths and moment arms

Simple Articular Musculotendon. SO is as a representative of simple articular musculotendon, which force action line, origin-insertion and moment arm are shown in Fig.5.7. Dynamic lengths and moment arms of SO are calculated by Eqs.(5.7)～(14).

$$l_1 = \sqrt{(O_x - A_x)^2 + (O_y - A_y)^2} \tag{5.7}$$

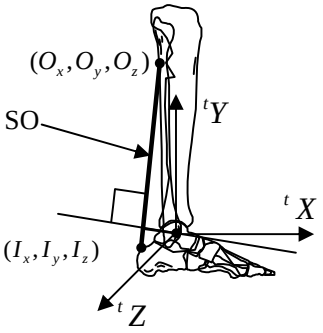

Fig.5.7 SO diagram in tibial coordinates.

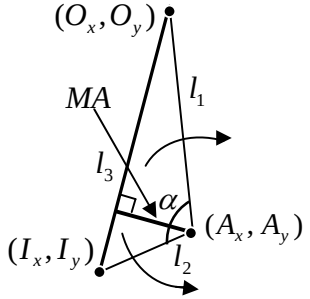

Fig.5.8 SO dynamic parameters

$$l_2 = \sqrt{(I_x - A_x)^2 + (I_y - A_y)^2} \tag{5.8}$$

$$l_3 = \sqrt{(O_x - I_x)^2 + (O_y - I_y)^2} \tag{5.9}$$

$$\alpha = \cos^{-1}\left(\frac{l_1^{\,2} + l_2^{\,2} - l_3^{\,2}}{2 \cdot l_1 \cdot l_2}\right) \tag{5.10}$$

$$\alpha' = \alpha + \theta_f - \theta_c \tag{5.11}$$

$$l_3' = \sqrt{l_1^{\,2} + l_2^{\,2} - 2 \cdot l_1 \cdot l_2 \cdot \cos(\alpha')} \tag{5.12}$$

$$\phi' = \cos^{-1}\left(\frac{l_1^{\,2} + (l_3')^2 - l_2^{\,2}}{2 \cdot l_1 \cdot l_3'}\right) \tag{5.13}$$

$$MA = l_1 \cdot \sin(\phi') \tag{5.14}$$

As is shown in Fig.5.8, *MA* is the dynamic moment arm of SO to ankle. l_3' is the dynamic length of SO. l_1 and l_2 are the lengths from the SO origin to the center of ankle and from the TA insert to the center of ankle respectively. α is the static included angle in the standard standing pose, and α' the dynamic included angle between the straight line l_1 and l_2. ϕ' is the dynamic included angle between the straight line l_1 and the dynamic lengths l_3' during gait.

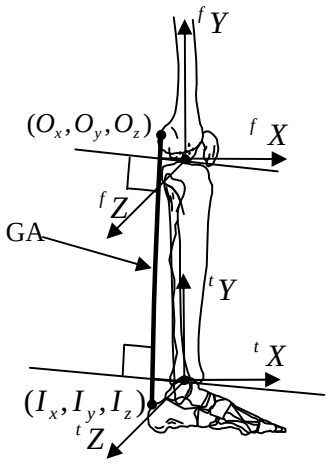

Fig.5.9 GA diagram in tibial-femoral coordinates

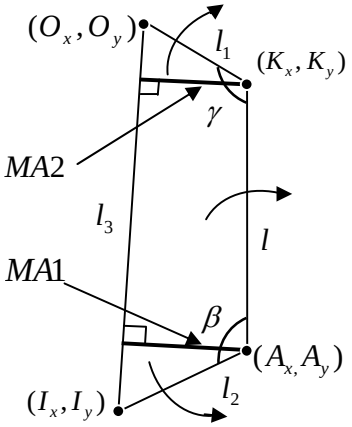

Fig.5.10 GA dynamic parameters

Biarticular Musculotendon. GA is as a representative of biarticular musculotendon, which force action line, origin-insertion and moment arm are shown in Fig.5.9. Dynamic lengths and moment arms of GA during gait are calculated by Eqs.(5.15)-(5.25). The biarticular musculotendon crosses two joints and produces the inverse joint moment between the two joints when the muscle is on contraction, and affects on the two joints mainly through the two different dynamic moment arms.

$$l_1 = \sqrt{(O_x - K_x)^2 + (O_y - K_y)^2} \tag{5.15}$$

$$l_2 = \sqrt{(I_x - A_x)^2 + (I_y - A_y)^2} \tag{5.16}$$

$$l_3 = \sqrt{(O_x - I_x)^2 + (O_y - I_y)^2} \tag{5.17}$$

$$l_4 = \sqrt{(I_x - K_x)^2 + (I_y - K_y)^2} \tag{5.18}$$

$$l_5 = \sqrt{(O_x - A_x)^2 + (O_y - A_y)^2} \tag{5.19}$$

$$\beta = \cos^{-1}\left(\frac{l^2 + l_2^2 - l_4^2}{2 \cdot l \cdot l_2}\right) \tag{5.20}$$

$$\gamma = \cos^{-1}\left(\frac{l^2 + l_1^{\,2} - l_5^{\,2}}{2 \cdot l \cdot l_1}\right) \tag{5.21}$$

$$\beta' = \beta + \theta_f - \theta_c \tag{5.22}$$

$$\gamma' = \gamma + \theta_t - \theta_c \tag{5.23}$$

$$MA1 = l_2 \cdot \sin(\beta') \tag{5.24}$$

$$MA2 = l_1 \cdot \sin(\gamma') \tag{5.25}$$

As is shown in Fig.5.10 and in the equations (5.13)-(5.20), $MA1$ and $MA2$ are GA dynamics moment arm lengths, β' and γ' are dynamic included angle during joint motion. Other parameters can be referred to the front Section.

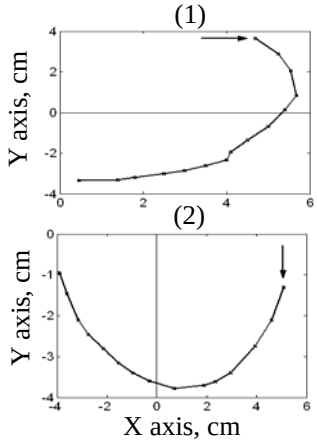

Fig.5.11 Moving patella trace curve following knee rotation. (1) Upper limbus point of patella. (2) Lower limbus point of patella.

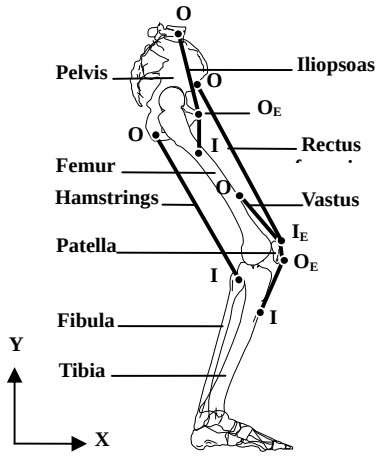

Fig.5.12 Force action line of HA, RF and VS. Origins (O), effective origins (O_E), insertions (I), and effective insertions (I_E) are indicated for HA, RF and VS.

Moving Patella Effects. Patella is the largest sesamoid of human body, and is wrapped in quadriceps tendon for raising quadriceps moment arm length to create better biomechanical condition during knee extension motion. The effect of the patella on moment arms and length of the quadriceps is also taken into account by modelling patella essentially as a frictionless moving pulley in the femoral reference frame. We got 15 trace points position with knee extension from 0

degree to 140 degree. As is shown in Fig.5.11, X-Y coordinates of patella point were drawn in femoral frame, and the arrows orientations are beginning point of knee rotation on 0 degree for upper and lower limbus point respectively. Both of upper and lower limbus points of patella don't move as a standard circle. The biggest differential values of the locus radius of the upper limbus point is 2.62 cm, being 43.67% of the maximal magnitude of the biggest trace radius, and the biggest differential values of the locus radius of the lower limbus point is 1.76 cm, being 33.46% of the maximal magnitude of the biggest trace radius.

If we use the distances from beginning point to original point as radius to describe the traces of patella limbus points following joint extension motion, the musculotendon lengths and moment arm lengths will produce more error relative to real activities of quadriceps. In our research, the irregular circle motion of the patella points was taken into account to calculate musculotendon length and moment arm. As is shown in Fig.5.12, origin of rectus femoris is on midpoint of anterior superior iliac spine, and insertion of rectus femoris is on midpoint of tibial tuberosity. Upper limbus point of patella as effective insertion of action line of musculotendon contraction is used to analyze moment arm of rectus femoris to hip joint motion, and lower limbus point of patella as effective origin of action line of musculotendon contraction is used to analyze moment arm of rectus femoris to knee joint motion. Accordingly, upper and lower limbus points of patella as medial sequential point for quadriceps, including vastus and rectus femoris, are used to analyze the musculotendon length. Length of each quadriceps is approximately described by three action lines (O-O_E-I_E-I), namely from origins to upper limbus point of patella, from upper limbus point of patella to lower limbus point of patella, and from lower limbus point of patella to insertions. Obviously, contrasting to hamstrings described by one action line (O-I) and Iliopsoas described by two action lines (O-O_E-I), quadriceps described by three action lines (O-O_E-I_E-I) more approximate to real activities of rectus femoris. We use origin and insertion coordinates to calculate musculotendon length and moment arm of SO, TA, BS, GU, VA, GA, and HA; origin, effective origin, and insertion to IL; origin, effective origin, effective insertion, and insertion to RF and VS.

5.5 Gait Experiments

Analysis processes of dynamic musculotendon parameters in our study can be seen in Fig. 5.13. 10 healthy subjects (8 males and 2 females) as volunteers cooperated with us for gait experiments. Their age is 28.1 ± 1.99 year-old (Mean $\pm$ S. D.), height 1.692 ± 0.0424 m, and weight 66.26 ± 9.179 kg. During gait experiments, each of the subjects wearing the sensor system was asked to normally walk on a force plate (EFP-S-2KNSA12, KYOWA); synchronously, the motion

information of the retro-reflective markers on the lower extremities of the subjects was captured by an optical camera system (Hi-DCam, NAC Image Tech.). The optical camera system is used as a reference to validate the wearable sensor system for measurement of segmental angular displacement.

Subsequently, the morphological parameters of the subjects were directly measured using anthropometric method. Anthropometric condition, measuring point and other anthropometric principles was obeyed by conferential materials[25, 26]. Simple anthropometer, slider calliper, spreading calliper, and measuring tape as main tools fulfilled the anthropometric task to confirm the skeletal morphological parameters of individual. For avoiding operation error, repetitive measurement process was repetitively executed for each subject. Then, the anthropometric data were inputted to the regression equations of musculutendon origin-insertion. At last, the data of kinematic analysis and musculotendons origin-insertion coordinates were inputted to the computer programming, and dynamic musculotendon parameters were calculated.

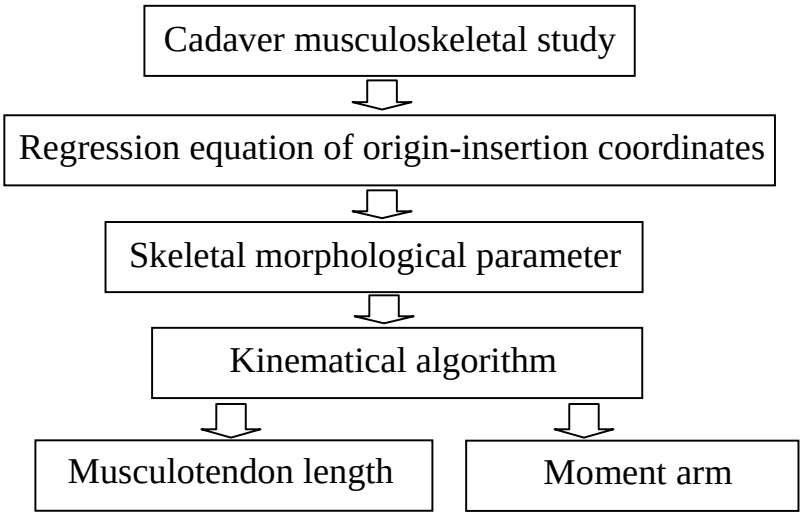

Fig. 5.13 Analysis processes of dynamic musculotendon parameters

5.6 Results and Discussions

Joint Angles. A representative result of segmental and joint angular displacements during one gait cycle is shown in Fig.5.14. The validation of the wearable sensor system was presented in our research[23].

The time of whole gait cycle is 147 seconds. Pre swing begins on the second of 70, when foot angular displacement is zero. Swing phase begins on the second of 102, when GRF signal is zero.

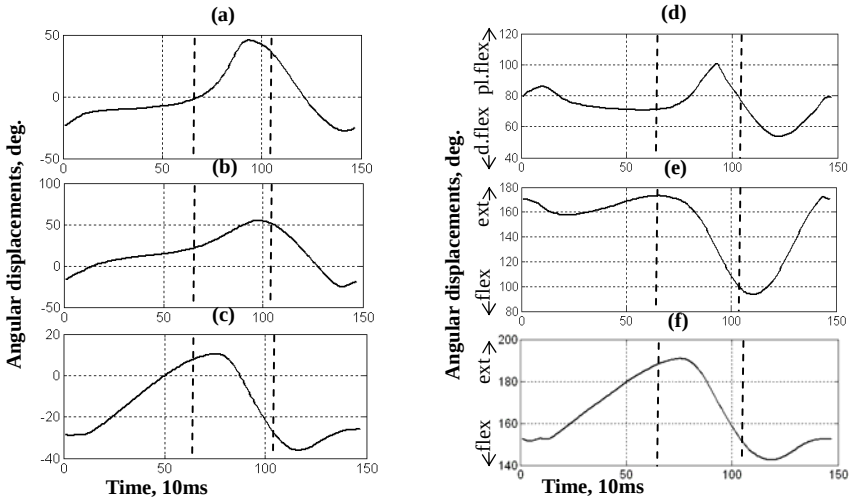

Fig.5.14 Segmental and joint angular displacements during one gait cycle. (a) Foot angular displacements. (b) Calf angular displacements. (c) Thigh angular displacements. (d) Ankle angular displacements. (e) Knee angular displacements. (f) Hip joint angular displacements. The first dashed vertical line means the beginning of pre swing phase, and the second dashed line is the beginning of swing phase.

In Fig. 5.14 (a)-(c), angular displacements of foot (θ_f), calf (θ_c) and thigh (θ_t) are presented respectively in one stride of gait. Please see Figure 1, θ_f is the included angle between the sole plane and the level ground in the sagittal plane (X-Y), θ_c is the included angle between the calf and the perpendicular line diverging from a common point – the center of the knee, and θ_t is the included angle between the thigh and the perpendicular line diverging from a common point – the center of the hip joint.

The directions of the angles of foot, calf and thigh are determined by Right-hand Grip Rule. The thumb's direction is orthogonal to the paper's plane (X-Y) and point to the reader. In detail, when the line of the thigh is in the left side of the perpendicular line, the angle of thigh is negative; on the contrary, the angle is positive. The angle of calf is defined as the thighs. When the sole plane incline to the level ground and the heel part of the foot is as a common point, the angle of the foot is negative; when the toe part of the foot is as a common point, the angle of the foot is positive.

The result of direction of hip extension in Fig. 5.14 (f) is validated by comparing to previous studies. I compared my results with the two references. One reference is Fig. 14-11 in book. The difference between my results and the results in the two references is only that the definition of joint angles is different. The definition in my paper is convenient to calculate the joint angles using the signals by the wearable sensor system. The angles of ankle, knee and hip

joints are defined as θ_a, θ_k and θ_h respectively in Fig.5.1. The definition is also convenient to calculate musculotendon parameters.

Musculotendon Lengths. A representative result of dynamic musculotendon lengths is shown corresponding to the joint angular displacements in Fig.5.16.

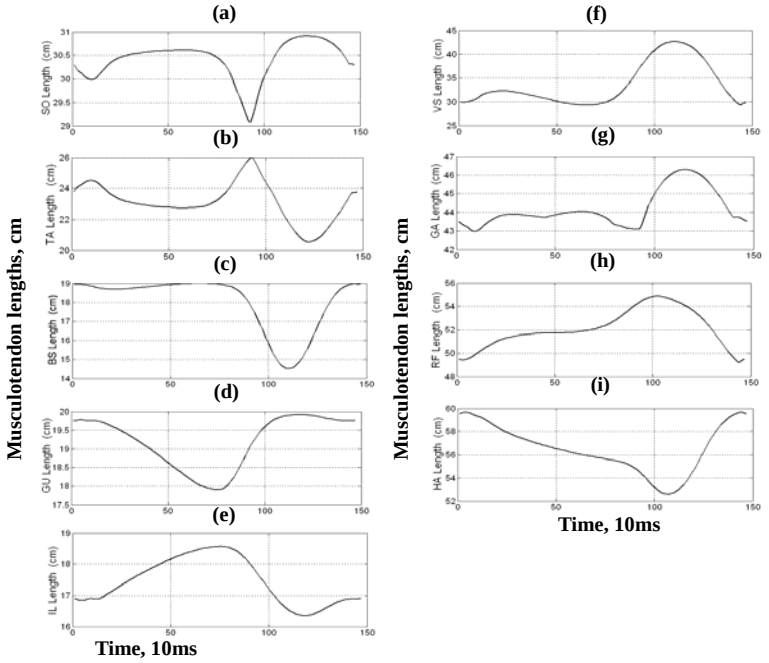

Fig.5.15 Musculotendon lengths of lower extremity during one normal walking cycle. (a) SO lengths. (b) TA lengths. (c) BS lengths. (d) GU lengths. (e) IL lengths. (f) VS lengths. (g) GA lengths. (h) RF lengths. (i) HA lengths.

Musculotendon length as a function of joint angle, the dynamic value during gait is also intensively affected by joint angular displacement. From the numerical analysis of the results of the dynamic musculotendon lengths, the numerical characters of the results are presented in Table 5.6. And the changing tendencies of the results can be distinctively observed in Fig.5.15.

Table 5.6 Numerical analysis of the dynamic musculotendon lengths

Name	Maximum length (cm)	Minimum length (cm)	Average (cm)	Maximal variation		Extreme point	
				Value (cm)	Percent to average (%)	Gait phase	Max. or Min.
SO	30.9146	29.0855	30.4107	1.8292	0.0601	Pre swing	Min.
TA	25.9765	20.5418	23.1378	5.4346	0.2349	Pre swing	Max.
BS	18.9843	14.5287	18.0140	4.4556	0.2473	Initial swing	Min.
GU	19.9186	17.9060	19.2029	2.0126	0.1048	Pre swing	Min.
IL	18.5673	16.3492	17.4493	2.2181	0.1271	Pre swing	Min.
VS	42.6806	29.3732	33.6788	13.3075	0.3951	Initial swing	Max.
GA	46.2875	42.9812	44.1957	3.3063	0.0748	Initial swing	Max.
RF	49.2171	54.8790	52.1105	5.6619	0.1087	Initial swing	Max.
HA	59.7016	52.6078	56.5138	7.0938	0.1255	Initial swing	Min.

Moment arms. A representative result of dynamic moment arms is shown corresponding to the joint angular displacements in Fig.5.16.

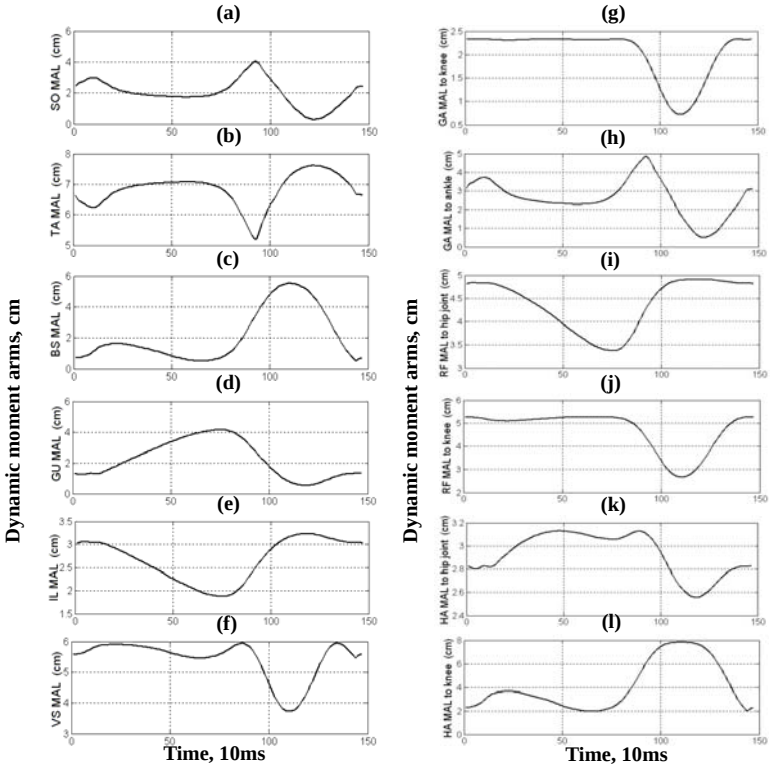

Fig.5.16 Dynamic moment arms in the sagittal plane during one gait cycle. (a) SO moment arms. (b) TA moment arms. (c) BS moment arms. (d) GU moment arms. (e) IL moment arms. (f) VS moment arms. (g) GA moment arms to knee. (h) GA moment arms to ankle. (i) RF moment arms to hip joint. (j) RF moment arms to knee. (k) HA moment arms to hip joint. (l) HA moment arms to knee.

Moment arm as a function of joint angle, the dynamic value during gait is intensively affected by joint angular displacement. From the numerical analysis of the dynamic moment arms

results, the numerical characters of the results are presented in Table 5. And the changing tendencies of the results can be distinctively observed in Fig.5.16.

Table 5 Numerical analysis of the dynamic musculotendon moment arms

Name	Maximum length (cm)	Minimum length (cm)	Average (cm)	Maximal variation		Extreme point	
				Value (cm)	Percent to average (%)	Gait phase	Max. or Min.
SO	4.0467	0.2863	2.0272	3.7604	1.8550	Pre Swing	Max.
TA	7.6118	5.2025	6.8248	2.4093	0.3530	Pre Swing	Min.
BS	5.5153	0.5115	2.1364	5.0038	2.3422	Initial Swing	Max.
GU	4.1461	0.5390	2.2380	3.6071	1.6118	Pre Swing	Min.
IL	3.2333	1.8784	2.6749	1.3549	0.5065	Initial Swing	Max.
VS	5.9438	3.7195	5.4238	2.2243	0.4101	Initial Swing	Min.
GA to knee	2.3332	0.7227	2.0286	1.6105	0.7939	Initial Swing	Min.
GA to ankle	4.8547	0.5079	2.6141	4.3468	1.6628	Pre Swing	Max.
RF to hip	4.9085	3.3765	4.3914	1.5320	0.3489	Pre Swing	Min.
RF to knee	5.2630	2.6794	4.6912	2.5835	0.5507	Initial Swing	Min.
HA to hip	3.1300	2.5563	2.9281	0.5737	0.1959	Initial Swing	Min.
HA to knee	7.8358	1.9643	4.1448	5.8715	1.4166	Initial Swing	Min.

5.7 Discussions and Conclusions

Estimation of individual dynamic musculotendon parameters is key problem to analyze subject's musculoskeletal motion in vivo. By integration of wearable sensor system and musculoskeletal model, whole practical processes to estimate individual dynamic musculotendon parameters were developed, and the method made it possible to further study personalized realistic musculoskeletal movements. The results testified the regression equations of muscle origin-insertion coordinate by inputting the morphological parameters of skeletal lower limb are accurate and serviceable. The whole processes of the method can be conveniently applied on musculotendon motion analysis in human daily activities.

The determination of the muscle force action line personalized to subject morphology is one of the major steps in the development of reliable musculoskeletal models. In order to apply origin-insertion data by the cadavers' studies on living subject, the regression equations to estimate musculotendon origin-insertion coordinates of lower limb were built by statistic analysis between origin-insertion coordinates and the morphological parameters. The statistic results indicated that the skeletal morphological parameters selected are appropriate to estimate individual musculotendon origin-insertion coordinates. Data from eight Asian cadavers' studies ensure the accuracy of musculoskeletal model. The skeletal morphological parameters were defined by anthropometric measurement of subject skeletal landmarks, and musculotendon origin-insertion coordinates were calculated by the morphological parameters. The origin-insertion coordinates and kinematical data from same subject gait experiments were

inputted into the algorithm to calculate the dynamic parameters. In whole processes, the data is uniform and intact. From the calculated results, the dynamic musculotendon lengths and moment arms as the functions of joint angular displacements are obviously following with the joint angular displacements in whole gait cycle. The extreme points of the musculotendon lengths and moment arms in Tables 5 and 6 are emerged in swing phases corresponding with body rapid forward movements in swing phase. The results are coherent with the role of the muscles[27]. However, how to control anthropometric measurement error is difficult, and the anthropometric accuracy should be improved in our future study.

In our experimental study, the angular displacemnts of ankle, knee and hip joints were collected using the wearable sensor system. Based on intact musculoskeletal model of lower limb, musculotendon origin-insert coordinates were calculated by the regression equations that were restructured the skeletal morphological parameters. The skeletal morphological parameters were measured by anthropometric method from the bony landmarks. For improvement of anthropometric accuracy, specific operations to comprehend the bony landmarks have been normalized for living body. The contents include how to confirm bony landmarks, subject physical structures, subject attitudes, and anthropometric techniques. Moreover, simple algorithm for calculation of musculotendon dynamic parameters was developed. The results of joint angular displacements, dynamic musculotendon lengths, and dynamic moment arms during gait testified that our practical method is feasible. The calculated results of the dynamic musculotendon parameters are apparently coherent with the role of the muscles. Our experimental study validated the wearable sensor system is not only feasible for joint kinetics analysis, but also feasible for musculotendon dynamic parameters analysis. More importantly, the dynamic musculotendon parameters analysis manifested individual musculoskeletal features, which means the analysis system may eventually become a convenient assisstant of medical or rehabilitation applications. In the next step, we will integrate the dynamic musculotendon parameters and the kinetics analysis by the wearable sensor system to predict muscle force based on a static optimization method, which provide details to deeply understand the physiological motion of human musculoskeletal mechanism.

References

(1) Zajac, F.E. and Gordon, M.E., Determining muscle’s force and action in multi-articular movement, Exercise and Sports Science Review, Vol. 17, No. 6, pp.187-230, 1989.

(2) Ahmet Erdemira, Scott McLeana, Walter Herzogb, Antonie J. van den Bogerta, Model based estimation of muscle forces exerted during movements, Clinical Biomechanics, Vol. 22, No. 2, pp. 131-154, 2007.

(3) Marjolein M. van der Krogt, Caroline A.M. Doorenbosch, Jaap Harlaar, Muscle length and lengthing velocity in voluntary crouch gait, Gait & Posture, Vol. 26, No. 4, pp. 532-538, 2007.

(4) R. A. Brand, R. D. Crowninshield, C. E. Wittstock, D. R. Pederson, C. R. Clark, A model of lower extremity muscular anatomy, Journal of Biomechanical Engineering, Vol. 104, No. 4, pp. 304-10, 1984.

(5) Melissa G. Hoy, Felix E. Zajac, Michael E. Gordon, A musculoskeletal model of the human lower extremity: the effect of muscle, tendon, and moment arm on the moment-angle relationship of musculotendon actuators at the hip, knee and ankle, Journal of Biomechanics, Vol. 23, No. 2, pp. 157-169, 1990.

(6) J.J. Visser, J.E. Hoogkamer, M.F. Bobbert, P.A. Huijing, Length and moment arm of human leg muscles as a function of knee and hip-joint angles, European Journal of Applied Physiology, Vol. 61, No. 5-6, pp. 453-460, 1990.

(7) Gunnar Nemeth, In vivo moment arm lengths for hip extensor muscle at different angles of hip flexion, Journal of Biomechanics, Vol. 18, No. 2, pp. 129-140, 1985.

(8) David Hawkins, Software for determining lower extremity muscle-tendon kinematics and moment arm lengths during flexion/extension, Computers in Biology and Medicine, Vol. 22, No. 1/2, pp. 59-71, 1992.

(9) Delp, S.L., Loan, J.P., A graphics-based software system to develop and analyze models of musculoskeletal structures, Computers in Biology and Medicine, Vol. 25, No. 1, pp. 21-34, 1995.

(10) Michael Damsgaard, John Rasmussen, Soren Torholm Christensen, Egidijus Surma, Mark de Zee, Analysis of musculoskeletal systems in the AnyBody Modeling System, Simulation Modelling Practice and Theory, Vol. 14, No. 8, pp. 1100-1111, 2006.

(11) Delp, S.L., Frank C. Andersen, Allison S. Arnold, Peter Loan, Ayman Habib, Chand T. John, Eran Guendelman, Darryl G. Thelen, OpenSim: open-source of software to create and analyze dynamic simulations of movement, IEEE Transactions on Biomechanical Engineering, Vol. 54, No. 11, pp. 1940-1947, 2007.

(12) Yamaguchi, G.T., et al., A survey of human musculotendon actuator parameters. In: Jack M. Winters, Savio L-Y. Woo, Multiple Muscle Systems: Biomechanics and Movement Organization, Spring-Verlag, pp. 727-773, 1990.

(13) M.D. Klein Horsman, H.F.J.M. Koopman, F.C.T. van der Helm, L. Poliacu Prose, Morphological muscle and joint parameters for musculoskeletal modeling of the lower extremity, Vol. 22, No. 2, pp. 239-247, 2007.

(14) Thomas M. Kepple, H. J. Sommer III, Karen Lohmann Siegel and Steven J. Stanhope, A three-dimension musculoskeletal database for the lower extremities, Journal of Biomechanics, Vol. 31, No. 1, pp. 77-88, 1998.

(15) Damao Shan, Brief introduction of research on model parameters of human lower body muscle function, Journal of Shanghai Physical Education Institute, Vol. 28, No. 4, pp. 63-68, 2004.

(16) Constantinos N. Maganaris, Imaging-based estimates of moment arm length in intact human muscle-tendons, European Journal of Applied Physiology, Vol. 91, No. 2-3, pp.130-139, 2004.

(17) Allison S. Arnold, Silivia Salinas, Deanna J. Asakawa, Scott L. Delp, Accuracy of muscle moment arms estimated from MRI-based musculoskeletal models of the lower extremity, Computer Aided Surgery, Vol. 5, No. 2, pp. 108-119, 2000.

(18) Constantinos N. Maganaris, Vasilios Baltzopoulos, Dimitrios Tsaopoulos, Muscle fiber length-moment arm ratios in the human lower limb determined in vivo, Journal of Biomechanics, Vol. 39, No. 9, pp. 1663-1668, 2006.

(19) Lennart Scheys, Arhur Spaepen, Paul Suetens, Ilse Jonkers, Calculated moment-arm and muscle-tendon lengths during gait differ substantially using MR based versus rescaled generic lower-limb musculoskeletal models, Gait & Posture, Vol. 28, No. 3, pp. 358-365, 2008.

(20) Lennart Scheys, Anja Van Campenhout, Arhur Spaepen, Paul Suetens, Ilse Jonkers, Personalized MR-based musculoskeletal models compared to rescaled generic models in the presence of increased femoral anteversion: Effect on hip moment arm lengths, Gait & Posture, Vol. 28, No. 4, pp. 640-648, 2008.

(21) A. Bonnefoy, N. Doriot, M. Senk, B. Dohin, D. Pradon, L. Cheze, A non-invasive protocol to determine the personalized moment arms of knee and ankle muscle, Journal of Biomechanics, Vol. 40, No. 8, pp. 1776-1785, 2007.

(22) H. Martin Schepers, H. F. J. M. Koopman, Peter H. Veltink, Ambulatory Assessment of ankle and foot dynamics, IEEE Transactions on Biomedical Engineering, Vol. 54, No. 5, pp. 895-902, 2007.

(23) Rencheng Zheng, Tao Liu, Yoshio Inoue, Kyoko Shibata, Kun Liu, Kinematics analysis of ankle, knee and hip joints using a wearable sensor system, Journal of Biomechanical Science and Engineering, Vol. 3, No. 3, pp. 343-355, 2008.

(24) Damao Shan, Study on the muscular function model and its application of human lower extremity, PhD Dissertation of Shanghai University of Sports, pp. 76-86, 2003. (in Chinese)

(25) Mochimaru Masaaki, Kouchi Makiko, Biomechanism Library, Measurement of Man: Size, Shape and Motion, Tokyo Denki University Press, pp. 1-34, 2006. (in Japanese)
(26) Kouchi Makiko, Reference Manual of Anthropometry in Ergonomic Design, Research Institute of Human Engineering for Quality Life, pp. 1-95, 1994. (in Japanese)
(27) Jennette L. Boakes, George T. Rab, Muscle activity during walking, In: Jessica Rose, James G. Gamble, Human Walking, Lippincotte Williams & Wilkins, pp. 103-118, 1994.
(28) Kenton R. Kaufman, David H. Sutherland, Kinematics of normal human walking, In: Jessica Rose, James G. Gamble, Human Walking, Lippincotte Williams & Wilkins, pp. 43-44, 2006.

6 Musculotendon Dynamics Analysis

Direct measurement of muscle forces is generally not feasible in a clinical setting, and optimization algorithm based on musculoskeletal model is an indispensable tool to estimate muscle forces for deeper understanding of neural control and tissue loading. Musculotendon dynamics analysis of lower limb is a complicated multi-body dynamics problem attracting researcher's interest for a long time. Physical muscles as a only motor system for human motion have an infinite number of cooperation manner to complete one motion task, optimization-based models of muscular cooperation considering physiological parameters are always built to solve the redundant problem. Static optimization, an inverse dynamics method, has been used extensively to estimate muscle force during gait on the basis of constrained nonlinear optimization technique.

Ordinarily, only one impact factors is adopted as objective function for the static optimization method; however, in fact muscle activation is obviously affected by more than one impact factors during gait. Human motion mechanism and physiological principles should be perfectly expressed through building reasonable mathematical algorithm. Linear-weight-sum method as a multiple objective optimization is more suitable than the single objective optimization to indicate the physiological principle of human walking. The weight value for each impact factor can also be adjusted according to a known physical performance of subject. For example, weight value to muscle fatigue function can be enhanced accordingly when subject is in fatigue condition. In our study, mean weight sum of three impact factor was applied to estimate muscle force for a healthy subject in a normal walking.

In this chapter, a linear-weight-sum method was proposed to solve the constrained nonlinear optimization problem combination static optimization, which method is used to estimate muscle force from joint moment based on musculoskeletal model of lower limb. Namely, muscle energy expenditure function, muscle fatigue function and muscle effort sense function are integrated into a minimization objective function in static optimization method. An antero-posterior human walking dynamic model of lower extremities was built, and each leg consist three joints and is controlled by nine Hill-type muscle-tendon groups. Maximal isometric muscle force is obtained by the velocity-length-force relation of muscle-tendon and the

parameters of physiological cross-sectional area (PCSA). The dynamic musculotendon parameters were estimated by the regression equation of musculotendon origin-insertion coordinates of a musculoskeletal model of lower limb. Both of them are respectively inputted into an inequality constraint equation and an equality constraint equation to express a relation between joint moments and muscle forces of lower limb during gait. Meanwhile, the joint moment of lower limb is calculated using an inverse dynamics method in accord with human walking performance principles. Kinematical data and ground reaction force (GRF) are measured for calculation of joint moments in gait laboratory.

The study validated that linear-weight-sum method is a promising optimization technique to estimate muscle force during gait based on multiple musculoskeletal model. Our experimental study was implemented on a subject with normal walking abilities who was asked to walk in a normal walking speed. The signals of surface Electromyography (EMG) were synchronously measured as a reference to evaluate the results of the estimated muscle force.

6.1 Introduction

Researcher commonly uses the musculoskeletal modeling method to analyze the muscle cooperation problem during human motion, since we can not destroy muscle organization and simultaneously maintain muscle lively. Correspondingly, estimation of muscle force is an important to understand muscle activities, and can provide diagnosis information for the relevant patient.

Recently, human motion modeling and simulation becomes a very active studying field. There is an increasing need of tools that permit to know or evaluate in vivo muscle force with noninvasive techniques. The most of studies is in virtue of the comprehensive achievements by Zajac[1-3]. Zajac[4,5] also suggested that dynamic optimization is a powerful method to estimate muscle force but static optimization has several disadvantages, even though static optimization has been used extensively to estimate in vivo muscle forces during gait.

Unfortunately, dynamic optimization incurs so much computational expense that relatively few dynamic solutions for gait have been found. Further, for gait, this approach has required that the dynamic models be simplified to such an extent that it has been difficult to ascertain whether its computational expense is justified. Thus, for normal gait, if one can accurately solve the inverse dynamics problem and if one seeks only to estimate muscle forces, the use of dynamic optimization rather than static optimization is currently not justified[6].

EMG-to-force processing approach[7-9] had became a reliable technique to estimate muscle force, Sofia[10] proposed static optimization method can get more accurate muscle force results

than EMG-to-force processing approach.

Since static optimization method may provide reasonably accurate estimation of muscle force during gait, objective function as an important impact factor to the estimation results had be paid a lot of attentions. Minimum energy expenditure, minimum muscle fatigue, and minimum sense of effort seem to be the most promising function to solve the optimization problem[(11)]. However, none of researchers integrated all of the three indexes to estimate muscle force, even though muscle activities is likely to be affected by the three indexes in the same time. In this chapter, whole flow of this study is introduced as technological processes to make clear the analysis method. At last, the results of optimal muscle force are evaluated by surface electromyography (EMG) signals synchronously measured in our gait experiments.

6.2 Inverse Dynamics Analysis Processes

Since wearable sensor system was used instead of the force plate and optical camera system in our experiments, the technical processes are obviously different with the method by other researchers. In Fig. 6.1, the whole technological processes are distinctly expressed for our study. The inverse method of dynamics analysis in our study insures that the method can be used in practice.

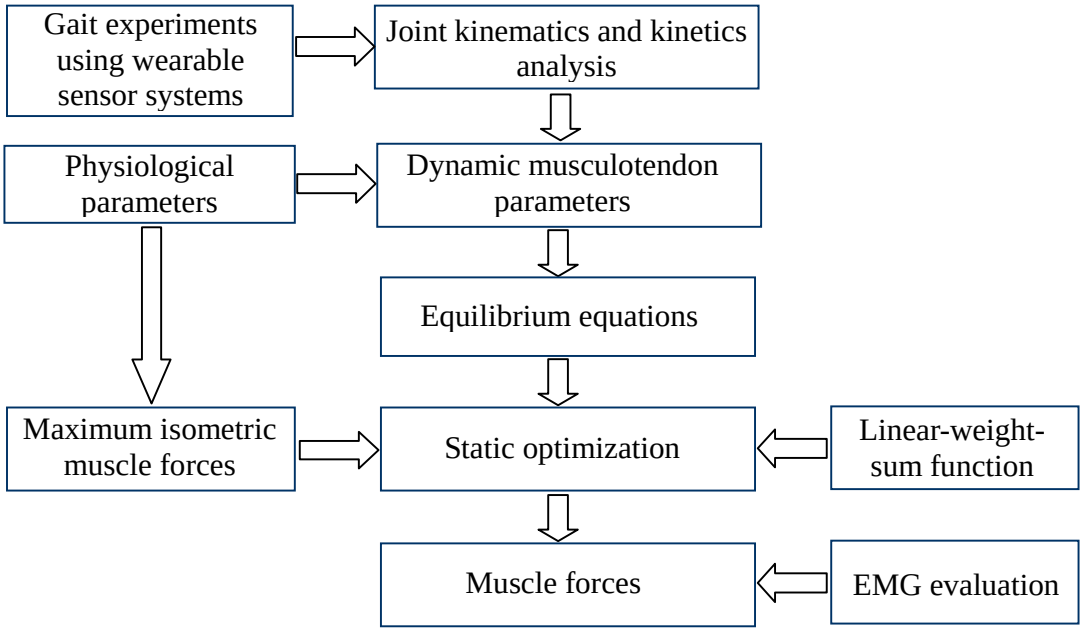

Fig. 6.1 Inverse dynamics analysis processes of estimation of optical muscle force using a wearable sensor system

6.3 Muscle Mechanical Properties

Before we begin to estimate muscle forces, some muscle mechanical properties have to be introduced. The properties are basic notions to understand muscles functions, and are also origin to resolve problems about muscles using modern mechanical theory.

Muscle activation mechanism. When the body performs a motor task, the central nervous system (CNS) excites muscles that subsequently develop forces that are transmitted by tendons to the skeleton to effect the task. Thus, muscles and tendons are the interface between the CNS and the articulated body segments. As was explained by Zajac[(1)] (1989), muscle activation mechanism can be simply represented by Fig. 6.2.

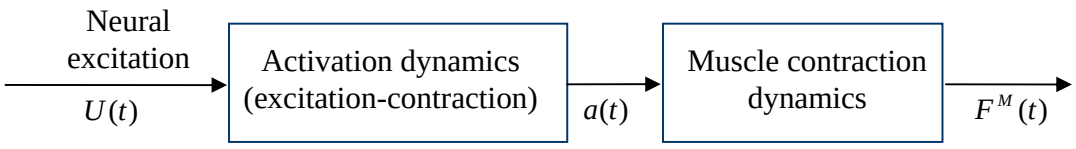

Fig. 6.2 Muscle tissue dynamics[()]. CNS excitation of muscle tissue (neural excitation, u(t)) acts through activationdynamics (EC coupling) to generate an internal muscle tissue state (muscle activation, a(t)), which is associated with the Ca^{++} activation of the contractile process. Through muscle contraction dynamics, this activation energizes the cross-bridges and muscle force $F^M(t)$ is developed.

Muscle Linear Dynamics. According to Lieber and Friden[(12)], muscle architecture is the primary determinant of muscle function. Understanding this structural and functional relationship is of great practical importance to provide a basic understanding of the physiological basis of muscle force production in human movement. Skeletal muscle architecture is defined as “the arrangement of muscle fibers within a muscle relative to the axis of firce generation”.

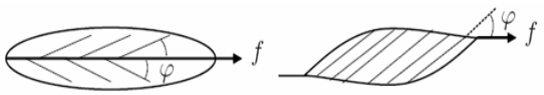

(a) Pennate muscle (b) Multipennate muscle

Fig. 6.3 Muscle architecture

Fig. 6.3 Schematic figures on two way of muscle fiber arrangement showing the angle of pennation, φ, in relation to the axis of force, f. Skeletal muscle function is defined as “the

arrangement of muscle fibers within a muscle relative to the axis of force generation".

Physiological cross-sectional area (PCSA) is proportional to the maximum tension generated by the muscle and is the major determinant of a muscle's strength. The functional difference of two muscles with identical fiber length and pennation angles but with different PCSA (large or small) is illustrated in Fig. 2.4.

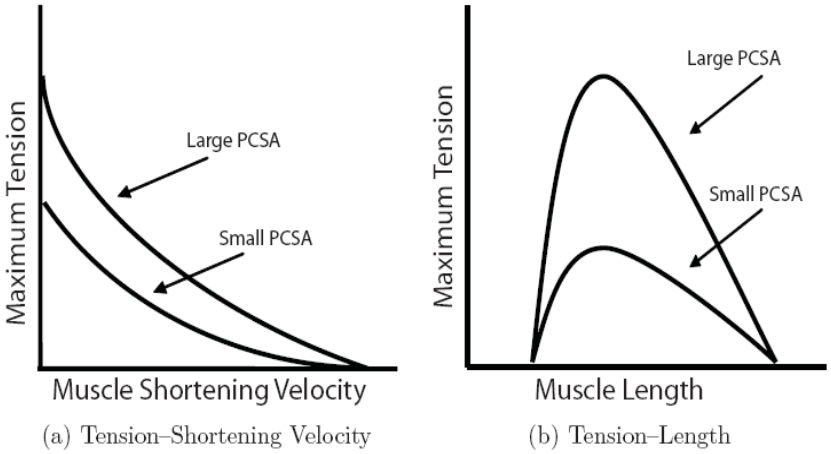

Fig. 6.4 The architectural properties of two muscles with small respective large PCSA. (a) showing the tension-shortening velocity relationship of a muscle in concentric contraction, (b) showing the tension-length relationship of the active muscle in concentric contraction.

Hill-type Musculotendon Model. Force produced by a muscle can be simulated in different ways. The most common numerical description of a muscle model is called Hill-model (see Fig. 6.5)

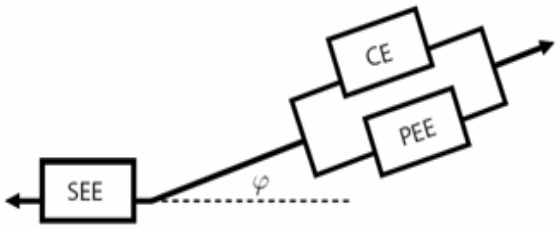

Fig. 6.5 The generic Three Component Hill-type muscle-tendon model described by Zajac in (1989). The model consist of one active contractile element (CE) in parallel with a passive elastic element (PEE), and in series with one non-linear elastic element (SEE) which is modeled with a pennation angle φ.

Force-length-velocity curve. A musculotendon actuator model based on the three component Hill-model was proposed by Zajac, including a pennation angle φ (Figures 2.5 and 2.6). Muscle architectural properties of the muscle force-fiber length, the muscle force-fiber velocity and tendon force-tendon length relationships, together with peak isometric force, optical muscle fiber length and pennation angle at optical fiber length, tendon slack length and maximum shortening velocity are used as inputs to the model. Muscle architectural properties were obtained from experimental studies.

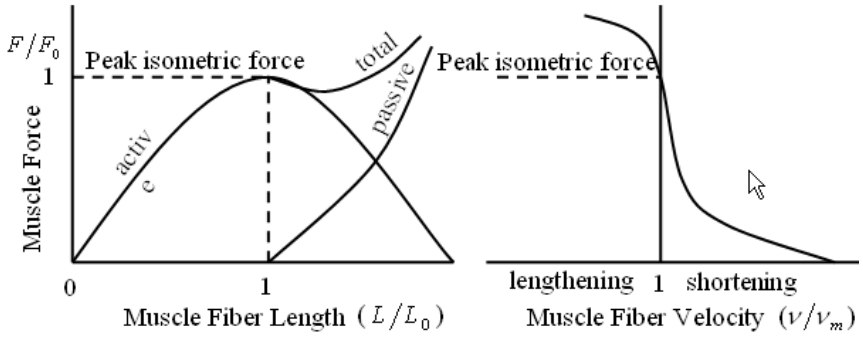

Fig. 6.6 Schematic figure of muscle properties used by the three component Hill-type musculotendon actuator model described by Zajac in (1989)

6.4 Static Optimization

The fact that the musculoskeletal system is redundant and that apparently only a limited number of Muscle Activation Patterns (MAP) are used in skilled tasks has led to the development of optimization-based models for estimating forces of individual muscles. The main assumption in these models is that the MAP is selected in such a way as to optimize a specific objective function or a combination of objective functions. We use static optimization method to estimate muscle force of lower extremity.

Redundant Problem. A musculoskeletal model of leg in the saggital plane is shown in Fig. 6.7.

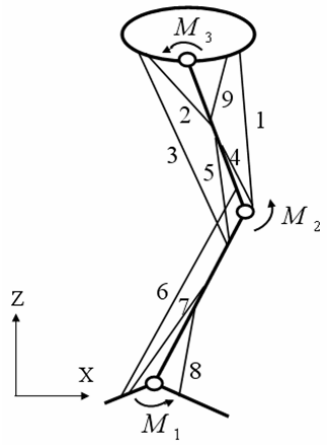

Fig. 6.7 Musculoskeletal model of lower limb in the sagittal plane. The musculoskeletal model of leg has three DoF and is controlled by main nine muscles. Therefore, thejoint moments of ankle, knee and hip joints can be produced by an infinite number of muscle force combinations theoretically. 1. Rectus Femoris (RF), 2. Glusteus Maximus (G-U), 3. Hamstring (HA), 4. Vastus (VA), 5. Biceps Femoris Caput Breve (BS), 6.Gastrocnemius (GA), 7. Soleus (SO), 8. Tibilis Anterior (TA), 9. Iliopsoas (IL).

In static optimization, it is assumed that the MAP at any movement instant is independent of those at other instants. Muscle forces are calculated for each time instant of a movement. Based on Fig. 6.7, four segmental models of the leg in the saggital plane, optimal forces of nine muscles can be found by solving the following static optimization problem for each time instant:

$$\begin{aligned} M_1 &= -a_{16}F_6 - a_{17}F_7 + a_{18}F_8 \\ M_2 &= a_{21}F_1 - a_{23}F_3 + a_{24}F_4 - a_{25}F_5 - a_{26}F_6 \\ M_3 &= a_{31}F_1 - a_{32}F_2 - a_{33}F_3 + a_{39}F_9 \end{aligned} \tag{6.1}$$

M_1, M_2 and M_3 are the joint moments of ankle, knee and hip, F_i is the muscle force of $i-th$ muscle, and $a_{j,i}$ is the dynamic moment arms of $i-th$ muscle with respect to $j-th$ joint. It is a typical redundant problem that the joint moments can be produced by infinite number force combinations in equation 6.1.

Constrained Nonlinear Optimization. Physical meaning of optimization-model is hypotheses of physiological behavior analysis about muscle cooperation. There are three behavior analyses: (1) nervo-musculo-skeletal system is almost same for different people, (2) physiological behavior is almost same for different people, (3) walking is daily, skilled and unconscious motion. So we can

get two hypotheses: (1) Law of muscle cooperation must be existed; (2) muscle cooperation is approximately optimal.

A constrained nonlinear optimization can be designed as following steps:

Objective function is

$$Z = f(F_1, F_2, \cdots, F_9), \tag{6.2}$$

Equality constraints function can be expressed by

$$\sum M_j = \sum a_{j,i} \cdot F_i \tag{6.3}$$

Inequality constraints function is

$$0 \le F_i \le F_{\max\_i} \tag{6.4}$$

where M_1, M_2, and M_3 are the joint moments of ankle, knee and hip joints respectively. F_i are the opti-mal force of i-th muscle. $a_{j,i}$ are the dynamic mom-ent arm length of i-th muscle with respect to j-th j-oint. $F_{\max\_i}$ is the maximum isometric force of i-thmuscle.

Linear-weight-sum Function. When we begin to use static optimization to estimate muscle force during gait, firstly, we assume that the muscle cooperation law exist for human motion considering two following reasons. One reason is that there is similar nerve-muscle-skeleton system for different people, for example similar neural system mechanism, similar muscle mechanical properties, and similar skeletal structure and functions. Another reason is that there are similar walking performances for different people, for examples, bimodality characteristic of ground reaction force (GRF), similar curve of joint moments, and similar wave of zero moment point of whole body. In the next, we assume that muscle cooperation must be an optimal processes since people is always choose the optimal way to finish his motion, more importantly, walking is daily, skilled and sometimes unconscious motion for human being.

With respect to objective function in static optimization, it is an important impact factor on the eventual result of muscle force. In the research, we assume that muscle activities are affected by multiple impact factors during gait, and choose a multiple objective function. Muscle energy expenditure function expressed in equation (6.5), muscle fatigue function in equation (6.6), and muscle effort sense function in equation (6.7) are considered in the optimization problem. The three impact factors constitute the minimizing objective function, and then a linear-weight-sum method is proposed to solve the minimizing objective function

$$Z_1(F_i) = \min_i \sum_{i=1}^{9} \left(F_i / F_{\max\_i}\right)^2, \quad i = 1, \cdots, 9 \tag{6.5}$$

$$Z_2(F_i) = \min_i \left\{ \sum_{i=1}^{9} \left(F_i / PCSA_i\right)^2 \right\}, \tag{6.6}$$

where $PCSA_i$ is the physiological cross-sectional area of i-th muscles.

$$Z_3(F_i) = \min_i \left\{ \sum_{i=1}^{9} a_i^{\,2} \cdot F_{\max\_i} \cdot v_{\max\_i} \cdot \phi(v_i / v_{\max\_i}) \right\}, \tag{6.7}$$

where Z_3 is the metabolic rate of the i-th muscle and function ϕ determines the metabolic cost; $F_{\max\_i}$ and $v_{\max\_i}$ are known as maximum force and maximum velocity of the i-th muscle respectively; v_i is instantaneous velocity of the i-th muscle; and a_i $(0 < a_i < 1)$ is the unknown normalizing activation of the i-th muscle, sought by minimizing criterion $Z_3(F_i)$. Moment constraints in equation (2) for this function take into account the force-velocity curve of muscle property.

When more impact factors are considered during human walking, the mathematical model to estimate muscle force have to be proposed by multiple objective function. Accordingly, a linear-weight-sum function can be structured by following equation to represent the optimization programming of multiple objective.

$$Z(F_i) = \min_i \left\{ \omega_1 Z_1(F_i)^2 + \omega_2 Z_2(F_i)^2 + \omega_3 Z_3(F_i)^2 \right\}, \quad i = 1, \cdots, 9 \tag{6.8}$$

where, ω_i is weight factor, $\omega_1 + \omega_2 + \omega_3 = 1$. The three weight factors are equivalent when we assume their weight is equal affected on the muscle activations. And each weight factor can be changed dependent on their physical meanings with corresponding to the body condition of subject.

Basic method to solve the multiple objective programming problem is evaluation function method. The basic method of the evaluation function is to structure evaluation function in virtue of geometric or direct-viewing background of the application, and translate multiple objective optimization problem to single objective optimization problem. Then, the optimal solution is obtained using the solving method of single objective optimization problem. The optimal solution of of single objective optimization is namely the solution of the multiple objective optimization.

For a multiple objective problem, rather large weight afford to the relatively important indexes, which mean the multiple objective function become a scalar problem of the weight-sum

for the integral objective function. Based on practical problem, evaluation function can be structured as follows.

$$\underset{F_i \in \Omega}{Z(F_i)} = \min_i \sum_{i=1}^{m} \omega_i Z_i(F_i)^2, \quad i = 1, \cdots, 9 \tag{6.9}$$

where, ω_i is weight factor, which can be chose by weight method, allowance method and weight factor decomposition method. Then, the problem is decomposed by standard unconstrained optimization method. At last, the multiple objective functions are integrated with the static optimization in section 2.1.1.

Maximum Isometric Muscle Force. In the static optimization method, the maximum isometric muscle force is an important constraints variable. Meanwhile, we have to consider the mechanical properties of muscle-tendon, mainly including the hill-type muscle-tendon model and velocity-length-force curve of muscle-tendon (Zajac, 1989). Based on the muscle mechanical properties, maximum isometric muscle forces can be approximately estimated by (Pedotti, 1978)

$$\begin{aligned} F_{\max\_i} &= \frac{b_i - 0.3V_i}{b_i + V_i} F_{a\_i} \quad for \quad V_i > 0 \\ F_{\max\_i} &= \left(\frac{-1.3V_i}{b_i} + 1 \right) F_{a\_i} \quad for \quad -\frac{b_i}{3} < V_i < 0 \\ F_{\max\_i} &= \left(\frac{1.3}{3} + 1 \right) F_{a\_i} \quad for \quad V_i < -\frac{b_i}{3} \end{aligned} \tag{6.10}$$

where b_i is the constant of the i-th muscle in Hill's equation, V_i is the velocity of shortening of the i-th muscle. F_{a_i} is given by

$$\begin{aligned} F_{a\_i} &= K \times PCSA_i \times [1 - K_1(l_{m\_i} - l_i)] \quad \text{for} \, V_i > 0 \\ F_{a\_i} &= K \times PCSA_i \times [1 - K_2(l_j - l_{m\_i})] \quad \text{for} \, l_i \le l_{m\_i} \end{aligned} \tag{6.11}$$

where K, K_1 and K_2 are the constants, l_i is the instantaneous length of the i-th muscle, l_{m_i} is the rest length of the i-th muscle.

Mathematical Algorithm. Using the static optimization to calculate of the optimal muscle forces, we have to design a programming algorithm(13) to solve the constrained nonlinear optimization

problem. Firstly, based on the optimization problem to certificate the existence of solution, Lagrange functions and Kuhn-Tucher conditions functions of Lagrange multiplier are applied in general processing. Then, Penalty function method is used to transform the constrained problem to the unconstrained one. And Newton-function-approximatioss method is built for searching the optimal solution. Mathematical algorithm was designed for resolving the optimization problem.

(1) Building of optimal conditions (Analyzing of the existence of solution)

Problem:

$$\begin{aligned} &\min \quad f(x) \\ &s.t. \quad g_i(x) \geq 0, i = 1,2,\cdots,m \\ &\qquad h_j(x) = 0,\ j = 1,2,\cdots,n \end{aligned} \tag{6.12}$$

Lagrange function:

$$\Delta_x L(x^*, \lambda^*, \mu^*) = \Delta f(x^*) - \sum_{i=1}^{m} \lambda_i{}^x \Delta g_i(x^*) - \sum_{j=1}^{n} \mu_j{}^x \Delta h_j(x) = 0 \tag{6.13}$$

Kuhn-Tucher conditions:

$$L(x, \lambda, \mu) = f(x) - \sum_{i=1}^{m} \lambda_i g_i(x) - \sum_{j=1}^{n} \mu_j h_j(x)$$

$$\lambda_i^* g_i(x^*) = 0, i = 1,2,\cdots,m \tag{6.14}$$

$$\lambda_i^* \geq 0, i = 1,2,\cdots,m$$

λ^*, μ^*, Lagrange multiplier

(2) Penalty function methods (Transforming constrained problem to unconstrained ones)

$$F_2(x, \sigma) = f(x) + \sigma \cdot P(x), \therefore P(x) = \sum_{i=1}^{m} \left[\max\{0, -g_i(x)\}\right]^{\alpha} + \sum_{j=1}^{n} \left|h_j(x)\right|^{\beta}, \tag{6.15}$$

$$\min F_2(x, \sigma) = f(x) + \sigma \cdot P(x)$$

(3) Newton-function-approximatioss methods (Researching the optimal solutions)

Problem: $\min f(x) \quad x \in R^1$

Making Second-order Newton-Thaler Polynomial:

$$\begin{aligned} &\phi(x) = f(x_k) + f(x_k)(x - x_k) + f'(x_k)(x - x_k)^2 / 2 \\ &\phi'(x) = f(x_k) + f(x_k)(x - x_k) = 0, \therefore x_{k+1} = x_k - \frac{f'(x_k)}{f''(x_k)} \end{aligned} \tag{6.16}$$

$\{ x_k \}$ is the optimal solutions by determinant.

6.5 Electromyography Experiments

In our gait lab, each of subjects wearing the sensor system was asked to normally walk on the level ground; synchronously, the motion information of the retro-reflective markers on the lower extremities of subjects was captured by an optical camera system (Hi-DCam, NAC Image Tech., Japan). The optical camera system is used as a reference to validate the wearable sensor system. Meanwhile, surface Electromyography (EMG) (Personal EMG Oisaka Development Ltd.) is stuck in body surface as is shown in figures 6.8-10. The detailed positions of surface EMG about individual muscle are guided by Edward[14].

Segmental inertial parameters of the lower extremities for calculation of joint moments were estimated by the empirical regression method. The morphological parameters of the subjects were directly measured, and were inputted to the regression equation of muscle-ten-don origin-insertion. The whole data from the gait experiments are inputted to the computational programming for off-line computing.

Fig. 6.8 Surface EMG processing

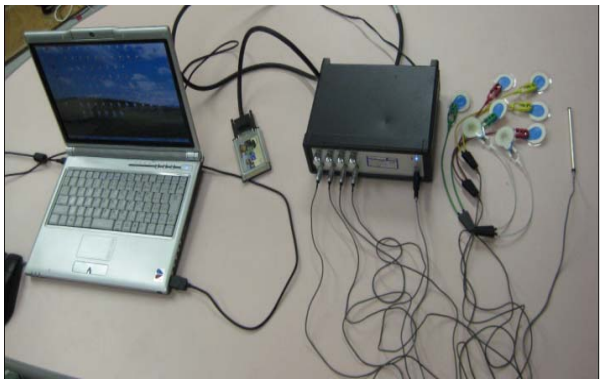

Fig. 6.9 Surface EMG equipment (Oisaka, Japan). 1) reference electrode sensor, 2) wet measurement electrode sensor, 3) EMG signal panel, 4) A/D Card, 5) Personal computer.

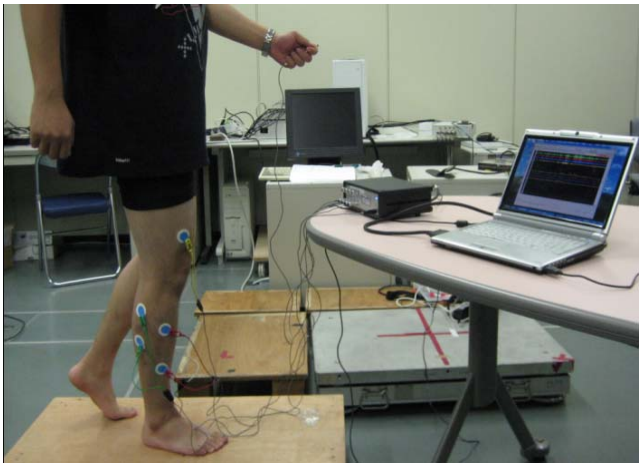

Fig. 6.10 Diagram of EMG experiments

6.6 Results and Discussions

The representative results of optimal muscle force during gait are presented in Fig. 11. Surface EMG signals synchronously measured in our gait experiments are used to evaluate the results of optimal muscle forces as a reference.

Fig. 11 Optical muscle forces and its surface EMG's signals

(a) TA forces and its EMG

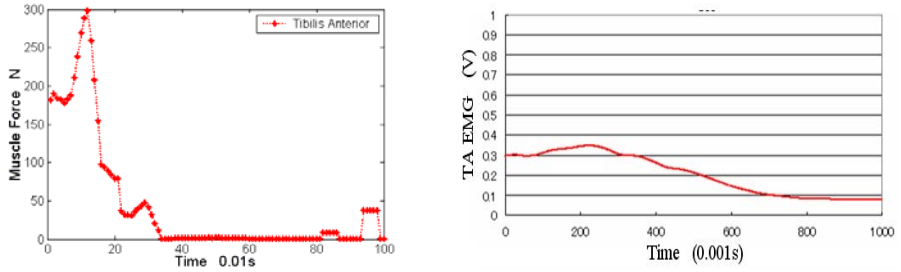

(b) SO forces and its EMG

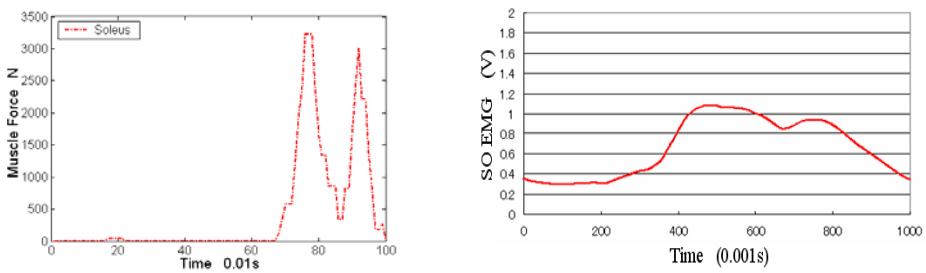

(c) GA forces and its EMG

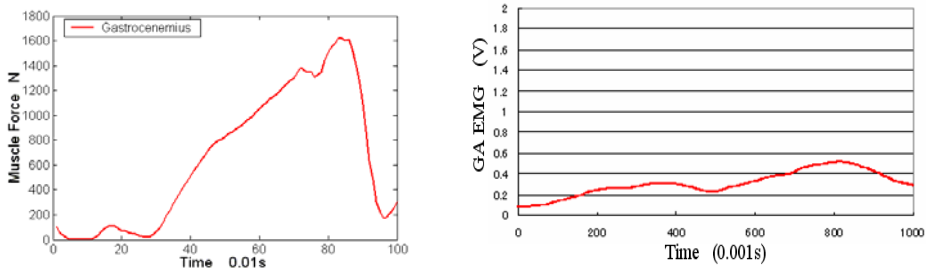

(d) GU forces and its EMG

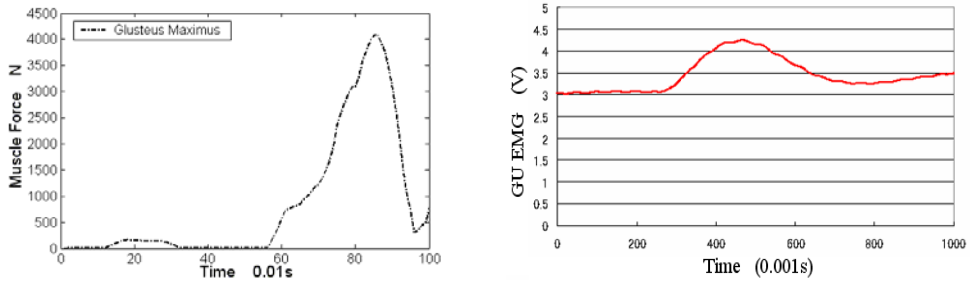

(e) RF forces and its EMG

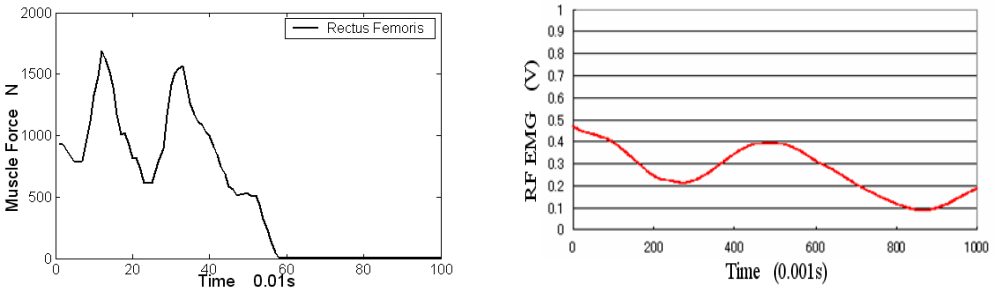

(f) VS forces and its EMG

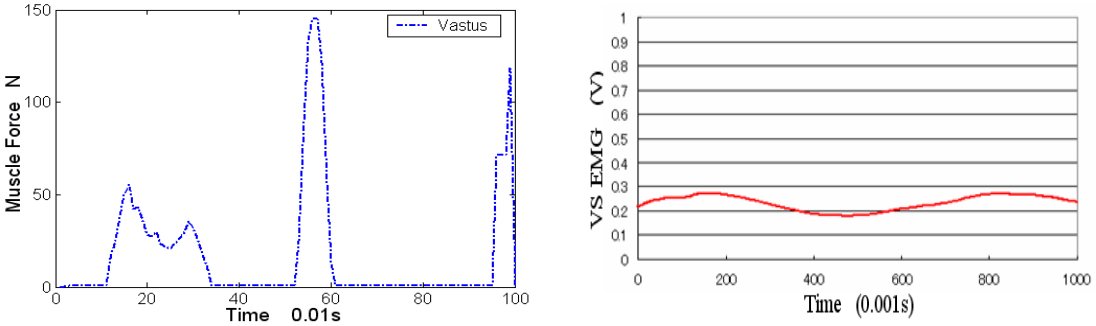

(g) BS forces and its EMG

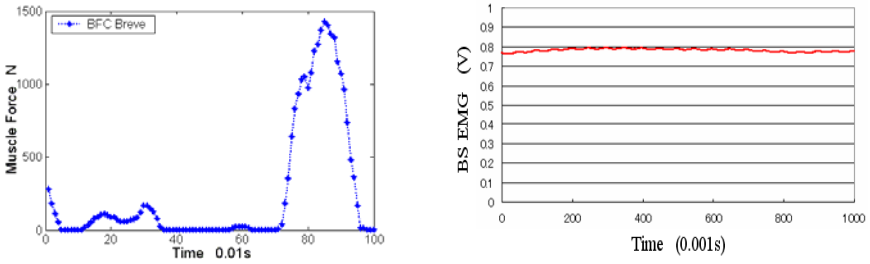

(h) IL forces and its EMG

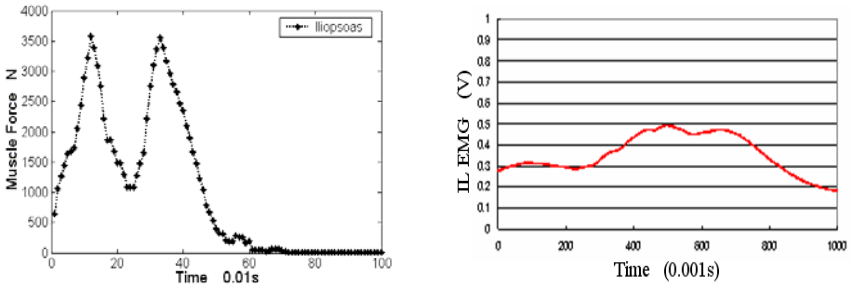

(i) HA forces and its EMG

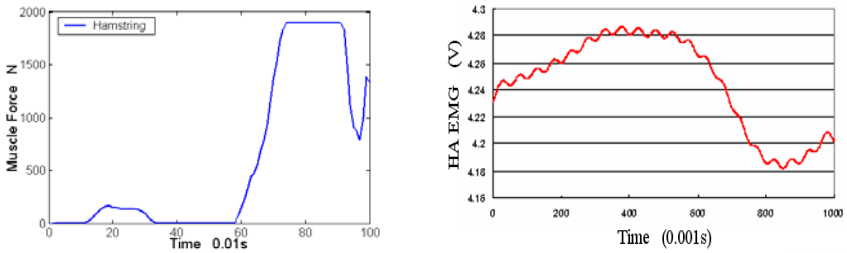

From the above results, we can find the results of the optical muscle force are principally consistent with the tendency of the results of the surface EMG signals. However, how to effectively evaluate accuracy of the estimating results of optimal muscle to the real muscle force, surface EMG signals as a common means are affected by many factors, and it is difficult to analyze its unstable signals in our experiment. In the other hand, since we used the some parameters values from the references, which maybe affected our results in some way. As a result, the linear-weight-sum method is a hoping method to estimate muscle force based on our study.

6.7 Conclusions

In the paper, the estimating processes of the optimal muscle forces based on multiple musculoskeletal model of leg are completely described. As a result, the following conclusions

have been drawn.

A. Linear-weight-sum method firstly is put forward as a new mathematical model to estimate the optimal muscle force for human walking. The method considers the three impact factors as minimizing objective function in static optimization, which apparently agree to the physical meanings of the human skilled motion, especially for human walking.
B. Through building the regression equations of muscle-tendon origin-insertion coordinates, then in vivo measurement of the morphological parameters of lower extremities of osteology to estimate dynamic muscle-tendon parameters, especially dynamic muscle-tendon moment arm length, provide a relative easy and accurate method that can be used in everyday medical application.
C. In the whole researching flow, the wearable sensor system is used as main equipments to measure human motion. The experiments verified that the system can be applied as a reliable instrument to motion evaluation in daily activities.

Reference

(1) Zajac Felix E., Muscle and tendon: properties, models, scaling, and application to biomechanics and motor control, Critical Reviews in Biomedical Engineering, Vol. 17, No. 4, pp.359-411, 1989.

(2) Zajac Felix E., Michael E. Gordon, Determining muscle's force and action in multi-articular movement, Exercise and Sport Science Reviews, Vol. 17, No. 6, pp.187-230, 1989.

(3) Zajac Felix E., Muscle coordination of movement: a perspective, Journal of Biomechanics, Vol. 26, Suppl. 1, pp.109-124, 1993.

(4) Zajac Felix E., Richard R. Neptune, Steven A. Kautz, Biomechanics and muscle coordination of human walking Part I: introduction of concepts, power transfer, dynamics and simulations, Gait & Posture, Vol. 16, No. 3, pp.215-232, 2002.

(5) Zajac Felix E., Richard R. Neptune, Steven A. Kautz, Biomechanics and muscle coordination of human walking Part II: Lessons from dynamical simulations and clinical implications, Gait & Posture , Vol. 17, No. 1, pp.1-17, 2003.

(6) Anderson Frank C., Marcus G. Pandy, Static and dynamic optimization solutions for gait are practically equivalent, Journal of Biomechanics, Vol. 34, No. 2, pp.153-161, 2001.

(7) David G. Lloyd, Thor F. Besier, An EMG-driven musculoskeletal model to estimate muscle forces and knee joint moments in vivo, Journal of Biomechanics, Vol. 36, No. 6, pp.765-776, 2003.

(8) Bogey R.A., J. Perry, A.J. Gitter, An EMG-to-force processing approach for determining ankle

muscle forces during normal human gait, Neural Systems and Rehabi-litation Engineering, Vol. 13, No. 3, pp.302-310, 2005.

(9) Louis N., A. Bonnefoy, D. Pradon, P. Gorce, A preliminary report. Muscle forces during reaching: EMG-to-force processing, Computer Methods in Biomechanics and Biomedical Engineering, Vol. 10, S. 1, pp.57-58, 2007.

(10) Sofia Heintz, Elena M Gutierrez-Farewik, Static optimization of muscle forces during gait in comparison to EMG-to-force processing approach, Gait & Posture, Vol. 26, No. 2, 2007.

(11) Prilutsky, Boris I., Zatsiorsky, Vladimir M., Optimization-based models of muscles coordination, Exercise & Sports Sciences Reviews, Vol. 30, No. 1, 2002.

(12) Sofia Heintz, Muscular forces from static optimization, Technical Report from Royal Institute of Technology, KTH Mechanics, 2006.

(13) Chao Weihua, Guo zheng, Optimization Technique and its MATLAB Realization, Chemistry Industrial Express, Beijing, 2004.

(14) Edward F. Delagi, Aldo O. Perotto, John Iazzetti, Daniel Morrison, Anatomical Guide for the Electromyographer,Charles C Thomas Publisher, Springfield, Illinois, U.S.A, 2005.

7 Conclusions

The goal of this dissertation was to explore the utilities of the wearable sensor system on human motion analysis in daily activities. To achieve this goal, we developed a whole inverse method of musculoskeletal kinematics and dynamics analysis of lower limb by the sensing signals. The summary result is that the wearable sensor system can be applied as a reliable musculoskeletal motion analysis system in daily activities. However, a significant amount of future work is needed to study pathological gait using the musculoskeletal dynamics analysis method by the wearable sensor systems. This chapter summarizes the contributions of this dissertation, outlines some of the limitations of the existing system and method, and lays out plans to expand the limits and applications of musculoskeletal dynamics analysis using the wearable sensor system.

7.1 Contributions

In the whole researching processes, the wearable sensor system is used as motion measuring equipment of lower limb. The studies verified that the wearable sensor system can be applied on musculoskeletal dynamics analysis as a reliable instrument in people daily activities. The main contributions in this dissertation are summarized as followings:

(1) Improvement of a wearable sensor system

The body motion analysis system is fundamental for rehabilitation and clinical diagnosis but data are commonly obtained by means of the laboratory-restricted equipment such as a force plate and optical camera system. A wearable sensor system was improved to facilitate assessment of body motion in daily activities. The sensor system is composed of a shoe-based force sensor which measures 3-dimension ground reaction force (GRF) and center of pressure (CoP), and a leg-attached motion sensor consisting of three uniaxial gyroscopes units which detect 2-dimension segmental motion of lower limb.

(2) Analysis of joint kinematics and dynamics

The kinematics and kinetics analysis of ankle, knee and hip joints during gait is critical for applications of the wearable sensor system. In order to estimate the joint kinematics and kinetics, an inverse method based on the sensing signals and gait characteristics was developed. The results of kinematics and kinetics analysis of ankle, knee and hip joints in the sagittal plane was

obtained by using the sensor system on human normal level walking during whole gait phases. In the validation experiments with 10 subjects, joint kinematics and kinetics was calculated using data synchronously measured by the sensor system and a force plate & optical camera system. The experimental results demonstrate the feasibility and effectiveness of the joint kinetics analysis using the wearable sensor system for a daily application of gait analysis.

(3) Calculation of dynamic musculotendon parameter

A reliable processing was successfully designed to estimate individual dynamic musculotendon length and moment arm of lower limb in the sagittal plane during gait by means of a wearable sensor system. A series of regression equations by inputting skeletal morphological parameters of lower limb was structured to calculate musculotendon origin-insertion coordinates in a musculoskeletal coordinates system. The anthropometric method of measuring skeletal morphological parameters of lower limb was developed to represent individual skeletal features, which method can be conveniently operated on subject's body in vivo. By integrating the kinematical data and the origin-insertion coordinates, an algorithm was developed to calculate dynamic musculotendon parameters. The experimental results suggest that the method used in our study is feasible for estimating personalized musculotendon dynamic parameters in human daily activities.

(4) Estimation of muscle force

Direct measurement of muscle forces is generally not feasible in a clinical setting. Static optimization method based on musculoskeletal model is indispensable tool to estimate muscle force for understanding of neural control and tissue loading. A linear-weight-sum algorithm is firstly proposed to solve the constrained nonlinear optimization problem, which is used to estimate muscle force from joint moment. Surface Electromyography signals were synchronously measured as a reference to evaluate the results of muscle force. The experimental study validated the method is a promising technique to estimate muscle force.

7.2 Applications

In virtue of the musculoskeletal dynamics analysis using the wearable sensor, clinical use of gait analysis can be used as an observation skill when physician, therapists, and prosthetists defined normal and abnormal limb motion and common deviations displayed by patients[(1)]. The dynamics analysis can be also used for motion abilities assessment for the elder and patient after operation. Motion mechanism of musculoskeletal is a complicated processes, many problem is not clear up to new. This kind of musculoskeletal dynamics analysis is helpful to understand the cooperation principles of musculoskeletal mechanism.

7.3 Future Work

(1) 3-Dimension wearable sensor system

In my research, the main limitation is that the existing wearable sensor system can only collect the motion signals of lower limb in the sagittal plane. However, motion analysis in the 3-dimensions becomes more and more important for clinical applications. In the next step, we have to develop 3-dimension motion sensor[(2)] to collect completed motion signals of lower limb, and more comfortable shoe-based force sensor to measure more accurate data of ground reaction force and center of pressure.

(2) 3-Dimension musculoskeletal dynamics analysis

Even though the analysis methods of musculoskeletal kinematics and dynamics in this study can be applied on 3-dimensional analysis, our studies is mainly based on the sagittal plane during human walking. For 3-Dimension musculoskeletal dynamics analysis, the key point is how to confirm the instant motion center of ankle, knee and hip joints during their moving. It is necessary to build the accurate joints model of lower limb, but how to estimate individual instant joints centers is puzzle.

(3) Seat-to-stand training strategy for the elder

Many elders are suffering by the muscle atrophy symptoms[(3)], including the atrophy of fast-switch muscles, reduced tendon stiffness, lower activation of agonist muscles and higher co-activation of antagonist muscles. Integrating the wearable sensor system and a standing-up training machine[(4)], a seat-to-stand[(5)] training system can be structured to improvement or recovery of elder's muscle strength of lower limb. Through comparison of the results in the condition of free passive motion, resistance passive motion and normal resistance training by the musculoskeletal dynamics analysis and surface electromyography signals experiments, an impedance control[(6)] system could be built to realize the suitable seat-to-stand training strategy. Out of question, it is a valuable study direction in the coming future.

Reference

(1) Janet M. Adams, Jacquenlin Perry, Gait analysis: Clinical decision making, Lippincott Williams & Wilkins, 2006.

(2) Ryo Takeda, Shigeru Tadano, Masahiro Todoh, Manabu Morikawa, Minoru Nakayasu, Satoshi Yoshinari, Gait analysis using gravitational acceleration measured by wearable sensors, Journal of Biomechanics, Vol. 42, No. 3, pp. 223-233, 2009.

(3) Elisabeth Barton,Carl Morris, Review Article: Mechanisms and Strategies to Counter Muscle Atrophy, The Journals of Gerontology Series A: Biological Sciences and Medical Sciences 58, pp. 923-926, 2003.

(4) Kyoko Shibata, Yoshio Inoue, Study on standing-up training machine with posture sensor system, Proceeding of the Welfare Engineering Symposium, Japan, pp. 41-43, 2007.

(5) Wim GM Janssen, Hans BJ Bussmann, Henk J Stam, Determinants of the sit-to-stand movement: a review, Physical Therapy, Vol. 82, No. 9, pp. 866-879, 2002.

(6) Hogan, N., Impedance control: An approach to manipulation: Part I - Theory. Part II - Implementation. Part III - Applications, ASME, Transactions, Journal of Dynamic Systems, Measurement, and Control, vol. 107, p. 1-24, 1985.

Appendix A

Origin-insertion coordinates of musculotendons of lower limb by cadaver study* (cm)

Number & Musculotendon**	X Coordinate	Y Coordinate	Z Coordinate	Reference frame
	Mean ± S.D.	Mean ± S.D.	Mean ± S.D.	
1 Psoas origin	-4.12 ± 0.80	18.73 ± 0.49	-5.23 ± 0.47	Pelvis
2 Tensor fasciae latae origin	4.07 ± 0.88	5.84 ± 0.06	5.06 ± 0.38	
3 Gluteus medius front origin	-0.35 ± 2.41	9.83 ± 0.13	3.09 ± 0.71	
4 Gluteus medius rear origin	-4.18 ± 1.24	8.04 ± 1.14	-1.37 ± 1.27	
5 Guteus minimus front origin	2.50 ± 1.45	4.89 ± 0.84	-1.37 ± 1.27	
6 Gluteus minimus rear origin	-1.75 ± 0.67	4.21 ± 1.09	0.56 ± 0.55	
7 Gluteus maximus upper origin	-7.07 ± 1.17	10.87 ± 1.70	-3.34 ± 1.08	
8 Gluteus maximus medium origin	-8.16 ± 0.23	5.40 ± 2.49	-5.40 ± 1.72	
9 Gluteus maximus lower origin	-8.76 ± 0.22	0.43 ± 1.39	-6.24 ± 0.50	
10 Gluteus maximus lower sequential origin	-6.10 ± 0.99	-6.67 ± 1.83	-1.33 ± 0.98	
11 Iliacus origin	-0.85 ± 0.33	7.98 ± 0.25	1.41 ± 0.08	
12 Iliopsoas effective origin	3.25 ± 0.90	1.05 ± 0.39	0.28 ± 0.23	
13 Sartorius origin	4.91 ± 0.32	5.44 ± 0.86	4.61 ± 0.48	
14 Rectus femoris origin	4.17 ± 0.50	2.59 ± 0.07	2.18 ± 0.50	
15 Pectineus origin	3.73 ± 0.58	-2.10 ± 0.88	-4.24 ± 0.42	
16 Adductor longus origin	2.23 ± 1.20	-4.47 ± 1.43	-6.06 ± 0.12	
17 Adductor brevis origin	3.32 ± 0.33	-4.50 ± 0.08	-6.11 ± 0.06	
18 Gracilis origin	0.80 ± 1.41	-6.29 ± 0.07	-5.65 ± 1.26	
19 Long head origin of biceps femoris	-5.52 ± 1.13	-5.44 ± 1.29	-1.68 ± 0.08	
20 Semitendinosus origin	-5.52 ± 1.13	-5.44 ± 1.29	-1.68 ± 0.08	
21 Semimembranosus origin	-4.18 ± 0.07	-5.04 ± 1.73	-0.59 ± 0.66	
22 Adductor magnus origin	-4.02 ± 1.46	-6.80 ± 0.16	-2.62 ± 1.06	
23 Musculus obturator externus origin	-0.44 ± 0.03	-4.27 ± 0.07	-3.55 ± 0.08	
24 Obturator externus effective origin	-5.50 ± 0.06	-1.72 ± 1.12	-2.09 ± 0.42	
25 Quadratus femoris origin	-3.65 ± 0.69	-5.36 ± 0.78	-1.23 ± 0.85	
26 Piriformis origin	-6.45 ± 1.45	3.65 ± 1.62	-5.44 ± 1.23	
27 Iliopsoas insertion	−1.93 ± 0.33	33.17 ± 2.18	1.16 ± 0.76	Pelvis

28 Gluteus maximus upper insertion	−1.36 ± 0.13	33.97 ± 2.18	5.97 ± 0.40	
29 Gluteus maximus medium insertion	−0.73 ± 0.30	29.30 ± 1.20	4.69 ± 0.79	
30 Gluteus maximus lower insertion	−0.25 ± 0.14	23.87 ± 0.43	3.51 ± 0.42	
31 Gluteus medius insertion	−0.72 ± 0.02	36.86 ± 0.91	6.97 ± 0.12	
32 Guteus minimus insertion	−1.49 ± 0.13	36.58 ± 3.63	6.85 ± 0.61	
33 Obturator externus insertion	−2.55 ± 0.02	37.22 ± 3.63	3.74 ± 0.26	
34 Musculus obturator externus insertion	−2.55 ± 0.02	37.22 ± 3.63	3.74 ± 0.26	
35 Piriformis insertion	−2.48 ± 0.18	38.33 ± 3.03	4.38 ± 0.55	
36 Quadratus femoris insertion	−2.83 ± 0.32	33.41 ± 4.88	3.45 ± 0.21	
37 Pectineus insertion	−0.80 ± 0.55	28.79 ± 3.97	2.36 ± 0.24	
38 Adductor longus insertion	0.21 ± 0.36	18.36 ± 4.31	1.70 ± 0.24	
39 Adductor brevis insertion	−0.57 ± 0.09	20.44 ± 8.31	2.56 ± 0.04	
40 Adductor magnus upper insertion	−0.85 ± 0.21	25.91 ± 3.51	3.28 ± 0.06	
41 Adductor magnus lower insertion	−0.78 ± 0.97	2.30 ± 0.37	−3.48 ± 0.13	
42 Adductor magnus medium insertion	0.65 ± 0.22	12.67 ± 0.57	2.34 ± 0.05	
43 Short head of biceps femoris origin	0.65 ± 0.22	12.67 ± 0.57	2.34 ± 0.05	
44 Vastus intermedius origin	2.75 ± 0.25	20.83 ± 1.45	2.33 ± 0.16	
45 Vastus medialis rigin	1.54 ± 0.34	20.78 ± 1.20	1.17 ± 0.34	
46 Vastus lateralis origin	2.23 ± 0.37	20.50 ± 1.00	3.43 ± 0.11	
47 Patella upper limbus point	4.70 ± 0.04	3.64 ± 0.74	−0.40 ± 0.58	
48 Biceps femoris effective origin	−0.04 ± 0.08	0.03 ± 0.22	4.15 ± 0.46	
49 Popliteus origin	−0.04 ± 0.08	0.03 ± 0.22	4.15 ± 0.46	
50 Lateral head origin of gastrocnemius	−0.23 ± 0.26	2.17 ± 0.81	2.38 ± 0.16	
51 Medial head origin of gastrocnemius	−0.35 ± 0.57	2.72 ± 0.41	−2.88 ± 1.07	
52 Lateral head effective origin of gastrocnemius	−2.11 ± 0.00	0.60 ± 0.36	−2.88 ± 1.07	
53 Medial head effective origin of gastrocnemius	−2.41 ± 0.58	0.56 ± 0.86	−2.04 ± 0.50	
54 Sartorius effective origin	−2.37 ± 0.93	−0.42 ± 0.32	−3.78 ± 0.15	
55 Gracilis effective origin	−3.12 ± 0.90	−0.25 ± 0.12	−3.59 ± 0.55	
56 Semitendinosus effective origin	−3.12 ± 0.90	−0.25 ± 0.12	−3.59 ± 0.55	
57 Semimembranosus effective origin	−3.12 ± 0.90	−0.25 ± 0.12	−3.59 ± 0.55	
58 Patella lower limbus point	5.10 ± 0.17	−1.30 ± 4.21	0.23 ± 0.79	
59 Quadriceps femoris insertion	4.34 ± 0.69	−7.10 ± 3.59	0.25 ± 0.26	
60 Biceps femoris insertion	−0. 33 ± 1.75	31.68 ± 3.11	4.99 ± 0.42	Femur
61 Tensor fasciae latae insertion	2.21 ± 1.43	32.62 ± 3.92	3.69 ± 0.40	
62 Sartorius effective insertion	−0.55 ± 1.29	30.17 ± 3.63	−1.63 ± 1.18	

63 Semitendinosus effective insertion	−0.55 ± 1.29	30.17 ± 3.63	−1.63 ± 1.18	
64 Semimembranosus effective insertion	−0.55 ± 1.29	30.17 ± 3.63	−1.63 ± 1.18	
65 Gracilis effective insertion	−0.55 ± 1.29	30.17 ± 3.63	−1.63 ± 1.18	
66 Sartorius insertion	1.38 ± 0.90	29.10 ± 4.88	−1.61 ± 0.82	
67 Semitendinosus origin	1.38 ± 0.90	29.10 ± 4.88	−1.61 ± 0.82	
68 Semimembranosus origin	1.38 ± 0.90	29.10 ± 4.88	−1.61 ± 0.82	
69 Gracilis insertion	1.38 ± 0.90	29.10 ± 4.88	−1.61 ± 0.82	
70 Popliteus effective insertion	−0.54 ± 0.22	26.83 ± 3.15	−1.06 ± 0.57	
71 Popliteus insertion	−0.54 ± 0.22	26.83 ± 3.15	−1.06 ± 0.57	
72 Peroneus longus origin	−0.82 ± 0.93	21.05 ± 6.60	3.55 ± 0.45	
73 Peroneus brevis origin	−0.99 ± 0.69	6.24 ± 2.63	2.67 ± 0.36	
74 Tibialis anterior origin	1.82 ± 0.40	20.91 ± 2.79	0.68 ± 0.35	
75 Extensor digitorum longus origin	0.37 ± 0.28	19.03 ± 1.84	2.88 ± 0.43	
76 Extensor hallucis longus origin	1.68 ± 0.20	16.58 ± 4.52	1.48 ± 0.80	
77 Tibialis anterior effective origin	2.08 ± 0.07	1.15 ± 0.04	−2.07 ± 1.05	
78 Extensor digitorum longus effective origin	2.28 ± 0.33	0.96 ± 0.70	1.14 ± 0.56	
79 Extensor hallucis longus effective origin	2.42 ± 0.45	1.41 ± 0.66	−0.47 ± 0.83	
80 Soleus origin	0.60 ± 0.36	24.72 ± 0.74	0.65 ± 0.27	
81 Posterior tibial origin	0.60 ± 0.36	24.72 ± 0.74	0.65 ± 0.27	
82 Flexor digitorum longus origin	−0.66 ± 0.90	16.92 ± 0.80	0.95 ± 1.16	
83 Flexor hallucis longus origin	−1.08 ± 0.15	12.47 ± 1.44	2.18 ± 0.29	
84 Posterior tibial effective origin	−1.17 ± 0.25	−0.26 ± 0.52	−2.46 ± 0.13	
85 Flexor digitorum longus effective origin	−2.07 ± 0.52	0.52 ± 1.07	−1.16 ± 0.65	
86 Flexor hallucis longus effective origin	−2.06 ± 0.63	0.58 ± 0.52	0.57 ± 0.41	
87 Peroneus longus effective origin	−1.87 ± 0.79	−1.07 ± 0.48	1.99 ± 0.11	
88 Peroneus brevis effective origin	−1.87 ± 0.79	−1.07 ± 0.48	1.99 ± 0.11	
89 Peroneus tertius effective origin	1.72 ± 0.14	0.64 ± 0.15	2.40 ± 0.07	
90 Tibialis anterior insertion	6.82 ± 1.17	-3.52 ± 0.08	-1.47 ± 0.12	Tibia
91 Extensor digitorum longus effective insertion	10.80 ± 0.45	-4.69 ± 0.68	-1.47 ± 0.12	
92 Extensor hallucis longus effective insertion	12.76 ± 0.73	-3.78 ± 1.15	2.57 ± 0.11	
93 Posterior tibial insertion	3.37 ± 2.14	-3.19 ± 0.22	-1.45 ± 0.08	
94 Flexor digitorum longus effective insertion	0.54 ± 0.02	−2.98 ± 0.13	−0.53 ± 0.07	
95 Flexor hallucis longus effective insertion	0.54 ± 0.02	−2.98 ± 0.13	−0.53 ± 0.07	
96 Peroneus longus effective insertion	4.51 ± 0.21	−5.90 ± 0.32	4.02 ± 0.81	
97 Peroneus brevis effective insertion	4.51 ± 0.21	−5.90 ± 0.32	4.02 ± 0.81	
98 Peroneus tertius effective insertion	5.19 ± 0.01	−4.72 ± 0.32	4.34 ± 0.11	

99 Triceps surae insertion	−4.06 ± 0.08	−4.68 ± 0.23	0.51 ± 0.08	
Joint Central Distance	Hip ~ Knee	40.82 ± 2.35	Knee ~ Ankle	38.00 ± 2.37

* The coordinates derived from Damao Shan (2003) unless otherwise noted.

** All of musculotendons and skeletons were named according to the reference - Manual of Structural Kinesiology (R.T. Floyd, McGraw-Hill, New York, 2007).

Appendix B

Skeletal morphological parameters of lower limb by cadaver study*

Table B1. Pelvic morphological parameters (cm)

Item	A1	A2	A3	A4	A5	A6	A7	A8
Mean value	23.74	8.76	27.72	15.84	20.36	21.22	14.84	17.08
S.D.	± 0.82	± 0.49	± 0.49	± 0.49	± 0.53	± 0.52	± 0.46	± 0.96

A1 is the intervals of the left anterior superior iliac spine to the right one.

A2 is the intervals between the left posterior superior iliac spine and the right one.

A3 is the intervals of the two iliac crest tuberosities.

A4 is the intervals between anterior superior iliac spine and posterior superior iliac spine.

A5 is the intervals between iliac crest tuberosity and coccyx apex.

A6 is the height of pelvic pedestal (intervals between ischium tuberosity and the upper limb of iliac crest).

A7 is the perpendicular distance from anterior superior iliac spine to ischium tuberosity (seating posture).

A8 is the perpendicular distance from posterior superior iliac spine to ischium tuberosity (seating postrure).

Table B2. Femoral morphological parameters (cm)

Item	B1	B2	B3	B4	B5	B6	B7	B8
Mean value	4.93	7.54	7.50	41.47	41.13	42.09	8.93	8.93
S.D.	± 0.16	± 0.18	± 0.27	± 0.97	± 1.55	± 1.50	± 0.18	± 0.17

B1 is the width of patella.

B2 is the intervals between the middle point of patella and lateral epicondyle.

B3 is the intervals between the middle point of patella and medial epicondyle.

B4 is the intervals between greater trochanter and the middle point of patella.

B5 is the intervals of greater trochanter apex and lateral epicondyle.

B6 is the intervals of greater trochanter apex and medial epicondyle.

B7 is the intervals between medial epicondyle and lateral epicondyle.

B8 is the vertical breadth of medial epicondyle and lateral epicondyle (Perpendicular distance from the frontal mid-point of patella to the link between the posterior border of medial epicondyle

and the posterior border of lateral epicondyle).

Table B3. Tibial morphological parameters (cm)

Item	C1	C2	C3	C4	C5	C6	C7	C8
Mean value	8.23	8.79	6.84	34.56	38.47	32.75	6.85	9.37
S.D.	± 0.23	± 0.27	± 0.09	± 1.38	± 1.39	± 1.68	± 0.38	± 0.40

C1 is the condyle intervals (transverse breadth of lateral condyle).

C2 is the vertical breadth of lateral condyle and medial condyle.

C3 is the width of malleolus (intervals between lateral malleolus to medial malleolus), C4 is the intervals from the head of fibula to medial malleolus.

C5 is the intervals between medial condyle and medial malleolus.

C6 is the intervals between tibial tuberosity and malleolus (between the middle point of tibial tuberosity and the middle point of the link of lateral malleolus and medial malleolus).

C7 is the tuberosity intervals of the head of fibula.

C8 is the tibial tuberosity intervals of medical condyle.

Table B4. Foot morphological parameters (cm)

Item	D1	D2	D3	D4	D5	D6	D7	D8
Mean value	7.81	7.63	17.99	8.53	6.84	14.11	14.54	2.11
S.D.	± 0.34	± 0.32	± 0.54	± 0.20	± 0.09	± 0.51	± 1.05	± 0.05

D1 is the foot height, namely perpendicular distance from the inner surface of lateral malleolus to the sole plane.

D2 is the intervals between tuber calcaneus and inner surface of lateral malleolus.

D3 is the foot length from the tuber calcaneus to middle point of first phalanx distal.

D4 is the foot width, namely intervals between the middle point of first phalanx distal and the middle point of fifth phalanx distal).

D5 is the malleolus width (intervals between lateral malleolus and medial malleolus).

D6 is the intervals between fifth metatarsals and lateral malleolus.

D7 is the intervals between first metatarsals and medial malleolus.

D8 is the ratio of foot length to foot width.

*The parameters derived from cadaver study by Dr. Damao Shan; all of musculotendons and skeletons were named according to the reference - Manual of Structural Kinesiology (R.T. Floyd, McGraw-Hill, New York, 2007).

Appendix C

Regression equations of origin-insertion coordinate by skeletal morphological parameters* (cm)

1 Psoas origin $X1 = 18.52 - 0.63 \times A1 - 0.42 \times A8, \quad (r = 0.853)$ ** $Y1 = -12.26 + 1.51 \times A7 - 0.66 \times A1, \quad (r = 0.986)$ $Z1 = 18.76 - 0.83 \times A5 - 0.29 \times A1, \quad (r = 0.888)$	2 Tensor fasciae latae origin $X2 = 2.42 - 0.27 \times A1 + 0.36 \times A5, \quad (r = 0.913)$ $Y2 = -25.25 + 1.18 \times A8 + 1.26 \times A2, \quad (r = 0.972)$ $Z2 = 8.4 - 0.7 \times A4 + 0.32 \times A1, \quad (r = 0.993)$
3 Gluteus medius front origin $X3 = 22.24 - 0.87 \times A5 - 0.44 \times A7, \quad (r = 0.989)$ $Y3 = -54.9 + 2.85 \times A4 + 0.82 \times A1, \quad (r = 0.947)$ $Z3 = 16.69 - 0.83 \times A8, \quad (r = 0.938)$	4 Gluteus medius rear origin $X4 = 1.93 - 0.53 \times A5 + 0.16 \times A1, \quad (r = 0.939)$ $Y4 = -34.54 + 1.63 \times A8 + 1.77 \times A2, \quad (r = 0.955)$ $Z4 = 32.19 - 1.28 \times A6 - 0.64 \times A2, \quad (r = 0.964)$
5 Guteus minimus front origin $X5 = 18.52 - 1.06 \times A5 - 0.24 \times A2, \quad (r = 0.993)$ $Y5 = -23.31 + 1.21 \times A8 + 0.93 \times A2, \quad (r = 0.977)$ $Z5 = 3.7 + 0.18 \times A1 - 0.22 \times A5, \quad (r = 0.956)$	6 Guteus minimus rear origin $X6 = 18.64 - 0.71 \times A5 - 0.28 \times A1, \quad (r = 0.871)$ $Y6 = -16.97 + 0.81 \times A8 + 0.92 \times A2, \quad (r = 0.845)$ $Z6 = -5.81 + 0.77 \times A2, \quad (r = 0.929)$
7 Gluteus maximus upper origin $X7 = 15.82 - 1.06 \times A5 - 0.24 \times A2, \quad (r = 0.993)$ $Y7 = -23.99 + 1.18 \times A6 + 0.37 \times A1, \quad (r = 0.938)$ $Z7 = 8.36 - 0.65 \times A6 + 0.12 \times A1, \quad (r = 0.914)$	8 Gluteus maximus medium origin $X8 = -2.45 - 0.56 \times A5 + 0.23 \times A1, \quad (r = 0.971)$ $Y8 = -18.7 + 0.64 \times A1 + 0.42 \times A8, \quad (r = 0.983)$ $Z8 = 20.9 - 1.01 \times A8 - 0.89 \times A2, \quad (r = 0.926)$
9 Gluteus maximus lower origin $X9 = 3.55 - 0.82 \times A7, \quad (r = 0.949)$ $Y9 = -37.47 + 1.22 \times A1 + 0.39 \times A5, \quad (r = 0.998)$ $Z9 = 6.82 - 0.58 \times A8 - 0.32 \times A2, \quad (r = 0.914)$	10 Gluteus maximus lower sequential origin $X10 = -8.83 + 0.47 \times A4 - 0.27 \times A2, \quad (r = 0.948)$ $Y10 = -12.16 + 0.61 \times A7 - 0.11 \times A5, \quad (r = 0.948)$ $Z10 = 23.13 - 0.9 \times A6 - 0.89 \times A2, \quad (r = 0.934)$
11 Iliacus origin $X11 = 7.88 - 0.41 \times A7 - 0.18 \times A4, \quad (r = 0.91)$ $Y11 = -40.79 + 2.19 \times A4 + 0.59 \times A1, \quad (r = 0.927)$ $Z11 = -1.57 + 0.2 \times A7, \quad (r = 0.709)$	12 Iliopsoas effective origin $X12 = 6.18 - 0.16 \times A1, \quad (r = 0.916)$ $Y12 = -18.13 + 0.3 \times A1 + 0.44 \times A7 + 0.3 \times A8, \quad (r = 0.938)$ $Z12 = 9.14 - 0.27 \times A5 + 0.18 \times A1, \quad (r = 0.775)$
13 Sartorius origin $X13 = 10.72 - 0.34 \times A1 + 0.11 \times A6, \quad (r = 1.00)$ $Y13 = -60.35 + 2.48 \times A5 + 0.67 \times A1, \quad (r = 0.978)$ $Z13 = 7.4 - 0.77 \times A4 + 0.38 \times A1, \quad (r = 0.999)$	14 Rectus femoris origin $X14 = 13.91 - 0.43 \times A1, \quad (r = 0.956)$ $Y14 = -9.74 + 0.9 \times A4 + 0.12 \times A1, \quad (r = 0.904)$ $Z14 = 3.19 - 0.27 \times A5 + 0.18 \times A1, \quad (r = 0.89)$
15 Pectineus origin $X15 = -4.33 + 0.42 \times A5, \quad (r = 0.894)$ $Y15 = -52.06 + 1.77 \times A5 + 0.56 \times A1, \quad (r = 0.975)$ $Z15 = 11.77 - 0.8 \times A5, \quad (r = 0.919)$	16 Adductor longus origin $X16 = -19.07 + 0.89 \times A4 + 0.27 \times A1, \quad (r = 0.87)$ $Y16 = -56.08 + 1.68 \times A5 + 0.69 \times A1, \quad (r = 0.982)$ $Z16 = 5.13 - 0.41 \times A8 - 0.47 \times A2, \quad (r = 0.745)$
17 Adductor brevis origin $X17 = -2.46 + 0.23 \times A4 + 0.11 \times A8, \quad (r = 0.972)$ $Y17 = -42.06 + 1.51 \times A5 + 0.29 \times A1, \quad (r = 0.972)$ $Z17 = 2.55 - 0.42 \times A5, \quad (r = 0.805)$	18 Gracilis origin $X18 = -21.56 + 0.88 \times A5 + 0.14 \times A1, \quad (r = 0.95)$ $Y18 = 10.02 + 2.99 \times A7 - 2.19 \times A3, \quad (r = 0.958)$ $Z18 = 18.9 - 0.93 \times A6 - 0.45 \times A2, \quad (r = 0.861)$
19 Long head origin of biceps femoris $X19 = -19.8 + 0.77 \times A4 + 0.14 \times A2, \quad (r = 0.967)$ $Y19 = -5.22 + 0.82 \times A2 - 0.41 \times A4, \quad (r = 0.977)$ $Z19 = 48.63 - 1.86 \times A6 - 1.24 \times A2, \quad (r = 0.906)$	21 Semimembranosus origin $X21 = 33.35 - 1.84 \times A7 - 0.43 \times A1, \quad (r = 0.969)$ $Y21 = 43.43 + 3.56 \times A2 - 2.83 \times A3, \quad (r = 0.979)$ $Z21 = 18.44 - 0.31 \times A1 - 0.43 \times A7 - 0.29 \times A8, \quad (r = 0.913)$
22 Adductor magnus origin $X22 = -15.84 + 0.63 \times A8, \quad (r = 0.963)$ $Y22 = -16.46 + 0.28 \times A1 + 0.32 \times A2, \quad (r = 0.962)$ $Z22 = 17.01 - 0.89 \times A6, \quad (r = 0.898)$	23 Musculus obturator externus origin $X23 = 6.75 - 0.3 \times A1, \quad (r = 0.817)$ $Y23 = -17.18 + 0.64 \times A5, \quad (r = 0.843)$ $Z23 = 21.17 - 0.31 \times A1 - 0.7 \times A7 - 0.41 \times A8, \quad (r = 0.899)$
24 Obturator externus effective origin	25 Quadratus femoris origin

$X\,24 = 1.98 - 0.29 \times A7 - 0.14 \times A1, \quad (r = 0.873)$ $Y\,24 = -14.65 + 0.27 \times A1 + 0.38 \times A7, (r = 0.942)$ $Z\,24 = 33.51 - 1.28 \times A6 - 0.93 \times A2, \quad (r = 0.884)$	$X\,25 = 4.77 - 0.55 \times A2 - 0.17 \times A1, \quad (r = 0.909)$ $Y\,25 = -20.38 + 0.34 \times A1 + 0.43 \times A7, (r = 0.931)$ $Z\,25 = 28.19 - 1.13 \times A6 - 0.55 \times A2, \quad (r = 0.932)$
26 Piriformis origin $X\,26 = 65.2 - 3.56 \times A3 + 2.97 \times A2, \quad (r = 0.984)$ $Y\,26 = -45.7 + 1.72 \times A6 + 0.49 \times A1, \quad (r = 0.97)$ $Z\,26 = 15.73 - 0.29 \times A1 - 0.5 \times A7 - 0.35 \times A8, (r = 0.92)$	27 Iliopsoas insertion $X\,27 = -23.38 + 3.26 \times B8 - 1.6 \times B1, (r = 0.977)$ $Y\,27 = 0.98 + 1.37 \times B6 - 0.58 \times B4, \quad (r = 0.992)$ $Z\,27 = 2.46 - 0.04 \times B6, \quad (r = 0.73)$
28 Gluteus maximus upper insertion $X\,28 = -7.05 + 0.14 \times B4, \quad (r = 0.54)$ $Y\,28 = -6.43 + 0.99 \times B6, \quad (r = 0.979)$ $Z\,28 = 7.74 + 0.92 \times B1 + 0.15 \times B4 - 1.42 \times B8, (r = 0.855)$	29 Gluteus maximus medium insertion $X\,29 = 6.34 - 0.97 \times B3, \quad (r = 0.948)$ $Y\,29 = 6.75 + 3.64 \times B7 - 1.21 \times B3, \quad (r = 0.988)$ $Z\,29 = 6.57 - 0.07 \times B1 + 0.01 \times B4 - 0.3 \times B8, (r = 0.307)$
30 Gluteus maximus lower insertion $X\,30 = 3.35 - 0.71 \times B1, \quad (r = 0.629)$ $Y\,30 = 40.7 - 6.44 \times B1 + 1.7 \times B8, (r = 0.982)$ $Z\,30 = 15.55 - 1.64 \times B2, \quad (r = 0.837)$	31 Gluteus medius insertion $X\,31 = 7.33 - 2.17 \times B1 + 1.94 \times B8, (r = 0.838)$ $Y\,31 = 0.47 + 0.88 \times B6, \quad (r = 0.986)$ $Z\,31 = 2.38 + 0.11 \times B6, \quad (r = 0.78)$
32 Guteus minimus insertion $X\,32 = 6.96 - 1.14 \times B3, \quad (r = 0.835)$ $Y\,32 = -1.4 + 0.96 \times B6, \quad (r = 0.984)$ $Z\,32 = 3.73 - 0.68 \times B3 + 0.87 \times B8, (r = 0.91)$	33 Obturator externus insertion $X\,33 = 5.18 - 0.72 \times B3 - 0.46 \times B!, \quad (r = 0.94)$ $Y\,33 = -38.15 + 2.68 \times B4 - 0.81 \times B5, (r = 0.997)$ $Z\,33 = 34.46 - 1.99 \times B3 - 1.79 \times B7, \quad (r = 0.963)$
35 Piriformis insertion $X\,35 = -20.25 - 1.98 \times B7, \quad (r = 0.932)$ $Y\,35 = -26.1 + 1.61 \times B4, \quad (r = 0.981)$ $Z\,35 = -2.41 - 1.23 \times B3 + 1.83 \times B8, (r = 0.955)$	36 Quadratus femoris insertion $X\,36 = 34.72 - 2.48 \times B3 - 2.15 \times B7, (r = 0.945)$ $Y\,36 = -30.41 + 1.62 \times B4, \quad (r = 0.968)$ $Z\,36 = -8.2 + 0.17 \times B5 + 0.63 \times B3, \quad (r = 0.777)$
37 Pectineus insertion $X\,37 = -16.53 + 2.11 \times B8 - 0.7 \times B!, (r = 0.865)$ $Y\,37 = 24.59 - 2.26 \times B3 + 2.68 \times B7, (r = 0.951)$ $Z\,37 = 5.29 - 0.07 \times B6, \quad (r = 0.826)$	38 Adductor longus insertion $X\,38 = -13.86 + 1.55 \times B7, \quad (r = 0.779)$ $Y\,38 = -38.15 + 2.68 \times B4 - 0.81 \times B5, (r = 0.981)$ $Z\,38 = 34.46 - 1.99 \times B3 - 1.79 \times B7, \quad (r = 0.931)$
39 Adductor brevis insertion $X\,39 = -9.97 + 1.05 \times B7, \quad (r = 0.843)$ $Y\,39 = 54.36 - 3.74 \times B3, \quad (r = 0.971)$ $Z\,39 = 10.39 - 0.19 \times B5, \quad (r = 0.828)$	40 Adductor magnus upper insertion $X\,40 = -6.86 + 1.16 \times B7 - 0.91 \times B1, (r = 0.937)$ $Y\,40 = 29.23 - 2.26 \times B3 + 1.8 \times B7, \quad (r = 0.976)$ $Z\,40 = 12.19 - 0.22 \times B5, \quad (r = 0.802)$
41 Adductor magnus lower insertion $X\,41 = -22.35 + 1.53 \times B3 + 1.21 \times B7, (r = 0.876)$ $Y\,41 = -2.82 + 0.84 \times B8 - 0.54 \times B1, (r = 0.743)$ $Z\,41 = -0.56 - 0.54 \times B4 + 2.14 \times B8, (r = 0.902)$	42 Adductor magnus medium insertion $X\,42 = 18.25 - 2.59 \times B8 + 0.63 \times B7, (r = 0.958)$ $Y\,42 = -63.91 + 7.3 \times B7 + 1.3 \times B8, \quad (r = 0.987)$ $Z\,42 = -0.91 + 0.43 \times B3, \quad (r = 0.728)$
44 Vastus intermedius origin $X\,44 = -11.33 + 1.6 \times B7 - 0.46 \times B1, (r = 0.916)$ $Y\,44 = 40.74 - 2.52 \times B3, \quad (r = 0.885)$ $Z\,44 = 5.15 - 0.6 \times B1, \quad (r = 0.662)$	45 Vastus medialis rigin $X\,45 = -29.81 + 0.76 \times B4, \quad (r = 0.961)$ $Y\,45 = 47.01 - 3.39 \times B3, \quad (r = 0.956)$ $Z\,45 = 1.29 - 0.26 \times B1 - 0.03 \times B4 + 0.27 \times B8, (r = 0.61)$
46 Vastus lateralis origin $X\,46 = -19.45 - 3.93 \times B7 - 0.33 \times B6, (r = 0.957)$ $Y\,46 = -48.99 - 3.71 \times B3, \quad (r = 0.941)$ $Z\,46 = -2.21 + 0.64 \times B7, \quad (r = 0.708)$	48 Biceps femoris effective origin $X\,48 = -4.2 + 0.33 \times B7 + 0.17 \times B3, (r = 0.995)$ $Y\,48 = 6.89 - 1.42 \times B1, \quad (r = 0.785)$ $Z\,48 = -2.31 + 0.76 \times B7, \quad (r = 0.778)$
50 Lateral head origin of gastrocnemius $X\,50 = -15.65 + 0.94 \times B3 + 0.96 \times B7, (r = 0.984)$ $Y\,50 = -20.78 + 2.14 \times B8 + 0.1 \times B6, \quad (r = 0.847)$ $Z\,50 = 7.69 - 0.78 \times B8 + 0.37 \times B1, \quad (r = 0.742)$	51 Medial head origin of gastrocnemius $X\,51 = 0.58 + 1.81 \times B1 - 1.06 \times B8, \quad (r = 0.95)$ $Y\,51 = -29.02 + 3.94 \times B8 - 0.42 \times B2, (r = 0.975)$ $Z\,51 = 37.12 - 2.96 \times B2 - 1.89 \times B8, \quad (r = 0.983)$
52 Lateral head effective origin of gastrocnemius $X\,52 = 9.81 - 1.04 \times B2 - 0.46 \times B8, \quad (r = 0.953)$ $Y\,52 = 12.86 - 1.33 \times B1 - 0.67 \times B7, \quad (r = 0.749)$ $Z\,52 = 7.32 - 0.35 \times B1 - 0.04 \times B4 - 0.11 \times B8, (r = 0.585)$	53 Medial head effective origin of gastrocnemius $X\,53 = 2.14 + 1.25 \times B3 - 1.6 \times B8, \quad (r = 0.97)$ $Y\,53 = -1.88 - 1.43 \times B1 + 0.99 \times B8, (r = 0.867)$ $Z\,53 = 15.83 - 4.54 \times B2 + 0.4 \times B6, \quad (r = 0.934)$
54 Sartorius effective origin $X\,54 = -21.06 + 0.27 \times B5 + 1.08 \times B3, (r = 0.925)$ $Y\,54 = 2.6 - 0.56 \times B1, \quad (r = 0.566)$ $Z\,54 = -5.72 - 0.1 \times B5 + 0.65 \times B8, \quad (r = 0.852)$	55 Gracilis effective origin $X\,55 = 2.16 + 1.88 \times B1 - 1.56 \times B8, (r = 0.975)$ $Y\,55 = 7.85 - 0.13 \times B5 - 0.35 \times B3, (r = 0.841)$ $Z\,55 = 12.05 - 1.59 \times B2 - 0.45 \times B3, (r = 0.90)$
60 Biceps femoris insertion $X\,60 = -14.43 + 0.5 \times C5 - 0.55 \times C7, (r = 0.947)$ $Y\,60 = -0.09 + 4.13 \times C1, \quad (r = 0.941)$ $Z\,60 = -4.99 + 1.26 \times C3 + 0.19 \times C2, (r = 0.855)$	61 Tensor fasciae latae insertion $X\,33 = 5.18 - 0.72 \times B3 - 0.46 \times B!, \quad (r = 0.94)$ $Y\,33 = -38.15 + 2.68 \times B4 - 0.81 \times B5, (r = 0.997)$ $Z\,33 = 34.46 - 1.99 \times B3 - 1.79 \times B7, \quad (r = 0.963)$
62 Sartorius effective insertion	66 Sartorius insertion

$X62 = 2.47 - 0.1 \times C5, \quad (r = 0.551)$ $Y62 = 5.88 + 0.69 \times C6 + 0.48 \times C2, (r = 0.986)$ $Z62 = -7.08 + 0.92 \times C3, \quad (r = 0.498)$	$X66 = -2.49 - 0.05 \times C2 + 0.26 \times C8, (r = 0.380)$ $Y66 = 22.73 + 0.73 \times C4 - 1.76 \times C2, (r = 0.964)$ $Z66 = 3.6 - 0.15 \times C5, \quad (r = 0.813)$
70 Popliteus effective insertion $X70 = 4.34 - 0.57 \times C1, \quad (r = 0.642)$ $Y70 = 11.85 - 0.95 \times C1 - 0.49 \times C2, (r = 0.996)$ $Z70 = 6.46 - 0.87 \times C1, \quad (r = 0.923)$	72 Peroneus longus origin $X72 = -9.91 + 0.28 \times C4, (r = 0.854)$ $Y72 = 5.595 + 2.445 \times C1, (r = 0.803)$ $Z72 = 6.42 - 0.37 \times C7, \quad (r = 0.699)$
73 Peroneus brevis origin $X73 = -6.17 + 0.65 \times C2, \quad (r = 0.634)$ $Y73 = 11.85 - 0.95 \times C2 + 0.12 \times C5, (r = 0.771)$ $Z73 = 5.44 - 0.37 \times C7, \quad (r = 0.776)$	74 Tibialis anterior origin $X74 = -3.63 + 0.17 \times C4, \quad (r = 0.693)$ $Y74 = 23.49 - 2.02 \times C8 + 2.66 \times C3, (r = 0.978)$ $Z74 = -4.99 + 1.26 \times C3 + 0.19 \times C2, (r = 0.695)$
75 Extensor digitorum longus origin $X75 = -9.58 + 0.25 \times C5, \quad (r = 0.908)$ $Y75 = 55.51 - 6.39 \times C3 + 0.98 \times C2, (r = 0.911)$ $Z75 = 1.84 + 0.35 \times C2 - 0.05 \times C6, \quad (r = 0.778)$	76 Extensor hallucis longus origin $X76 = -3.99 + 0.85 \times C3, \quad (r = 0.632)$ $Y76 = -2.08 + 1.9 \times C7 + 1.01 \times C2, (r = 0.958)$ $Z76 = 8.96 - 0.43 \times C7 - 0.58 \times C2, (r = 0.916)$
77 Tibialis anterior effective origin $X77 = 7.03 - 0.57 \times C2, \quad (r = 0.714)$ $Y77 = 10.18 - 1.03 \times C2, \quad (r = 0.729)$ $Z77 = -5.74 + 0.08 \times C5, (r = 0.56)$	78 Extensor digitorum longus effective origin $X78 = 20.84 - 2.32 \times C3 - 0.28 \times C2, \quad (r = 0.891)$ $Y78 = 3.83 + 0.04 \times C2 - 0.04 \times C5 - 0.13 \times C8, (r = 0.522)$ $Z78 = 0.404 + 0.09 \times C6 - 0.29 \times C2, \quad (r = 0.874)$
79 Extensor hallucis longus effective origin $X79 = 12.11 - 0.67 \times C2 - 0.09 \times C5, (r = 0.872)$ $Y79 = 11.13 - 0.58 \times C2 - 0.5 \times C1, \quad (r = 0.954)$ $Z79 = -5.59 + 0.13 \times C4, \quad (r = 0.816)$	80 Soleus origin $X80 = 4.51 - 1.05 \times C2 + 0.55 \times C8, \quad (r = 0.913)$ $Y80 = -12.23 + 3.97 \times C1 + 0.55 \times C2, (r = 0.988)$ $Z80 = -1.67 - 0.68 \times C2 + 1.24 \times C3, \quad (r = 0.809)$
82 Flexor digitorum longus origin $X82 = 3.13 - 0.38 \times C1, \quad (r = 0.546)$ $Y82 = -14.64 + 2.67 \times C1 + 1.48 \times C3, \quad (r = 0.995)$ $Z82 = 1.399 - 0.29 \times C2 - 0.02 \times C5 + 0.21 \times C8, (r = 0.713)$	83 Flexor hallucis longus origin $X83 = -3.88 - 0.31 \times C2 + 0.08 \times C5 + 0.28C8, (r = 0.608)$ $Y83 = -1.77 + 2.73 \times C1 - 0.22 \times C6, \quad (r = 0.856)$ $Z83 = 1 - 0.67 + 0.26 \times C2 + 0.1 \times C8, \quad (r = 0.352)$
84 Posterior tibial effective origin $X84 = 7.58 - 0.22 \times C5, \quad (r = 0.825)$ $Y84 = 12.25 - 1.38 \times C5, \quad (r = 0.882)$ $Z84 = 4.98 - 0.55 \times C2 - 0.37 \times C7, (r = 0.779)$	85 Flexor digitorum longus effective origin $X85 = -1.74 - 0.05 \times C6 + 0.2 \times C2, (r = 0.885)$ $Y85 = 2.44 - 0.18 \times C5 + 0.65 \times C2, (r = 0.825)$ $Z85 = 10.25 - 0.78 \times C2 - 0.49 \times C1, (r = 0.872)$
86 Flexor hallucis longus effective origin $X86 = 8.498 - 0.18 \times C5 - 0.37 \times C2, (r = 0.937)$ $Y86 = 4.21 - 0.1 \times C6, \quad (r = 0.748)$ $Z86 = 9.04 - 1.17 \times C2 + 0.3 \times C7, \quad (r = 0.949)$	87 Peroneus longus effective origin $X87 = 24.63 - 2.83 \times C3 - 0.75 \times C2, (r = 0.964)$ $Y87 = 3.14 - 0.91 \times C2 + 0.45 \times C8, \quad (r = 0.812)$ $Z87 = -6.1 + 1.75 \times C1 - 0.92 \times C3, \quad (r = 0.96)$
89 Peroneus tertius effective origin $X89 = 11.14 - 1.39 \times C3, \quad (r = 0.705)$ $Y89 = 7.696 - 0.33 \times C8 - 0.45 \times C2, \quad (r = 0.738)$ $Z89 = 1.09 + 0.23 \times C2 + 0.02 \times C5 - 0.14 \times C8, (r = 0.928)$	90 Tibialis anterior insertion $X90 = 9.04 - 1.05 \times D2 + 0.78 \times D4, \quad (r = 0.98)$ $Y90 = -14.34 + 0.54 \times D4 + 1.07 \times D5, (r = 0.738)$ $Z90 = -2.47 + 1.13 \times D2 - 0.9 \times D4, \quad (r = 0.928)$
91 Extensor digitorum longus effective insertion $X91 = 87.19 - 13.6 \times D5 + 2.17 \times D1, \quad (r = 0.989)$ $Y91 = -19.49 + 2.35 \times D4 - 0.39 \times D7, (r = 0.991)$ $Z91 = 1.05 + 0.66 \times D2 - 1.63 \times D8, \quad (r = 0.881)$	92 Extensor hallucis longus effective insertion $X92 = -0.54 + 0.4 \times D3 + 0.96 \times D5, \quad (r = 0.971)$ $Y92 = -16.64 - 1.65 \times D6 + 5.16 \times D5, (r = 0.975)$ $Z92 = 10.63 - 1.33 \times D4 - 0.1 \times D2, \quad (r = 0.992)$
93 Posterior tibial insertion $X93 = 6.05 - 3.32 \times D8 + 0.68 \times D4, (r = 0.719)$ $Y93 = 4.82 - 3.86 \times D8, \quad (r = 0.595)$ $Z93 = -15.34 + 1.82 \times D2, \quad (r = 0.933)$	94 Flexor digitorum longus effective insertion $X94 = -50.3 + 6.45 \times D5 + 0.47 \times D6, (r = 0.984)$ $Y94 = 35.68 - 4.22 \times D5 - 0.55 \times D3, (r = 0.98)$ $Z94 = 11.04 - 1.16 \times D4 - 0.12 \times D7, (r = 0.88)$
96 Peroneus longus effective insertion $X96 = -1.32 + 0.78 \times D2, \quad (r = 0.809)$ $Y96 = -0.63 - 1.63 \times D1 + 1.07 \times D5, (r = 0.979)$ $Z96 = 20.14 - 1.82 \times D4, \quad (r = 0.943)$	98 Peroneus tertius effective insertion $X98 = -21.91 + 7.44 \times D5 - 11.27 \times D8, (r = 0.951)$ $Y98 = 8.29 - 9.07 \times D8 + 0.7 \times D4, \quad (r = 0.98)$ $Z98 = 9.1 - 2.05 \times D4 + 1.85 \times D5, \quad (r = 0.947)$
99 Triceps surae insertion $X98 = 9.74 - 0.9 \times D3 + 0.17 \times D7, \quad (r = 0.994)$ $Y98 = -1.67 + 0.56 \times D7 - 0.61 \times D3, \quad (r = 0.913)$ $Z98 = 10.18 - 1.1 \times D4, \quad (r = 0.998)$	
20 Semitendinosus origin $X20 = X19; \quad Y20 = Y19; \quad Z20 = Z19$	34 Musculus obturator externus insertion $X34 = X33; \quad Y34 = Y33; \quad Z34 = Z33$
43 Short head of biceps femoris origin $X43 = X42; \quad Y43 = Y42; \quad Z43 = Z42$	49 Popliteus origin $X49 = X48; \quad Y49 = Y48; \quad Z49 = Z48$

56 Semitendinosus effective origin $X56 = X55;\ \ Y56 = Y55;\ \ Z56 = Z55$	57 Semimembranosus effective origin $X57 = X55;\ \ Y57 = Y55;\ \ Z57 = Z55$
63 Semitendinosus effective insertion $X63 = X62;\ \ Y63 = Y62;\ \ Z63 = Z62$	64 Semimembranosus effective insertion $X64 = X62;\ \ Y64 = Y62;\ \ Z64 = Z62$
65 Gracilis effective insertion $X65 = X62;\ \ Y65 = Y62;\ \ Z65 = Z62$	67 Semitendinosus origin $X67 = X66;\ \ Y67 = Y66;\ \ Z67 = Z66$
68 Semimembranosus origin $X68 = X66;\ \ Y68 = Y66;\ \ Z68 = Z66$	69 Gracilis insertion $X69 = X66;\ \ Y69 = Y66;\ \ Z69 = Z66$
71 Popliteus insertion $X71 = X70;\ \ Y71 = Y70;\ \ Z71 = Z70$	81 Posterior tibial origin $X88 = X87;\ \ Y88 = Y87;\ \ Z88 = Z87$
88 Peroneus brevis effective origin $X88 = X87;\ \ Y88 = Y87;\ \ Z88 = Z87$	95 Flexor hallucis longus effective insertion $X95 = X94;\ \ Y95 = Y94;\ \ Z95 = Z94$
97 Peroneus brevis effective insertion $X97 = X96;\ \ Y97 = Y96;\ \ Z97 = Z96$	
47 Patella upper limbus point $X47 = 17.1 - 0.14 \times B6 - 0.62 \times B8,\ \ (r = 0.957)$ $Y47 = -0.59 + 0.76 \times B1,\ \ (r = 0.703)$ $Z47 = -10.66 + 1.06 \times B3 + 0.6 \times B1,\ \ (r = 0.946)$	58 Patella lower limbus point $X58 = 26.1 - 1.57 \times C2 - 0.86 \times C1, (r = 0.952)$ $Y58 = 2.71 + 1.25 \times C4 - 0.92 \times C2, (r = 0.998)$ $Z58 = 55.35 - 8.47 \times C3,\ \ (r = 0.937)$
59 Quadriceps femoris insertion $X59 = -5.71 + 1.22 \times C1,\ \ (r = 0.871)$ $Y59 = 4.59 + 1.1 \times C6 - 0.2 \times C5,\ \ (r = 0.998)$ $Z59 = 26.14 - 2.8 \times C3 - 0.82 \times C2,\ \ (r = 0.941)$	
Central distance of hip-knee joints $HK = -1.235 + 1.020 \times B6,\ \ (r = 0.911)$ $HK = 34.113 + 2.494 \times B6 - 2.349 \times B4,\ \ (r = 0.968)$ $HK = 98.833 + 3.090 \times B6 - 6.652 \times B4 + 2.156 \times B5, (r = 1.000)$	Central distance of knee-ankle joints $KA = 2.612 + 1.052 \times C4,\ \ (r = 0.980)$ $KA = -0.610 + 0.575 \times C5 + 0.514 \times C4,\ \ (r = 0.996)$ $KA = -10.394 - 0.131 \times C5 + 3.050 \times C4 - 1.558 \times C6, (r = 1.000)$

* The regression equations derived from cadaver study by Dr. Damao Shan, but some uncompleted regression equations in the doctoral dissertation of Dr. Damao Shan were supplemented by the author.

**The skeletal morphological parameters are referred to Appendix B; and ‘r’ is correlation coefficient to present the closeness between the results of origin-insertion coordinates of musculotendons, which calculated by the regression equations, and the results, which measured by the specimens in the cadaver study.

Appendix D

Table 1 Anthropometric results of skeletal morphological parameters of lower limb* (cm)

Item	Subject number										Mean value	S. D.
	1	2	3	4	5	6	7	8	9	10		
Age	30	23	23	29	27	28	33	25	33	28	27.9	3.5730
Height	160	178	171	170	168	165	178	171	166	172	169.9	5.8523
Weight (kg)	63.5	73	60	61.8	64	80	70	68	67	68	67.53	5.8734
A1	23.60	26.10	23.70	23.90	22.80	22.20	23.52	22.65	24.10	24.21	23.586	1.0795
A2	10.85	10.50	8.89	8.12	8.62	8.63	9.51	8.94	8.59	9.21	9.1834	0.8696
A3	28.21	28.90	28.34	27.30	25.91	25.80	27.34	26.82	28.12	27.31	27.4084	1.0246
A4	16.75	16.60	15.62	16.40	15.51	16.40	16.03	15.12	16.12	15.94	16.0494	0.5155
A5	20.54	19.80	20.61	20.40	20.56	20.80	21.60	20.25	21.01	22.12	20.776	0.6666
A6	21.25	21.60	21.28	21.00	21.42	21.60	22.42	21.65	21.36	22.58	21.608	0.5057
A7	15.33	16.20	14.94	15.80	15.40	16.20	16.24	15.62	15.72	15.31	15.677	0.4478
A8	17.14	18.10	17.70	17.80	17.61	17.50	18.46	17.72	18.12	17.41	17.752	0.3898
B1	3.88	4.64	4.39	4.64	4.83	5.24	5.07	4.90	4.98	4.86	4.7434	0.3858
B2	5.54	8.59	7.82	7.51	7.27	7.51	7.32	7.62	7.18	7.88	7.4236	0.7772
B3	6.40	8.75	7.97	7.74	7.54	7.74	7.72	7.52	7.53	8.51	7.7422	0.6315
B4	41.00	39.50	39.21	41.10	41.52	38.90	41.82	41.33	41.32	41.81	40.7474	1.1134
B5	38.40	38.50	38.80	39.80	39.92	37.60	41.20	41.20	40.20	41.52	39.71	1.3561
B6	40.10	40.40	40.22	42.30	42.03	39.40	42.21	42.31	43.42	42.71	41.514	1.3482
B7	8.53	10.20	9.34	9.14	8.82	9.03	9.16	9.12	9.32	9.42	9.2112	0.4439
B8	7.29	10.20	9.40	8.82	9.23	9.21	9.06	9.07	9.32	9.12	9.0668	0.7167
C1	8.47	9.51	8.91	8.47	8.43	9.18	8.41	8.27	8.21	8.36	8.622	0.4312
C2	8.94	8.81	9.57	8.62	8.92	9.54	8.88	8.72	8.56	8.94	8.9498	0.3451
C3	7.33	8.17	7.62	6.66	6.89	6.71	6.89	6.57	6.08	7.11	7.0032	0.5898
C4	29.50	37.50	35.62	34.10	34.20	33.90	37.20	35.23	34.81	33.62	34.5706	2.2277
C5	30.01	38.30	36.85	37.20	37.72	36.20	39.22	37.82	37.62	36.72	36.7672	2.5230
C6	26.34	36.10	32.43	31.20	31.40	31.60	33.12	32.94	32.41	32.81	32.031	2.4352
C7	7.79	7.11	7.46	6.95	6.54	6.92	7.07	6.88	6.78	7.64	7.1138	0.3962
C8	7.40	8.75	8.46	8.92	9.06	9.08	9.21	9.45	8.67	9.18	8.8184	0.5750
D1	8.26	8.49	8.90	8.02	7.29	8.03	7.86	7.56	7.63	8.07	8.0106	0.4684
D2	9.27	9.32	8.19	7.53	7.81	7.78	7.62	7.78	7.36	8.62	8.1278	0.7083
D3	17.86	17.70	14.43	18.40	18.12	18.00	18.03	18.52	18.35	18.12	17.7504	1.1951
D4	8.28	8.67	7.78	8.13	8.49	8.57	8.57	7.81	7.81	8.42	8.2534	0.3482
D5	7.33	8.17	7.62	6.66	6.89	6.71	6.89	6.57	6.08	7.11	7.0032	0.5898
D6	11.63	13.9	13.64	13.80	12.12	12.40	13.80	14.14	13.31	13.72	13.2508	0.8694
D7	23.60	15.2	13.17	14.2	13.58	14.1	14.68	14.64	14.14	14.14	14.1086	0.6357
D8	10.85	2.04	1.86	2.26	2.13	2.10	2.10	2.37	2.35	2.15	2.15172	0.1499

*The skeletal morphological parameters are referred to Appendix B.

Table 2 A representative anthropometric results

of skeletal morphological parameters of lower limb* (cm)

Item	Anthropometric times					Mean value	S.D.
	1st times	2nd times	3rd times	4th times	5th times		
A1	23.60	23.62	23.58	23.60	23.60	23.6000	0.0141
A2	11.00	10.80	10.92	10.75	10.80	10.8540	0.1029
A3	28.20	28.10	28.12	28.40	28.25	28.2140	0.1076
A4	16.90	16.75	16.82	16.70	16.60	16.7540	0.1023
A5	20.45	20.80	20.60	20.40	20.45	20.5400	0.1462
A6	21.60	21.70	21.80	20.60	20.55	21.2500	0.5550
A7	15.20	15.40	15.50	15.20	15.35	15.3300	0.1166
A8	17.40	17.00	17.10	17.05	17.15	17.1400	0.1393
B1	3.80	3.85	3.91	3.91	3.95	3.8840	0.0528
B2	5.55	5.25	5.58	5.60	5.70	5.5360	0.1516
B3	6.48	6.38	6.30	6.50	6.35	6.4020	0.0765
B4	40.82	41.00	41.20	40.80	41.20	41.0040	0.1745
B5	38.20	38.40	38.30	38.60	38.50	38.4000	0.1414
B6	40.00	40.10	39.90	40.20	40.30	40.1000	0.1414
B7	8.50	8.45	8.60	8.61	8.50	8.5320	0.0624
B8	7.30	7.32	7.20	7.30	7.32	7.2880	0.0449
C1	8.35	8.55	8.48	8.48	8.49	8.4700	0.0654
C2	8.97	8.88	9.00	8.98	8.86	8.9380	0.0567
C3	7.44	7.30	7.21	7.39	7.32	7.3320	0.0788
C4	29.4	29.22	29.41	29.80	29.65	29.4960	0.2044
C5	30.11	30.00	30.02	29.98	29.95	30.0120	0.0542
C6	26.40	26.50	26.60	26.20	26.00	26.3400	0.2154
C7	7.80	7.75	7.81	7.78	7.80	7.7880	0.0213
C8	7.38	7.42	7.34	7.38	7.50	7.4040	0.0542
D1	8.29	8.26	8.23	8.31	8.19	8.2560	0.0427
D2	9.23	9.12	9.32	9.34	9.33	9.2680	0.0838
D3	17.89	17.90	17.91	17.72	17.90	17.8640	0.0723
D4	8.59	8.12	8.26	8.16	8.29	8.2840	0.1652
D5	7.44	7.30	7.21	7.39	7.32	7.3320	0.0788
D6	11.71	11.78	11.59	11.58	11.48	11.6280	0.1053
D7	13.07	13.29	13.40	13.31	13.31	13.2760	0.1098
D8	2.0827	2.2044	2.1683	2.1716	2.1592	2.1572	0.0403

* Subject is 30 years old, 160cm high, and 63.5 kg weight; see the items; the skeletal morphological parameters are referred to Appendix B.

List of Publications

Paper of Academic Journals

1. Rencheng Zheng, Tao Liu, Yoshio Inoue, Kyoko Shibata, Kun Liu, Kinetics analysis of ankle, knee and hip joints using a wearable sensor system, Journal of Biomechanical Science and Engineering, Vol. 3, No. 3, 2008, pp. 343-355.
2. Rencheng Zheng, Tao Liu, Yoshio Inoue, Kyoko Shibata, Kun Liu, In vivo estimation of dynamic musculotendon parameters of lower limb during gait, Journal of Biomechanical Science and Engineering. (Conditionally Accepted)
3. Rencheng Zheng, Tao Liu, Yoshio Inoue, Kyoko Shibata, Kun Liu, Prediction of muscle force using a wearable sensor system, Journal of Biomedical Engineering. (Prepare to submit)

Proceeding of International Conference

1. Rencheng Zheng, Tao Liu, Yoshio Inoue, Kyoko Shibata, Kun Liu, Linear-weight-sum method to estimate muscle force based on multiple musculoskeletal model, 4th Asian Conference of Multibody Dynamics, Jeju, Korean, 2008, pp. 838-845. (Poster Presentation Award)
2. Rencheng Zheng, Tao Liu, Yoshio Inoue, Kyoko Shibata, Kun Liu, In vivo estimation of dynamic muscle-tendon moment arm length using a wearable sensor system, Proceeding of the 2008 IEEE/ASME International Conference on Advanced Intelligent Mechatronics, Xi'an China, 2008, pp. 647-652.
3. Rencheng Zheng, Tao Liu, Yoshio Inoue, Kyoko Shibata, Calculation of joint moment using wearable sensor systems, 3rd Asian Pacific Conference on Biomechanics, Tokyo, Japan, 2007, pp. 192.
4. Rencheng Zheng, Tao Liu, Yoshio Inoue, Kyoko Shibata, Estimation of muscle force during gait using wearable sensor systems, 3rd Asia-Pacific Conference on Exercise and Sports Science, Hiroshima, Japan, 2007, pp. 79.
5. Tao Liu, Yoshio Inoue, Kyoko Shibata, Rencheng zheng, Measurement of Human Lower Limb Orientations and Ground Reaction Forces Using Wearable Sensor System, Proceedings of 2007 IEEE/ASME International Conference on Advanced Intelligent Mechatronics, September 4-7, ETH Zurich, Switzerland,2007, pp. 1-6.